PERIODICAL Kobe marine Obsw.
#11 memoirs
label
p.31
#1

神戸海洋氣象台

歐文報告

第拾壹卷

THE MEMOIRS OF THE KOBE MARINE OBSERVATORY KOBE, JAPAN

Vol. XI

KOBE

MAY - 1954

Contents

Mathematical Studies of Surf and Breakers—Nonlinear Wave Theory in Shallow Water of Constant Slope—(II)

On the Sea Level Variations Accompanied with the Travelling Atmospheric Disturbances

Notes on the Theory of the Wind-driven Oceanic Circulation

On the Variation of Oceanic Circulation. (III)

On the Variation of Oceanographical Elements due to the Tidal Currents

A Short Note on Energy Transfer from Wind to Waves and Currents

Some Remarks on the Non-linear Theory of Shallow Water Waves on a Sloping Beach

Tidal Variations of Oceanographical Elements

On the Variation of Oceanic Circulation. (IV)

On the Abnormal High Waters in Rivers

With the Author's Compliments

Mathematical Studies of Surf and Breakers— Nonlinear Wave Theory in Shallow Water of Constant Slope—(II)

By

M. Miyazaki

Reprinted from the *Oceanographical Magazine* Vol. 4. No. 1
August 1952

Mathematical Studies of Surf and Breakers—Nonlinear Wave Theory in Shallow Water of Constant Slope—(II).

By

Masamori MIYAZAKI

(Kobe Marine Observatory)

§ 6. *Breaker elements* (i)

In this paragraph we shall determine the wave elements (stationary and first order terms) of the breakers. As we have already stated, the quantity S^2 is no longer negligible for 1 at the breaking point. Therefore, we must return back to the fundamental equations (2.9), (2.10), and (2.12).

(a) *Stationary terms*—We easily obtain

$$S_0^4+S_0^2+2\zeta_0 S_0'=0 \qquad \text{at} \quad x=x_c \tag{6.1}$$

from the exact equation (3.5), provided $a\ll 1$. Therefore, the second derivative of the surface elevation S_0' must be positive at the breaking point. This means that the shoreward inclination S_0 reaches a maximum value at the immediate neighbourhood of x_c, since S_0' is always negative in the region of $S_0^2\ll 1$. Then we shall have a sharp reverse zone between this maixmum point and x_c, where S_0 rapidly decreases again to the shore.

Now we have, from the first equation of (2.9),

$$\frac{d^2\phi_0^0}{dx^2}\Big/\frac{d\phi_0^0}{dx}=\frac{S_0}{2\zeta_0}+\frac{S_0S_0'}{1+S_0^2}\,, \tag{6.2}$$

which is generally negative in sign, and, excepting the close neighbourhood of of x_c, decreases to the shore. But in the reverse zone of S_0 close to x_c, the right hand terms rapidly increase again to the shore. Then, it will be very natural to take that $\dfrac{d^2\phi_0^0}{dx^2}$ is equal to zero at $x=x_c$. This assumption will be easily permitted since we have an arbitrary constant η which is to be significant near the breaking point. It immediately leads us the result that the surface (shoreward) flow gains its maximum speed at $x=x_c$.

By use of this condition, we easily obtain

$$\left.\begin{aligned} &S_0=1\,, \\ \text{and}\quad &S_0'=3/h. \end{aligned}\right\} \qquad \text{at} \quad x=x_c \tag{6.3}$$

from (6.1) and (6.2). Substituting (6.3) into (2.9) and (2.10), we have

$$\left.\begin{aligned} &\phi_1^0=-\frac{1}{2}\frac{d\phi_0^0}{dx}\ , \quad \frac{d\phi_1^0}{dx}=0\ , \\ &\phi_2^0=\frac{3}{8h}\frac{d\phi_0^0}{dx} \quad \text{and} \quad \frac{d\phi_2^0}{dx}=-\frac{9}{16h^2}\frac{d\phi_0^0}{dx}\ . \end{aligned}\right\} \quad \text{at} \quad x=x_c \tag{6.4}$$

The velocity eomponents at the breaking point will be then

$$u_0=\left\{\frac{3}{16}+\frac{9}{8}\left(\frac{y}{h}\right)-\frac{9}{16}\left(\frac{y}{h}\right)^2\right\}\left(\frac{d\phi_0^0}{dx}\right),$$

$$\text{and} \quad v_0=\left\{-\frac{3}{4}+\frac{3}{4}\left(\frac{y}{h}\right)\right\}\left(\frac{d\phi_0^0}{dx}\right). \qquad \left[\frac{d\phi_0^0}{dx}=-\frac{2}{3}\sqrt{3gh}\right] \tag{6.5}$$

(b) *First order terms*—According to the fundamental equations (2.9), (2.10), and (2.12), it is easily found that the first order motion has generally four degrees of freedom. Two of them are determined by the amplitude and phase of the initial incoming waves, but two independent constants are still remained undetermined. Therefore, the wave height and the amplitude of the particle velocity fluctuations can be adjusted to have their maximum values at $x=x_c$.

By use of these conditions and the first relation of (6.3), we have

$$|s_1|=\sqrt{s_1 s_1^*}=1, \quad \text{and} \quad \arg s_1=\arg \zeta_1+\pi \tag{6.6}$$

at the breaking point, where s_1^* denotes the conjugate complex variable of s_1.

Now, substituting the same condition into (2.9) and (2.12), we have

$$\left.\begin{aligned} &\frac{d\phi_0'}{dx}\left(\frac{d\phi_0'}{dx}+2V\right)=-2g(\zeta_1+\zeta_0 s_1)\ , \\ \text{and} \quad &2s_1\left(3\frac{d\phi_0^0}{dx}+2V\right)=-\frac{\zeta_1}{\zeta_0}\frac{d\phi_0^0}{dx}\ , \end{aligned}\right\} \tag{6.7}$$

at this point, provided $a\ll 1$.

We next consider the breaking condition, that is, the maximum particle velocity at the surface must become equal to the phase velocity V. Expressing this relation in formula, we have

$$|u|_{\max}=-\frac{d\phi_0^0}{dx}+\left|\frac{d\phi_0'}{dx}\right|=V \qquad \text{at} \quad x=x_c \tag{6.8}$$

Substitnting (6.6) and (6.8) into (6.7), we have

$$\left.\begin{aligned} &4\mu^2+6\mu+3=3\nu \\ \text{and} \quad &4\mu+6=3\nu-\frac{\nu\alpha}{2\mu^2}-\frac{\nu\alpha}{\mu} \end{aligned}\right\} \tag{6.9}$$

where $\mu=V\Big/\frac{d\phi_0{}^0}{dx}$, $\nu=|\zeta_1|\Big/h$, and $\alpha=\frac{\sigma^2 h}{g}$.

To obtain the approximate solution of (6.9), we expand μ and ν in the series of α. If we neglect the terms of order α^3 and higher, we obtain

$$\left.\begin{aligned}\mu&=-(1.151+0.056\,\alpha-0.022\,\alpha^2)\,,\\ \text{and}\qquad \nu&=\ (0.465-0.060\,\alpha-0.019\,\alpha^2)\,.\end{aligned}\right\} \tag{6.10}$$

We can compute the breaker height and velocity from the depth of breaking by use of (6.10). The ratio of the depth of breaking to the breaker height will be discussed again in § 7.

The wave length at the breaking point is computed from the relation

$$L=\frac{2\pi}{\sigma}V, \tag{6.11}$$

i. e.,

$$L/h=\alpha^{-1/2}(8.351+0.406\,\alpha-0.160\,\alpha^2)\,, \tag{6.12}$$

where L is the wave length of the breakers.

§ 7. *Breaker elements* (ii)

In § 6 we have studied the wave elements and their variations of breakers. However, one of the most important relations—the relation between the breaker height and the initial wave height—is still not investigated.

Now we make an elementary assumption that the shorewad energy flow is conserved. The average wave energy transmitted shoreward per unit time equals

$$\frac{1}{16}\rho g H_0{}^2 V_0=\frac{1}{16\sigma}\rho g^2 H_0{}^2 \tag{7.1}$$

at the initial deep sea waves, where H_0 is the initial wave height, and V_0 is the initial wave velocity. Then, according to our assumption, the average wave energy transmitted per unit time at the breaking point must be equal to (7.1).

(a) *Potential and kinetic energy at the breaking point*—We now consider the unit width of a thin vertical layer (thickness : dx) at the breaking point, which spreads from the surface to the bottom. The potential energy in this layer is

$$\frac{1}{2}\rho g\zeta^2 dx$$

Average value of its variable part is

$$\frac{1}{4}\rho g h^2 \nu^2 dx \qquad (7.2)$$

The kinetic energy is

$$\frac{1}{2}\rho\phi_0\left\{(1+s^2)\phi_1+s\frac{d\phi_0}{dx}\right\}dx$$

(LAMB, 1932; p. 66). Average part of its variable part is

$$\frac{1}{4}\rho\left|\phi_0'\left(2\phi_1'+\frac{d\phi_0'}{dx}\right)\right|dx$$

By use of the first relation of (2.10), it becomes

$$\frac{1}{4}\rho V\left|\zeta_1\frac{d\phi_0'}{dy}\right|dx=\frac{1}{3}\rho g h^2\mu\nu(\mu+1)dx \qquad (7.3)$$

Two energies (7.2) and (7.3) are not equal to each other, but (7.2) is generally far larger than (7.3), At the first approximation, where the terms containing α are all neglected, (7.2) is just twice as large as (7.3). It is a very important conclusion, which can not be expected by previous investigations. Sufficient discussions is earnestly hoped for this problem.

(b) *Breaker height and the depth of breaking*—The average energy transmitted shoreward per unit time at the breaking point is given by (7.2) and (7.3), i. e.,

$$\rho g h^2 \mu\nu\left\{\frac{\nu}{4}+\frac{1}{3}\mu(\mu+1)\right\}\frac{d\phi_0{}^0}{dx} \qquad (7.4)$$

Equating (7.1) and (7.4), and substituting the formulas (6.10), we have

$$H_0/H=\beta^{1/4}(1.434+0.228\,\beta+0.030\,\beta^2) \qquad (7.5)$$

where H is the breaker height (twice amplitude), and $\beta=\dfrac{\sigma^2 H}{g}$. (7.5) shows that the ratio H/H_0 is a unique function of β. Then, it is evident that H/H_0 is also represented as a unique function of $\dfrac{\sigma^2 H_0}{g}$, or the initial steepness H_0/L_0 (L_0 is the initial wave length). Just the same are the ratios h/H and H/L.

The relation between h/H and H_0/L_0, which is computed from (6.10) and (7.5), is represented in Fig. 6. This figure shows that h/H must slightly increase with the increasing initial steepness. Its numerical values very from 1.08 to 1.15 in the effective range of the steepness.

The ratio h/H has been discussed by various authorities from the results of

the observations and the approximate theories. These values are largely fluctuated, but their average values range from 1.0 to 1.5. According to the solitary wave theory (MUNK, 1949), h/H is to be constant and equal to 1.28. However, the observed $h/H-$ values quoted in MUNK's paper seem to have, in the average, the similar features of the variation to our result.

The relation between H/H_0 and H_0/L_0 is shown in Fig. 7. H/H_0 varies as $(H_0/L_0)^{-1/5}$ in the first approximation. Therefore, the inclination of the curve is more gentle than that of the solitary wave theory, and more steep than that of AIRY's theory.

The observed data quoted in MUNK's paper are also plotted in this figure. The mean curve of the observation has a point of inflexion at $H/H_0=1.27$ and $H_0/L_0=0.017$. H/H_0 is a little larger than our theory in this neighbourhood. But our result is generally in good agreement with the observation.

(c) *Wave length and the steepness of breakers*—The mutual relations among H/L, L/L_0 and H_0/L_0 are shown in Fig. 8. The theoretical relationships according to LARRAS (1937) and the solitary wave theory (MUNK, 1949) are also represented in this figure. They are fairly different from our results. A few measurements of the breaker steepness (LARRAS, 1937) are in agreement with our result, but the numbers of the reliable observation are, in the present days, too small to examine these theoretical relationships.

(d) *The constant c*—The constant c, which was given in § 2, is easily computed from these figures, since

$$c^2=\frac{8}{27}gh^3$$

§ 8. *Pressure distribution*

The pressure distribution is calculated by use of the surface elevation and the velocity terms, i. e., from equations (2.2), (2.6), and (2.11), we have

$$\left.\begin{aligned} -\frac{P_1}{\rho}+g&=\frac{\partial\phi_1}{\partial t}+2\phi_2\frac{\partial\zeta}{\partial t}+\left(\frac{\partial\phi_0}{\partial x}+\phi_1 s\right)\left(\frac{\partial\phi_1}{\partial x}+2\phi_2 s\right)+2\phi_1\phi_2\,,\\ \text{and}\quad -\frac{P_2}{\rho}&=\frac{\partial\phi_2}{\partial t}+\left(\frac{\partial\phi_0}{\partial x}+\phi_1 s\right)\frac{\partial\phi_2}{\partial x}+\frac{1}{2}\left(\frac{\partial\phi_1}{\partial x}+2\phi_2 s\right)^2\,. \end{aligned}\right\} \tag{8.1}$$

Except for the close neighbourhood of x_c, s^2 can be neglected for 1. In this range, the pressure distribution is expressed by the hydrostatic formula

$$P=\rho g(y+\zeta) \tag{8.2}$$

in sufficient approximation,

The assumption of the hydrostatic pressure on longer holds near the breaking point in general cases, since s^2 can not be neglected for 1. Therefore, the strict equations (8.1) must be used in this range to determine the pressure distribution. However, at the breaking point and at the breaking instant, all hydrodynamical terms vanish and the hydrostatic pressure (8.2) holds. This fact is easily proved from (8.1), since s, ϕ_1, and $\frac{\partial \zeta}{\partial t}$ become equal to zero in this special case.

The pressure distribution at any point near the breaking point will be also calculated for anyinstant, but we shall not touch on such a process in the present paper.

§9. *Effects of the return flow*

In the foregoing paragraphs we have not considered the effects of the return flow, due to the result that the assumption of the irrotational motion no longer holds after the breaking takes place. However, in actual cases, the shoreward flow accompanied by the incoming waves is partly cancelled by the return flow, although a part of it returns back in the form of the rip currents.

For instance, we suppose that the return flow is strictly radial, and disregard the second order terms and the terms of the lateral mixing. Then, the radial velocity u_r and the surface elevation ζ are given by

$$\left.\begin{aligned} u_r &= b^2(\theta_0^2-\theta^2)/r\,, \\ \text{and} \qquad \zeta &= b^2 A/gr^2\,. \end{aligned}\right\} \tag{9.1}$$

where the origin of the circular cordinate (r, θ) is taken on the shore line, θ_0 is the angle of the bottom inclination, A is the coefficient of the eddy viscosity, and b is a constant.

Therefore, the observed fact that the mean surface is heaved at the breaking point from the undisturbed surface, which could not be explained by our irrotational theory, will be considered as the effect of the return flow. Of course (9.1) is mere a first order approximation of the strict solution, and even if the strict solution is given, it can not be linearly superimposed to the solution of the solution of the irrotational motion, owing to the existence of the interaction terms. More perfect solutions are expected.

§ 10. *Summary*

(i) The irrotational motion of waves cannot be maintained on the inclined bottom within a finite depth, which is considered to be the depth of the breaking.

(ii) In the surf zone, the stationary shoreward flow remains and is enlarged with the decrease of the depth (Fig. 2). Accordingly, the mean surface will gradually fall (Fig. 1), and at the breaking point the amount of the descention becomes one third of the depth. The observed elevation of the mean surface at the breaking point will be considered as the effect of the return flow.

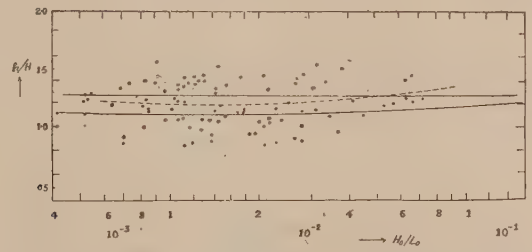

Fig. 6. Relation between g/H and H_0/L_0.

The lower solid curve denotes the theoretical relationship according to our theory, and the upper solid line represents the formula $h=1.28\,H$ of the solitary wave theory. The dashed curve is the empirical relationship.

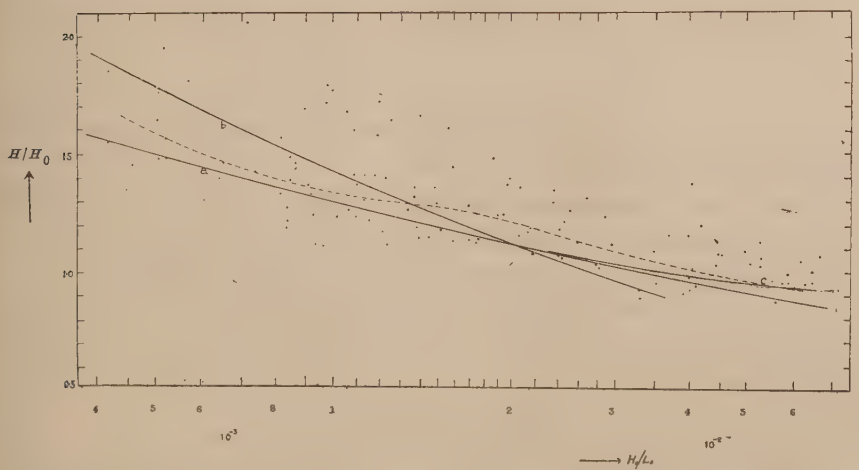

Fig. 7. Relation between H/H_0 and H_0/L_0.

The solid curves denote the theoretical relationships. The curve marked (a) represents our theory, the curve marked (b) represents the solitary wave theory, and the curve marked (c) represents AIRY's theory. The dashed curve is the empirical relationship.

(iii) The wave amplitude varies in the deeper surf region similar to the linear theory of AIRY, but becomes more larger in the shallower region (Fig. 4); while the wave velocity is generally larger than the result of the linear theory (Fig. 3 and Fig. 5). Wave velocity reaches a minimum value at $1.39x_c$.

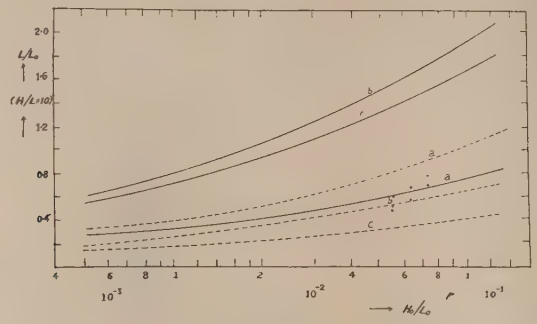

Fig. 8. Relations among H/L, L/L_0, and H_0/L_0.

The solid curves represent the relation between H/L and H_0/L_0, and the dashed curves the relation between L/L_0 and H_0/L_0. The meaning of the marks is as follows:

a. our theory, b. theory of LARRAS, c. solitary wave theory.

(iv) At the breaking point the wave height and the velocity are given by

$$H=0.930\,h, \quad \text{and} \quad V=1.329\sqrt{gh}$$

in the first approximation. But, strictly speaking, they are the functions of the initial wave height and the initial steepness.

(v) The nondimensional quantities h/H, H/H_0, and H/L are represented as the functions of the initial steepness. They are shown in figures 6—8.

The ratio h/H is nearly constant, but slightly increases with H_0/L_0.

The ratio H/H_0 varies as $(H_0/L_0)^{-1/5}$ in the first approximation. (According to the solitary wave theory it varies as $(H_0/L_0)^{-1/3}$).

Acknowledgement

The author wishes to express his hearty thanks to Dr. Masito Nakano, who kindly read this paper before printing. The author is also indebted to Mr. Kozo Yoshida for his kind advices and encouragement.

REFERENCES.

LAMB, H: *Hydrodynamics*, 6th Ed., 1932.

LARRAS, M. J.: Le defelement des Lames sur les jeties verticales. *Ann. d. Ponts et Chaussees*, 1937.

MUNK, W. H.: The solitary wave theory and its application to surf problems. *Ann. New York Acad Sci.* **51**, 3, 1949.

ERRATA FOR THE PART I (Oceanogr. Mag. 3, 3, 1951)

Page	Line	For	Read
68	last	$\cos\left(\frac{4}{3}\right)$	$\cos\left(\frac{\varphi}{3}\right)$
70	21 and 22 (Formula 3.9)	$\frac{d\phi_0{}^0}{dx}=\frac{3c}{2ax_c}$, and $\phi_1{}^0=-\frac{3cs_{0c}}{2ax_c}$.	$\frac{d\phi_0{}^0}{dx}=\frac{3c}{2ax_c}\sqrt{1+s_{0c}^2}$, and $\phi_1{}^0=-\frac{3cs_{0c}}{2ax_c}\Big/\sqrt{1+s_{0c}^2}$.
71	Fig. 2	reverse	

昭和27年10月5日　印刷
昭和27年10月10日　發行

編集兼發行人　中央氣象臺
東京都千代田區大手町一の七

印刷人　笠井康賴
東京都千代田區富士見町一の十

印刷所　國際文献印刷社
東京都千代田區富士見町一の十

With the Author's Compliments

On the Sea Level Variations Accompanied with the Travelling Atmospheric Disturbances

By

M. Miyazaki

Reprinted from the *Oceanographical Magazine* Vol. 4. No. 1
August 1952

On the Sea Level Variations Accompanied with the Travelling Atmospheric Disturbances.

By

Masamori MIYAZAKI

(Kobe Marine Observatory)

1. *Introduction*

In this paper the author intends to investigate the sea-level variations caused in the open and bounded seas by the travelling winds and the pressure disturbances. Due to the great importance of this problem, various typical cases have been discussed and solved by many students. Therefore, some elementary characters of the sea-level variations are now familiar to us, but they are of course not the whole. For instance, the effects of the Coriolis force and the bottom friction have been, until now, merely treated for some specialized cases. In the following sentenses, an attempt will be made to demonstrate these effects on the sea-level variations from more generalized point of view.

2. *General solutions of the forced oscillation*

Our first course is to obtain the equations of the forced oscillation accompanied with the travelling atmospheric disturbances—surface pressure fluctuations and the tangential stresses at the surface—in the form of $f(x-Vt, y)$ and $f(x-Vt)$. The solution for the open sea will be given from these equations.

We now consider a left-hand rectangular coordinate, and choose the z-axis vertically downwards from the mean surface. If we disregard the vertical velocity component, the inertia terms, and the lateral mixing terms, the hydrodynamical equations of motion are represented by

$$\left.\begin{aligned} \frac{\partial u}{\partial t}-\lambda v &= -g\frac{\partial}{\partial x}(\zeta-\zeta_0)+\nu\frac{\partial^2 u}{\partial z^2}, \\ \text{and}\qquad \frac{\partial v}{\partial t}+\lambda u &= -g\frac{\partial}{\partial y}(\zeta-\zeta_0)+\nu\frac{\partial^2 v}{\partial z^2}, \end{aligned}\right\} \qquad (1)$$

where t is the time, u and v are x- and y-components of the velocity, λ is the Coriolis parameter, g is the accerelation due to the gravity, ζ is the forced oscillation of the sea surface, ζ_0 is the hydrostatic elevation of the surface (sea surface fall divided by $g\rho$), ρ is the sea-water density, and ν is the z-component of the

eddy viscosity coefficient. λ and ν are regarded to be invariable in this paper.

The continuity equation is

$$\frac{\partial \zeta}{\partial t} = -\int_0^h \left(\frac{\partial u}{\partial x} + \frac{\partial v}{\partial y} \right) dz , \tag{2}$$

where h is the water depth. The surface condition is

$$\left.\begin{aligned} \frac{\partial u}{\partial z} &= -\frac{1}{\nu\rho} T_x , \\ \text{and} \qquad \frac{\partial v}{\partial z} &= -\frac{1}{\nu\rho} T_y , \end{aligned}\right\} \quad \text{at} \quad z=0 \tag{3}$$

where T_x, and T_y are x- and y-components of the surface tangential stress. The bottom condition is

$$u=v=0 \qquad \text{at} \quad z=h \tag{4}$$

(i) *Disturbance in the form of* $f(x-Vt, y)$

We first consider the case where the disturbance propagates with a constant speed V along the x-axis, so that T_x, T_y, and ζ_0 are all represented as the functions of $x-Vt$ and y.

It will be evident that the forced oscillation is also represented as the functions of $x-Vt$ and y. Provided that the disturbance vanishes at infinite distances, we can put

$$u=v=\zeta=0 \quad \text{at} \quad x-Vt \equiv x' = \pm\infty \quad \text{or} \quad y=\pm\infty \tag{5}$$

Then, by use of the Fourier transformation, (1) becomes

$$\left.\begin{aligned} ipV\bar{u} + \lambda\bar{v} &= ipg(\bar{\zeta}-\bar{\zeta}_0) - \nu\frac{d^2\bar{u}}{dz^2} , \\ \text{and} \qquad ipV\bar{v} - \lambda\bar{u} &= iqg(\bar{\zeta}-\bar{\zeta}_0) - \nu\frac{d^2\bar{v}}{dz^2} , \end{aligned}\right\} \tag{6}$$

where $$\bar{\phi}(z) = \int_{-\infty}^{+\infty}\int_{-\infty}^{+\infty} \phi(x',y) e^{-ipx'-iqy} dx'dy .$$

(6) immediately leads us to the relation

$$\left.\begin{aligned} \frac{d\bar{m}}{dz} &= Ae^{(\alpha-\alpha i)z} + Be^{-(\alpha-\alpha i)z} , \\ \text{and} \qquad \frac{d\bar{n}}{dz} &= A'e^{(\beta-\beta i)z} + B'e^{-(\beta-\beta i)z} , \end{aligned}\right\} \tag{7}$$

where $\bar{m}=\bar{u}+i\bar{v}$, $\bar{n}=i\bar{u}+\bar{v}$, $\alpha=\sqrt{\frac{PV-\lambda}{2\nu}}$, and $\beta=\sqrt{\frac{PV+\lambda}{2\nu}}$. Substituting (3) into (7), we have

$$\left.\begin{aligned} A+B&=-\frac{1}{\nu\rho}(\bar{T}_x+i\bar{T}_y)\equiv\bar{M}\,,\\ \text{and}\quad A'+B'&=-\frac{1}{\nu\rho}(i\bar{T}_x+\bar{T}_y)\equiv\bar{N}\,. \end{aligned}\right\} \tag{8}$$

Once integrates (7) with respect to z, and substitutes the condition (4) and (8), then we obtain

$$\left.\begin{aligned} \bar{m}&=-\frac{1}{2\alpha}(\bar{M}+i\bar{M})e^{-(\alpha-\alpha i)z}+\frac{1}{\alpha}(A+iA)\cosh(\alpha-\alpha i)z+m_0\,,\\ \text{and}\quad \bar{n}&=-\frac{1}{2\beta}(\bar{N}+i\bar{N})e^{-(\beta-\beta i)z}+\frac{1}{\beta}(A'+iA')\cosh(\beta-\beta i)z+n_0\,, \end{aligned}\right\} \tag{9}$$

where

$$\left.\begin{aligned} \bar{m}_0&=\frac{1}{2\alpha}(\bar{M}+i\bar{M})e^{-(\alpha-\alpha i)h}-\frac{1}{\alpha}(A+iA)\cosh(\alpha-\alpha i)h\,,\\ \text{and}\quad \bar{n}_0&=\frac{1}{2\beta}(\bar{N}+i\bar{N})e^{-(\beta-\beta i)h}-\frac{1}{\beta}(A'+iA')\cosh(\beta-\beta i)h\,. \end{aligned}\right\} \tag{10}$$

On the other hand, (6) requires

$$\left.\begin{aligned} \bar{m}_0&=\frac{(p+iq)g}{2\nu\alpha^2}(\bar{\zeta}-\bar{\zeta}_0)\,,\\ \text{and}\quad \bar{n}_0&=\frac{(ip+q)g}{2\nu\beta^2}(\bar{\zeta}-\bar{\zeta}_0)\,. \end{aligned}\right\} \tag{11}$$

Substituting (9) into the continuity equation (2), and eliminating four parameters $\bar{m}_0$, $\bar{n}_0$, A, and A' by use of (10) and (11), we finally obtain

$$\left.\begin{aligned} -4ipV\bar{\zeta}&=-2\int_0^h\{(pi+q)\bar{m}+(p+qi)\bar{n}\}dz\\ &=-(-p+qi)K_\alpha\bar{M}-(pi+q)K_\beta\bar{N}-\frac{(\bar{\zeta}-\bar{\zeta}_0)ig}{\nu}(L_\alpha+L_\beta)(p^2+q^2)\,, \end{aligned}\right\} \tag{12}$$

where $K_\alpha=\{\mathrm{sech}\,(\alpha-\alpha i)h-1\}/\alpha^2$, $K_\beta=\{\mathrm{sech}\,(\beta-\beta i)h-1\}/\beta^2$,

$L_\alpha=\left\{\alpha h-\frac{1+i}{2}\tanh(\alpha-\alpha i)h\right\}\Big/\alpha^3$, and $L_\beta=\left\{\beta h-\frac{1+i}{2}\tanh(\beta-\beta i)h\right\}\Big/\beta^3$.

It is very easy to obtain the formal solution of ζ from (12), i. e.,

$$\zeta=\frac{1}{4\pi^2}\int_{-\infty}^{+\infty}\int_{-\infty}^{+\infty}\int_{-\infty}^{+\infty}\int_{-\infty}^{+\infty}\frac{iM(k,l)(p-qi)K_\alpha+N(k,l)(p+qi)K_\beta-\frac{g}{\nu}\zeta_0(k,l)(p^2+q^2)(L_\alpha+L_\beta)}{4pV-\frac{g}{\nu}(p^2+q^2)(L_\alpha+L_\beta)}$$
$$\times e^{-ip(k-x')-iq(l-y)}dkdld\,pdq\,. \tag{13}$$

(ii) *Disturbance in the form of* $f(x-Vt)$

When the disturbance is represented as the function of $x-Vt$ only, and vanishes at $x-Vt\equiv\pm\infty$, we shall obtain

$$\zeta=\frac{1}{2\pi}\int_{-\infty}^{+\infty}\int_{-\infty}^{+\infty}\frac{iM(\mu)K_\alpha+N(\mu)K_\beta-\frac{gp}{\nu}\zeta_0(\mu)(L_\alpha+L_\beta)}{4V-\frac{gp}{\nu}(L_\alpha+L_\beta)}e^{-ip(\mu-x')}d\mu dp \qquad (14)$$

instead of (13).

§ 3. *Two special cases*

In this paragraph, we shall calculate the difinite integral (14) for two special cases. Two dimensional case (13) will be treated in the later paper.

(i) *Case 1 : very deep sea.*

When the water is sufficiently deep, we can put

$$\left.\begin{aligned} &K_\alpha\approx-\frac{1}{\alpha^2}=-\frac{2\nu}{pV-\lambda}\,,\quad K_\beta\approx-\frac{1}{\beta^2}=-\frac{2\nu}{pV+\lambda}\,,\quad L_\alpha\approx\frac{h}{\alpha^2}=\frac{2\nu h}{pV-\lambda}\\ &\text{and}\quad L_\beta\approx\frac{h}{\beta^2}=\frac{2\nu h}{pV+\lambda}\,,\end{aligned}\right\} \qquad (15)$$

in the formula (14), except for the close neighbourhood of $p=\pm\frac{\lambda}{V}$,

Therefore, (14) is approximated by

$$\begin{aligned}2\pi\zeta=&\int_{-\infty}^{+\infty}\int_{-\infty}^{+\infty}\frac{F(\mu)}{(c^2-V^2)p^2+\lambda^2}e^{-ip(\mu-x')}d\mu dp+\int_{-\infty}^{+\infty}d\mu\int_{-\frac{\lambda}{V}-\varepsilon}^{-\frac{\lambda}{V}+\varepsilon}\Bigg[f_{14}\\ &-\frac{F(\mu)}{(c^2-V^2)p^2+\lambda^2}e^{-ip(\mu-x')}\Bigg]dp\\ &+\int_{-\infty}^{+\infty}d\mu\int_{\frac{\lambda}{V}-\varepsilon}^{\frac{\lambda}{V}+\varepsilon}\left[f_{14}-\frac{F(\mu)}{(c^2-V^2)p^2+\lambda^2}e^{-ip(\mu-x')}\right]dp\,,\end{aligned} \qquad (16)$$

in this case, where $c=Vgh$, $F(\mu)=-\frac{1}{\rho}\frac{dT_x}{d\mu}+\frac{\lambda}{\rho V}T_y-c^2\frac{d^2\zeta_0}{d\mu^2}$, f_{14} is the integrated function of (14), and $\varepsilon>0$ represents the limit where $|\alpha h|$ and $|\beta h|$ are sufficiently larger than 1. As long as the water is deep enough, so that $\frac{2\nu}{h^2}\ll\lambda$, ε can be taken far smaller than λ/V. Then, the second and the third integrals of (16) become

$$\int_{-\infty}^{+\infty} d\mu \int_{-\gamma_0+\gamma_0 i}^{\gamma_0-\gamma_0 i} \frac{\phi(\mu)\gamma^2}{2\gamma-\tanh\gamma} \cos\frac{\lambda}{V}(\mu-x')d\gamma$$

$$-\int_{-\infty}^{+\infty} d\mu \int_{-\gamma_0+\gamma_0 i}^{\gamma_0-\gamma_0 i} \frac{4Vi\nu\gamma}{c^2h^2\lambda^2} F(\mu)\cos\frac{\lambda}{V}(\mu-x')d\gamma=0\,,$$

where $\gamma_0=\sqrt{\frac{\varepsilon V}{2\nu}}h$, and $\phi(\mu)$ is a function of μ. (16) is then simplified as follows:

$$\zeta=\frac{1}{2\pi}\int_{-\infty}^{+\infty}\int_{-\infty}^{+\infty}\frac{F(\mu)}{(c^2-V^2)p^2+\lambda^2}e^{-ip(\mu-x')}d\mu dp\,. \tag{17}$$

Therefore, we have no effects of the bottom friction in this case.

Calculating (17), we finally obtain

$$\zeta=\frac{1}{2\alpha\lambda}\left[e^{-x'\frac{\lambda}{\alpha}}\int_{-\infty}^{x'}F(\mu)e^{\mu\frac{\lambda}{\alpha}}d\mu+e^{x'\frac{\lambda}{\alpha}}\int_{x'}^{\infty}F(\mu)e^{-\mu\frac{\lambda}{\alpha}}d\mu\right] \tag{18}$$

for $c^2-V^2\equiv\alpha^2>0$, and

$$\zeta=\frac{1}{2\alpha'\lambda}\left[\sin\frac{\lambda}{\alpha'}x'\int_{-\infty}^{+\infty}F(\mu)\cos\frac{\lambda}{\alpha'}\mu d\mu-\cos\frac{\lambda}{\alpha'}x'\int_{-\infty}^{+\infty}F(\mu)\sin\frac{\lambda}{\alpha'}\mu d\mu\right], \tag{19}$$

for $c^2-V^2\equiv-\alpha'^2<0$.

Formulas (18) and (19) are sufficiently correct under the condition $h^2\gg\frac{2\nu}{\lambda}$. For instance, when $\nu=10^2$ c.g.s., it corresponds to the water depth larger than a few hundred meters at the middle latitudes.

(ii) *Case 2: very shallow sea*

If, in contrast with it, the water depth is very small, we have

$$K_\alpha\approx K_\beta\approx h^2 i \qquad \text{and} \qquad L_\alpha\approx L_\beta\approx-\frac{2}{3}h^3 i \tag{20}$$

except for very large and small values of p.

Then (14) becomes

$$\zeta=\frac{1}{2\pi}\int_{-\infty}^{+\infty}\int_{-\infty}^{+\infty}\frac{G(\mu)}{pi+\frac{3V\nu}{c^2h^2}}e^{-p(\mu-x')}d\mu dp\,, \tag{21}$$

in sufficient approximation, where $\frac{3}{2\rho c^2}T_x+\frac{d\zeta_0}{d\mu}$. The effects of the Coriolis force do not appear in this case.

Calculating (21), we have

$$\zeta = e^{-ax'} \int_{-\infty}^{x'} G(\mu) e^{a\mu} d\mu \,, \tag{22}$$

for $V>0$, and

$$\zeta = -e^{ax'} \int_{x'}^{\infty} G(\mu) e^{-a\mu} d\mu \,, \tag{23}$$

for $V<0$, where $a=\dfrac{3V\nu}{c^2h^2}$.

(22) and (23) are strictly correct under the condition $h^2 \ll \dfrac{2\nu}{\lambda}$. When $\nu=10$ c.g.s., it corresponds to the water depth smaller than about 10 meters at the middle latitudes.

§ 4. *Effects of the straight coast*

If there exists a coast which limits the sea, the free oscillation $\zeta_2(x,t)$ is accompanied with the forced oscillation $\zeta_1(t-\dfrac{x}{V})$ so as to satisfy the boundary condition. Let the coast be $x=0$ (sea spreads in the range $x>0$), and the motion be uniform in the direction of y, the boundary condition becomes

$$\frac{\partial \zeta_2}{\partial x} = -\frac{\partial \zeta_1}{\partial x} \,. \tag{24}$$

We now consider the solution for two special cases which we have treated in the foregoing paragraph.

(i) *Case 1 : very deep sea*

According to (14) and (17), it is evident that the free oscillation satisfies the differential equation

$$\frac{\partial^2 \zeta_2}{\partial t^2} - c^2 \frac{\partial^2 \zeta_2}{\partial x^2} + \lambda^2 \zeta_2 = 0 \,, \tag{25}$$

in this case. The suitable solution of (25) is given by

$$\begin{aligned} \zeta_2 = &\int_{\lambda}^{\infty} E_1(s) \cos\left(st \pm \sqrt{\frac{s^2-\lambda^2}{c}}\, x\right) ds + \int_{\lambda}^{\infty} E_2(s) \sin\left(st \pm \sqrt{\frac{s^2-\lambda^2}{c}}\, x\right) ds \\ &+ \int_0^{\lambda} E_3(s) \sin st\, e^{-\sqrt{\frac{\lambda^2-s^2}{c}}\, x} ds + \int_0^{\lambda} E_4(s) \cos st\, e^{-\sqrt{\frac{\lambda^2-s^2}{c}}\, x} \end{aligned} \tag{26}$$

where $E_1(s)$, $E_2(s)$, $E_3(s)$, and $E_4(s)$ are unknown functions of s, and the double sign $\begin{matrix}+\\-\end{matrix}$ corresponds to $V \begin{matrix}>0\\<0\end{matrix}$.

We can determine four unknown functions of s by use of the boundary condition (24), taking the relation

$$\zeta_1=\frac{1}{\pi}\int_0^{\infty}\cos s\left(t-\frac{x}{V}\right)ds\int_{-\infty}^{+\infty}\zeta_1(k)\cos ksdk+$$

$$+\frac{1}{\pi}\int_0^{\infty}\sin s\left(t-\frac{x}{V}\right)ds\int_{-\infty}^{+\infty}\zeta_1(k)\sin ksdk\,, \qquad (27)$$

into account. The final solution is

$$\zeta=\zeta_1\left(t-\frac{x}{V}\right)+\frac{c}{\pi V}\left[\pm\int_{\lambda}^{\infty}\frac{s}{\sqrt{s^2-\lambda^2}}ds\int_{-\infty}^{+\infty}\zeta_1(k)\cos\left(st\pm\frac{\sqrt{s^2-\lambda^2}}{c}x-ks\right)dk\right.$$

$$\left.+\int_0^{r}\frac{s}{\sqrt{\lambda^2-s^2}}e^{-\frac{\sqrt{\lambda^2s^2}}{c}x}ds\int_{-\infty}^{+\infty}\zeta_1(k)\sin(st-ks)dk\right]. \qquad (28)$$

where the double sign $\underset{-}{+}$ also eorresponds to $V\underset{<0}{>0}$.

The former integral of (28) represents a group of the reflected waves whose velocities are equal to or larger than $c=\sqrt{gh}$, and the latter integral shows the boundary standing waves generated by the existence of the Coriolis force.

(ii) *Case 2; very shallow sea*

According to (14) and (21), the equation of the free oscillation is given by

$$\frac{\partial\zeta_2}{\partial t}+\frac{1}{3}\frac{gh^3}{\nu}\frac{\partial^2\zeta_2}{\partial x^2}=0\,, \qquad (29)$$

in this case. Solving (29) under the boundary condition (24), we have

$$\zeta=\zeta_1\left(t-\frac{x}{V}\right)+\frac{1}{\pi}\int_0^{\infty}\sqrt{\frac{s}{Va}}e^{-\sqrt{\frac{sa}{2V}}x}ds\int_{-\infty}^{+\infty}\zeta_1(k)\sin\left(st+\sqrt{\frac{sa}{2V}}x+ks+\frac{\pi}{4}\right)dk \qquad (30)$$

Therefore, in this case, the free oscillation always propagates offwards (not shoreward even when $V>0$), and are damped with the increassing distance from the coast.

§ 5. *Some typical examples*

In the second to fourth paragraphs, we have obtained the formulas of the sea-level variations in an open or bounded sea accompanied with the travelling atmospheric disturbance for general and special cases. Our second course is to demonstrate the characteristic features of these variations by some typical models of the disturbance and the boundary configuration. We shall take two special cases into account. One is the case where the warm or cold front passes on a deep infinite or semi-infinite sea. The other is the case where the developed low propagates on a shallow infinite or semiinfinite channel.

(i) *Pass of the front on a deep infinite or semi-infinite sea*

We now consider the front which propagates with a constant speed V along the x-axis. Then, the stress and the pressure distribution at the sea surface can be schematically taken as follows;

$$\left.\begin{aligned} &T_x = T_0 + T_1 e^{-\theta x'}, && = T_0 + T_1 e^{\theta x'}, \\ &T_y = T_2 e^{-\theta x'} \quad (x'>0) && = -T_2 e^{\theta x'}, \quad (x'<0) \\ \text{and}\quad &\frac{d^2\zeta_0}{dx'^2} = 0 && = 0 \end{aligned}\right\} \tag{31}$$

where T_0, T_1, and T_2 are all dimensional constants, which are positive for $V>0$, and negative for $V<0$. (31) is a simple but representative model of the atmospheric disturbances accompanied with the travelling front. The constant θ is generally far larger than λ/V.

If $c^2>V^2$, substituting (31) into (18), we easily obtain

$$\left.\begin{aligned} &\zeta = \frac{T\theta}{\rho(\alpha^2\theta^2-\lambda^2)}\left(e^{-\frac{\lambda}{\alpha}x'} - e^{-\theta x'}\right), \quad \text{for } x'>0, \\ \text{and}\quad &= \frac{T\theta}{\rho(\alpha^2\theta^2-\lambda^2)}\left(e^{\theta x'} - e^{\frac{\lambda}{\alpha}x'}\right), \quad \text{for } x'<0, \end{aligned}\right\} \tag{32}$$

where $T = T_1 + \dfrac{\lambda}{V\theta}T_2$. (32) represents the sea-level variations in an open sea. A numerical example of this case is shown in Fig. 1. The sea-level rapidly rise in the upper side of the propagation, reachs a maximum value at a finite distance from the front, and then gradually decrease again to the mean sea-level. Variations are in opposite sign but of the same magnitude in the lower side.

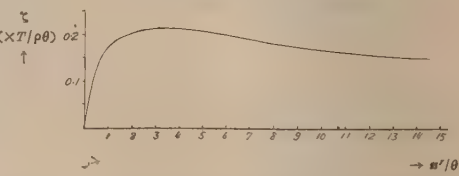

Fig. 1. Sea-level variatien on a deep open sea accompanied with the travelling front, where we take $\lambda = 7\times10^{-5}$ sec^{-1}, and $d\theta = 2\times10^{-3}$ sec^{-1}. The curve is anti-symmetric with the center of the disturbance ($x'=0$).

If the sea is bounded by a straight coast $x=0$, the sea-level variations are given by (see (28))

$$\zeta = \zeta_1(x-Vt) \pm \frac{2T\theta}{\rho(\alpha^2\theta^2-\lambda^2)}\int_\lambda^\infty \left(\frac{1}{\theta^2V^2+s} - \frac{1}{\frac{\lambda^2V^2}{\alpha^2}+s^2}\right)\frac{s^2}{\sqrt{s^2-\lambda^2}}$$
$$\times \sin\left(st \pm \sqrt{s^2-\lambda^2}\,x\right)ds - \frac{2T\theta}{\rho(\alpha^2\theta^2-\lambda^2)}\int_0^\lambda \left(\frac{1}{\theta^2V^2s^2} - \frac{1}{\frac{\lambda^2V^2}{\alpha^2}+s^2}\right)$$
$$\times \frac{s^2}{\sqrt{\lambda^2-s^2}}\cos st\, e^{-\frac{\sqrt{\lambda^2-s^2}}{c}x}\,ds, \tag{33}$$

instead of (32). Provided that $\theta V \gg \lambda$, and $c \gg V$, the variations at the coast will become

$$\left.\begin{aligned} \zeta &= \frac{|T|\theta}{\rho(\alpha^2\theta^2-\lambda^2)}\left[e^{-\theta|V|t}-2e^{-\frac{\lambda|V|t}{\alpha}}-\frac{c}{V}\{J_0(\lambda t)-e^{-\theta|V|t}\}\right] && \text{for } t>0 \\ \text{and} \quad &= \frac{|T|\theta}{\rho(\alpha^2\theta^2-\lambda^2)}\left[-e^{\theta|V|t}+\frac{c}{V}\{J_0(\lambda t)-e^{\theta|V|t}\}\right] && \text{for } t<0 \end{aligned}\right\} \quad (34)$$

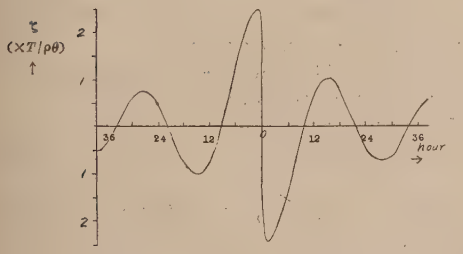

Fig. 2. Timely variation at the coast, where we take $\lambda = 7\times10^{-6}$ sec^{-1}, $\alpha\theta = 2\times10^{-3}$ sec^{-1}, and $c/V = 10$.

in sufficient approximation (cf. Watson (1922) P. 170, and Haan (1935) T. 52, 13). A numerical example of (34) is shown in Fig. 2. The sea-level varies nearly as $J_0(\lambda t)$ in this case, but the sign changes on both sides of $t=0$. The chief origin of this undulation is the interference of reflected waves. The maximum rise takes place slightly before ($V>0$) or after ($V<0$) the center ($t=0$), and reaches about $|T/\rho cV\theta|$.

(ii) *Sea-level variations in a shallow channel caused by the storm*

We next consider the case where the disturbance in the type of

$$\left.\begin{aligned} T_x &= -\tau x' e^{-bx'} \\ \zeta_0 &= \eta e^{-bx'} \end{aligned}\right\} \quad (x'>0) \qquad \left.\begin{aligned} &= -\tau x' e^{bx'} \\ &= \eta e^{bx'} \end{aligned}\right\} \quad (x'<0) \qquad (35)$$

propagates on to the shallow channel. (35) schematically represents the disturbances accompanied with the developed low such as the typhoon or the hurricane. τ and η are positive dimensional constants.

According to (22) and (23), the forced oscillation is given by

$$\left.\begin{aligned} \zeta &= (A_1+B_1)e^{-a|x'|}-A_1e^{-b|x'|}-A_2|x'|e^{-b|x'|}, && \text{for } Vx'>0, \\ \text{and} \quad &= B_1e^{-b|x'|}+B_2|x'|e^{-b|x'|}, && \text{for } Vx'<0, \end{aligned}\right\} \quad (36)$$

in this case, where $A_1 = \dfrac{b\eta}{a-b} - \dfrac{3\tau}{2\rho c^2(a-b)^2}$, $B_1 = \dfrac{b\eta}{a+b} + \dfrac{3\tau}{2\rho c^2(a+b)^2}$, $A_2 = \dfrac{3\tau}{2\rho c^2(a-b)}$, and $B_2 = \dfrac{3\tau}{2\rho c^2(a+b)}$. (36) represents the solution for the open channel. A numerical example of this case is shown in Fig. 3. The sea-level

is highest at the center, and is about twice η in this example. Generally, variations are nearly symmetric with the center of the disturbance, but slightly larger in the lower side.

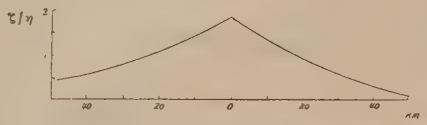

Fig. 3. Sea-level variation on a shallow open channel caused by the propagation of the developed low. Numerical values are taken as follows;
$a=3.06\times10^{-8}$ sec^{-1}, $b=5.00\times10^{-7}$ sec^{-1},
$V=10^3$ cm/sec, and $\tau/\rho=2.57\times10^{-7}$ c.g.s.

If an end of the channel $x=0$ is closed, the sea-level variations are fairly different from (36). That is, by use of (30), we have

$$\left.\begin{aligned}\zeta&=(A_1+B_1)e^{-aVt}+\{B_1-A_1(b/a)^{1/2}+\frac{A_2}{2}(ab)^{-1/2}\}e^{-bVt}\\&\quad+\{B_2-A_2(b/a)^{1/2}\}Vte^{-bVt}, \qquad \text{for } Vt>0\\ \text{and}\\ \zeta&=(A_1+B_1)\{\cosh aVt-R_1(aVt)\}\\&\quad-[A_1e^{bVt}+A_1(b/a)^{1/2}\{\cosh bVt-R_1(bVt)\}+B_1(b/a)^{1/2}\\&\quad\times\{\sinh bVt+R_1(bVt)\}]\\&\quad-[A_2Vte^{bVt}-A_2(ab)^{-1/2}\{bVt\cosh bVt+\frac{1}{2}\cosh bVt+R_2(bVt)\}\\&\quad+B_2(ab)^{-1/2}\{bVt\sinh bVt+\frac{1}{2}\sinh bVt-R_2(bVt)\}], \qquad \text{for } Vt<0\end{aligned}\right\}\quad(37)$$

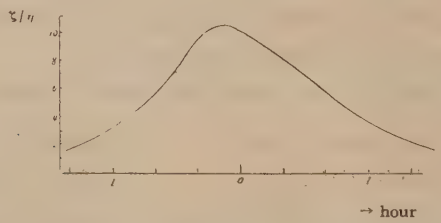

Fig. 4. Timely variation at the coast. Numerical values of the constants are equal to the case of Fig. 3. The curve is drawn for $V>0$.

at $x=0$, where

$$R_1(z)=\sum_{n=0}^{\infty}\frac{(-Z)^{2n+\frac{3}{2}}}{\Gamma\left(2n+\frac{5}{2}\right)} \quad \text{and} \quad R_2(Z)=\sqrt{2\pi}\sum_{n=0}^{\infty}\frac{(n+1)(-Z)^{2\eta+\frac{3}{2}}}{\Gamma\left(2n+\frac{5}{2}\right)},$$

(cf. Watson (1922) p. 434, and Haan (1935) T. 177, 29; T. 178, 12–15).

Fig. 4 represents a numerical example of (37). The sea-level reachs a maximum at $t\approx\pm 10$ min. ($\pm$ for $V\gtrless 0$), and becomes about ten times η in this example. The asymmetry becomes more remarkable and contrarily to the case of the open channel.

§ 6. *Summary*

In this paper, we have first derived the general solutions of the forced oscillation of the sea-level corresponding to the atmospheric disturbance in the type of $f(x-Vt, y)$ and $f(x-Vt)$, where the effects of the Coriolis parameter and the eddy viscosity terms have been both taken into account. When the water depth is either very large or very small, the solutions are simplified for the latter form of the disturbance. The effect of the bottom friction can be neglected for the very deep sea, and the effect of the Coriolis force can be neglected for the very shallow sea.

In a bounded sea, the terms of the free oscillation must be added so as to satisfy the boundary condition. In this paper we also treat the case where the sea is bounded by a straight coast for two special cases.

As the typical examples of these cases, we have calculated the sea-level variations in an open sea and near the straight coast accompanied with the pass of the front, and those in a shallow channel caused by the propagation of the developed low. These examples show that the rise of the sea-level becomes far larger at the coast than in the open sea. Numerical examples of these cases are shown in Fig. 1–4, whose characteristic features are presented in § 5.

Acknowledgements

In conclusion, the author expresses his hearty thanks to Dr. M. Nakano, who kindly read this paper before printing. The author is also indebted to Mr. K. Akedo and Mr. K. Kanaya for their kind advices on meteorological problems.

REFERENCES

G. N. Watson: *A treatise on the theory of Bessel functions*, Cambridge, 1922.

B. d. Haan: *Nouvelles tables d' intégrales définies*, reprinted by Iwanami, 1935.

昭和27年10月5日　印刷
昭和27年10月10日　發行

編集兼發行人　中央氣象臺
東京都千代田區大手町一の七

印刷人　笠井康賴
東京都千代田區富士見町一の十

印刷所　國際文献印刷社
東京都千代田區富士見町一の十

With the Authors' Compliments

Notes on the Theory of the Wind-driven Oceanic Circulation

By

M. Miyazaki

Reprinted from the *Oceanographical Magazine* Vol. 4. No. 2
October 1952

Notes on the Theory of the Wind-driven Oceanic Circulation.

By

Masamori MIYAZAKI

(Kobe Marine Observatory)

Abstract :

The wind-stres exerted on the ocean surface is supposed to have a gyral structure. And, in the coastal region, the lateral mixing coefficient will have the smaller values than those in the offing.

Chief process of this paper is to calculate the distribution of the mass transport under these circumstances by using Munk's fundamental equation. These conditions make possible to adjust the absolute quantities of the mass transport to the observed data, and to explain the existence of the counter currents near the western edge of the ocean.

§ 1. *Introduction*

In these few years, the drift current theory has made a great progress by the serial investigations of Stommel (1948), Reid (1948), Munk (1950), Munk and Carrier (1950), Hidaka (1949, 1950 a, b, c), and others. Through these works we know that two important factors, the lateral mixing and the variation of the Coriolis parameter with latitude, are closely related with the real circulation. Some important features of the oceanic circulation, such as the remarkable westward intensification of the current system, are explained by these investigations.

However, inconsistency exists between theory and observation at least in two points. That is, (i) the absolute value of the mass transport is not in agreement with the observation, and (ii) the inshore counter currents can not be explained by these theories. Recently, Munk, Groves, and Carrier (1950) calculated the more exact cases by taking the inertia terms into account, but the results were not noticeably improved.

The author is of the opinion that the distribution of the wind-stress exerted on the ocean surface is represented by a few sets of gyres (cyclonic or anticyclonic) which correspond to the tropical low, subtropical high, subpolar low, etc, and that the lateral mixing coefficient will noticeably decrease in the coastal region. In the following paragraphs, we shall calculate two new models of the oceanic circulation by taking these effects into account.

§ 2. *The Oceanic Circulation Caused by the Gyral Distribution of the Wind-Stress*

According to Munk (1950), the stream function of mass transport ψ is given by the differential equation

$$\left(A\Delta^2-\beta\frac{\partial}{\partial x}\right)\psi=-\operatorname{rot}_z\tau\,, \tag{1}$$

where the axes x and y are taken eastward and northward, respectively.

A is the lateral component of the kinetic eddy viscosity, $\beta=\frac{\partial f}{\partial y}$, f the Coriolis parameter, and τ the wind-stress.

When we consider a zonal region of the ocean bounded by two straight coasts $x=0$ and a, the boundary conditions will become

$$\left.\begin{aligned}&\psi=0\,,\\ \text{and}\quad&\frac{\partial\psi}{\partial x}=0\,.\end{aligned}\right\}\quad(\text{at } x=0 \text{ and } a) \tag{2}$$

Munk (1950) expressed the wind-stress as the function of y only, but it will be more natural to assume the gyral distribution such as

$$\left.\begin{aligned}&\tau_x=-\tau_0\sin mx\cos ny\,,\\ \text{and}\quad&\tau_y=\frac{m}{n}\tau_0\cos mx\sin ny\,,\end{aligned}\right\}\quad(\text{non-divergent case}) \tag{3}$$

where $m=\frac{2\pi}{a}$, and $\tau_0>0$. Although, owing to the large fluctuations of the oceanic wind data, our assumption is not sufficiently accepted by the wind charts, yet it will be strongly suggested by the use of the mean isobaric charts (Schott 1926, Tsukuda and Yoshikawa 1931). From these charts, cyclonic or anticyclonic gyres of the wind system will by supposed to be corresponding to the tropical low, subtropical high, and the subpolar low.

Now, substituting (3) into (1), we have

$$\left(\Delta^2-K^3\frac{\partial}{\partial x}\right)\psi=B\sin mx\sin ny\,, \tag{4}$$

where $K=\sqrt[3]{\beta/A}$, and $B=\frac{\tau_0 n}{A}\left(1+\frac{m^2}{n^2}\right)$. K and B are supposed to be constant in this paper. A particular solution of (4) is given by

$$\psi_P=\frac{B}{mK^3}\cos mx\sin ny\,, \tag{5}$$

provided $K^3\gg m^3$, n^3. The solution of the homogeneous equation

$$\left(\Delta^2-K^3\frac{\partial}{\partial x}\right)\psi=0 \qquad (6)$$

is, in sufficient approximation, given by the product of $\sin ny$ and a function of x as follows:

$$\psi_h=(P_1e^{-\frac{K}{2}x}\cos\frac{\sqrt{3}}{2}Kx+q_1e^{-\frac{K}{2}x}\sin\frac{\sqrt{3}}{2}Kx+P_2e^{Kx}+P_3)\sin ny\,, \qquad (7)$$

where P_1, q_1, P_2, and P_3 are all integral constants. The suitable solution of (4) is represented by the sum of (5) and (7).

Determining the four integral constants by using the boundary conditions (2), we finally obtain

$$\psi=\frac{B}{mK^3}\left[\cos mx-\frac{4}{\sqrt{3}}e^{-\frac{K}{2}x}\cos\left(\frac{\sqrt{3}}{2}Kx-\frac{\pi}{6}\right)+1\right]\sin ny\,, \qquad (8)$$

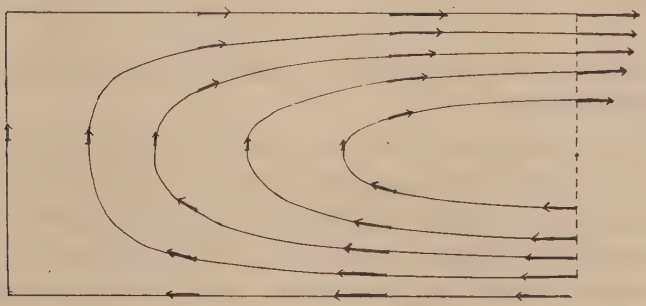

Fig. 1. Schematic distribution of the wind-stress in the western half of the ocean. The fine lines represent the stream-lines of the wind.

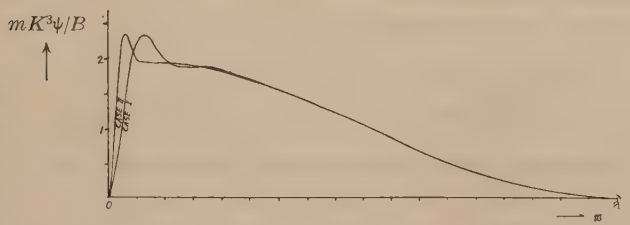

Fig. 2. Zonal distribution of $mK^3\psi/B$ at $y=\frac{\pi}{2m}$. The curve marked with "CASE I" corresponds to the case $m/K=\frac{\sqrt{3}}{30}$, and the curve marked with "CASE II" to the case $m/K=\frac{\sqrt{3}}{60}$.

provided $e^{-\frac{Ka}{2}} \ll 1$. Zonal distributions of ψ are shown in Fig. 2 for $m/K = \frac{\sqrt{3}}{30}$ and $\frac{\sqrt{3}}{60}$. Since, for instance, in the subtropical current system of the Northern Pacific (Kuroshio and its extension) we may take $m = 3.0 \times 10^{-9}$ cm^{-1}, and $\beta = 1.93 \times 10^{-13}$ cm^{-1} sec^{-1} (latitude 32.5°N), these two cases correspond to the lateral mixing coefficients 1.38×10^{9} cm^2 sec^{-1}, and 1.72×10^{8} cm^2 sec^{-1}, respectively.

General patterns of two curves in Fig. 2 are nearly similar to the solutions of Munk (1950), and of Munk and Carrier (1950), but fairly different in magnitude. The total mass transport of the Kuroshio Current becomes about 3×10^{13} g. sec^{-1} according to them, and becomes about 5.6×10^{13} g. sec^{-1} in our cases, since $n/m = 4.2$ and $\tau_0 = 1.02$ dynes cm^{-2} for this region. The latter value is nearly twice the former and in fair agreement with the observed value 6.4×10^{13} g. sec^{-1} (cf. Sverdrup, et al. 1942, p 727).

§ 3. *The case where the Lateral Mixing Coefficient takes a Smaller Value in the Coastal Region*

As we have already shown, the lateral mixing effect is concentrated near the western coast, and in this region the value A will play an important part. In the last paragraph, we have considered A to be always constant. However, strictly speaking, this assumption is not true. It is easily expected that A will noticeably decrease closely near the western coast, where the mixing length takes very small values. Perhaps, the existence of the shallow continental shelf and the large velocity gradients in the west side of the main stream will strengthen the contrast of its values.

In this paragraph, we simply suppose that

$$\left.\begin{aligned} &K = K_0 = \text{const.} \quad \text{for} \quad 0 \leq x < b, \\ \text{and} \quad &K = K_0' = \text{const.} \quad \text{for} \quad b < x \leq a, \end{aligned}\right\} \tag{9}$$

where $K_0 > K_0'$. The boundary conditions will then become

$$\left.\begin{aligned} &\psi = \frac{\partial \psi}{\partial x} = 0 && \text{at} \quad x = 0, \\ &\psi = \psi', \quad \frac{\partial \psi}{\partial x} = \frac{\partial \psi'}{\partial x}, \quad \frac{\partial^2 \psi}{\partial x^2} = \frac{\partial^2 \psi'}{\partial x^2} && \text{at} \quad x = b, \\ \text{and} \quad &\psi' = \frac{\partial \psi'}{\partial x} = 0 && \text{at} \quad x = a, \end{aligned}\right\} \tag{10}$$

where ψ and ψ' represent the mass transport stream functions at the coastal and the off-sea regions, respectively. Of course, the circumstance will be similar near the eastern coast, but we need not consider this effect, since the lateral mixing effect itself can be disregarded from our solution in this region.

If we take $K_0=4K_0'$ and $b=\frac{4\pi}{3\sqrt{3}K_0}$, the solutions become

$$\left.\begin{aligned}\psi &= \frac{B}{mK_0^3}\left[\cos mx+0.5148e^{-\frac{K_0}{2}x}\cos\left(\frac{\sqrt{3}}{2}K_0x-\frac{\pi}{6}\right)-1.4458\right]\sin ny\,,\\ \text{and}\quad \psi' &= \frac{B}{mK_0^3}\left[\cos mx+5.0367e^{-\frac{K_0'}{2}x}\cos\left(\frac{\sqrt{3}}{2}K_0'x+1.3828\right)+1\right]\sin ny\,.\end{aligned}\right\} \tag{11}$$

Zonal distributions of ψ and ψ' are shown in Fig. 3 taking $m/K_0'=\frac{\sqrt{3}}{30}$, which corresponds to the lateral mixing coefficient 2.16×10^7 cm^2 sec^{-1} in the coastal region and 1.38×10^9 cm^2 sec^{-1} in the offing.

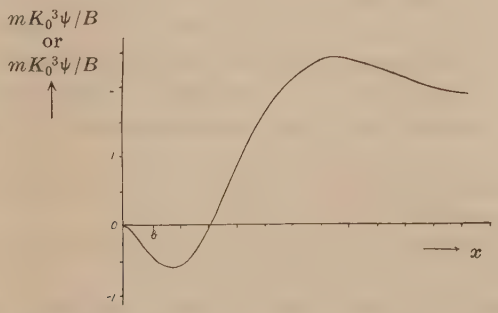

Fig. 3. Zonal distribution of $mK_0^3\psi/B$ and $mK_0^3\psi/B$ near the western coast $\left(y=\frac{\pi}{2n}\right)$, where we take $K_0=4K_0'$, $b=\frac{4\pi}{3\sqrt{3}K_0}$, and $m/K_0'=\frac{\sqrt{3}}{30}$.

One of the most attractive features of this curve is the counter currents on the western edge of the ocean. The existence of such counter currents was already proposed by Rossby (1936) using his wake stream theory. However, the origin of the counter currents is somewhat different in these two theories. According to Rossby, the water column shrinks when it approaches the wake stream region, and this makes the counter currents occur on the western side of the main stream. In contrast with it, our results shows that the counter currents are caused by the sharp decrease of the lateral mixing coefficient near the western edge.

In our example the total transport of the western counter currents is about one fifth of that of the main stream. But it is merely a special case, and the details of the stream pattern must be discussed from a more generalized viewpoint.

Acknowledgements

The author wishes to express his hearty thanks to Dr. M. Nakano, who kindly read this paper before printing. He is also indebted to Mr. K. Kajiura, Tokyo University, for his useful advices.

References

Hidaka, K., 1949: Mass transport in ocean currents and the lateral mixing. *Geophys. Notes, Tokyo Univ.* **2**, 3.

Hidaka, K., 1950 a: Wind-driven currents and surface contours in an enclosed ocean, and the lateral mixing. *Geophys. Notes, Tokyo Univ.* **3**, 12.

Hidaka, K., 1950 b: Drift currents in an enclosed ocean, Part 1. *Geophys. Notes.* **3**, 23.

Hidaka, K., 1950 c: Drift currents in an enclosed ocean, Part 2. *Geophys. Notes*, **3**, 38.

Munk, W. H., 1950: On the wind-driven ocean circulation. *J. Met.* **7**, 2, pp. 79-93.

Munk, W. H., and G. F. Carrier, 1950: The wind-driven circulation in ocean basin of various shapes. *Tellus*, 2, 3, pp. 158-167.

Munk, W. H., G. W. Groves, and G. F. Carrier, 1950: Notes on the dynamics of the Gulf Stream. *J. Mar. Res.* 9, 3, pp. 218-238.

Reid, R. O., 1948: The Equatorial Currents of the Eastern Pacific as maintained by the stress of the wind. *J, Mar. Res.* 7, 2, pp. 74-99.

Rossby, C. G., 1936: Dynamics of steady ocean currents in the light of experimentarl fluid mechanics. *Pap. phys. Ocean. Meteorol., M. I. T. and Woods Hole O. I.* **5**, 1.

Schott, G., 1926: *Geographie des Atlantischen Ozeans*, 2. Aufl., Hamburg. Tafeln 20, 21.

Stommel, H., 1948: The westward intensification of the wind-driven ocean currents. *Trans. Amer. Geophys. Un.* **29**, 2, pp. 202-206.

Sverdrup, H. U., et. al. 1942: *The oceans, their physics, chemistry, and general biology.* Prentice-Hall, New York, 1087 pp.

Tsukuda, J., and T. Yoshikawa, 1931: On the distribution of the pressure, cloudiness and the surface water temperature of the northern Pacific (In Japanese). *Jap. Mem. Imp. Marine Obs.* **37**.

昭和27年10月23日　印刷
昭和27年10月28日　發行

編集兼發行人　中央氣象臺
東京都千代田區大手町一の七

印刷人　笠井康賴
東京都千代田區富士見町一の十

印刷所　國際文献印刷社
東京都千代田區富士見町一の十

With the Authors' Compliments

On the Variation of Oceanic Circulation. (III)

By

T. Ichiye

Reprinted from the *Oceanographical Magazine* Vol. 4. No 2
October 1952

On the Variation of Oceanic Circulation. (III)

By

Takashi ICHIYE

(Kobe Marine Observatory)

§1. In his previous papers (1) and (2) the author discussed two types of annual variation of ocean current. Here he treats the problem more empirically and has sought the annual variation of oceanic circulation due to the fluctuation of the wind system over the Pacific Ocean. First the wind stresses are determined by use of the "Atlas of Climatic Charts of the Oceans" of U.S. Weather Bureau. The mean wind velocity and direction for each five-degree sector in each month is obtained from the Charts, and the wind stresses are calculated by the formula of Reid[3] considering the constancy of the wind. From the constancy of wind direction, we put the wind stress as $T(1-a)$, where a is the constant determined by the standard deviation of wind direction, which is given by the formula $\Phi\left(\frac{d}{\sigma}\right)=1-p/100$, where Φ is the error function, and p the percentage constancy of wind direction given in the Charts. Then, taking $d=30°$, we obtain σ for any p, and further putting $a=\sigma/360°$, the values of a are 0, 0.10, 0.15, 0,24, 0.50, 1.00, corresponding to $p=100$, 80, 60, 40, 20, 0(%), respectively. For the standard deviations σ_1 of wind velocity which are necessary for the calculation of T, we use the wind force w appearing in 60% or more of the time in the Charts and take $\sigma_1=0.43w$, where $\frac{1}{2}\Phi(0.43)=0.60$, and then we can compute T by the formula

$T=0.9\times10^{-6}(\bar{u}^2+\sigma_1^2)$ ($\bar{u}<3$ Beaufort), $2.0\times10^{-6}(\bar{u}^2+0.85\bar{u}\sigma_1+\sigma_1^2)$ ($\bar{u}=4$ Beaufort)
$9.0\times10^{-6}(\bar{u}^2+\sigma_1^2)$ ($\bar{u}>4$ Beaufort), (u, σ= cm/sec).

The zonal and meridional mean values of wind stresses are shown in Tables 1 and 2, where T_x is E−W component, and T_y N−S component. Further, from the zonal mean of T_x we obtain the coefficients T_1 and T_2 by the method of least squares,

where $$T_x=T_0+T_1\cos\frac{\pi y}{a}+T_2\cos\frac{2\pi}{a}y$$

and the results are shown in Table 3.

In the following discussions we take $x=0$, a for 130°E and 110°W, and $y=0$, b for 10°S and 50°N, respectively.

And from the formulae given in one of the previous papers[4]

$$u=-\frac{a}{\beta D}\left(\frac{\pi}{b}\right)^2\left(T_1\cos\frac{\pi y}{b}+4T_2\cos\frac{2\pi y}{b}\right)$$
$$\times\left\{\left(\frac{x}{a}-1\right)+\frac{2}{\sqrt{3}}e^{-\alpha_2 x/2}\cos\left(\frac{\sqrt{3}}{2}\alpha_2 x-\frac{\pi}{6}\right)\right\},$$
$$v=-\frac{2}{\sqrt{3}}\cdot\frac{a\pi}{bD}\beta^{-2/3}K^{-1/3}\left(T_1\sin\frac{\pi y}{b}+2T_2\sin\frac{2\pi y}{b}\right)e^{-\alpha_2 x/2}\sin\frac{\sqrt{3}}{2}\alpha_2 x,$$

where $\alpha_2=(\beta/K)^{1/3}$, $a=0.7\times10^9$(cm), $b=1.2\times10^9$(cm), $\beta=10^{-13}$
$K=10^8$, $D=2\times10^4$(cm).

In the present case, we can calculate the maximum values of velocity components u and v near the western boundary and their annual variations are shown in Fig. 1 for the latitudes of $y=0$, $b/2$, b for u, and $y=b/4$, $b/2$, $3b/4$ for v, respectively. The curves indicate that the two maxima and minima exist, although the phases are somewhat different in each latitude. The northern current is strongest at $y=\frac{3b}{4}$ and the maxima occur in late spring and early winter, whereas at $y=\frac{b}{4}$ the phase lag is about two or three months. From the variations of u we can see that the current corresponding to the equatorial current is much weaker than the west wind drift and in spring it flows towards west, which seems to be rather unlikely. But, for the meridional current system the effect of the zonal distribution of wind stresses is more predominant, and it is difficult to make a conclusion only from the meridional distribution.

§ 2. Next, for the discussion of the effect of the zonal distribution of wind stresses, the coefficients of Fourier series are calculated by the ordinary method of harmonic analysis and the results are shown in Table 4,

where

$$T_x=\sum_{n=0}^{2}\left(p_n\cos\frac{2n\pi}{b}y+q_n\sin\frac{2n\pi}{b}y\right)\cdot\sum_{m=0}^{4}\left(A_m\cos\frac{2m\pi}{a}x+B_m\sin\frac{2m\pi}{a}\right),$$

and

$$T_y=\sum_{n=0}\left(p_n'\cos\frac{2n\pi}{b}y+q_n'\sin\frac{2n\pi}{b}y\right)\cdot\sum_{m=0}^{4}\left(A_m'\cos\frac{2m\pi}{a}x+B_m'\sin\frac{2m\pi}{a}x\right).$$

In the present research, however, as the coefficients such as

$$T_x=\sum_{j=1,2}\cos\frac{j\pi y}{b}\left(A_{j_0}+A_{j_1}\cos\frac{2\pi x}{a}+B_{j_1}\sin\frac{2\pi x}{a}+\cdots\right)$$

and

$$T_y=\sum_{j=1,2}\sin\frac{j\pi y}{b}\left(A'_{j_0}+A'_{j_1}\cos\frac{2\pi x}{a}+B'_{j_1}\sin\frac{2\pi x}{a}+\cdots\right)$$

Table 1. The zonal mean values of wind stresses over the Pacific Ocean.
(dyne/cm², T_x=E Comp., T_y=N Comp.)

Lat.	Jan.		Feb.		Mar.		Apr.		May		June	
	T_x	T_y	T_x	T_y	T_x	T_y	T_x	T_y	T_x	T_y	T_x	T_y
45°N	0.5	0.2	0.4	0.3	0.7	0.3	0.7	0.2	0.5	0.2	0.3	0.2
40	0.6	−0.1	0.6	−0.1	0.6	0.1	0.7	0.1	0.5	0.2	0.2	0.1
35	0.7	−0.2	0.7	−0.0	0.5	−0.1	0.4	−0.0	0.4	0.2	0.2	0.0
30	0.6	−0.3	0.6	−0.2	0.4	−0.3	0.0	−0.2	−0.1	−0.3	0.0	−0.1
25	0.1	−0.4	0.3	−0.4	−0.1	−0.5	−0.9	−0.5	−0.4	−0.4	−0.4	−0.3
20	−0.6	−0.6	−0.5	−0.6	−0.6	−0.5	−1.3	−0.6	−0.8	−0.3	−0.7	−0.4
15	−0.6	−0.7	−0.5	−1.0	−0.6	−1.0	−1.0	−0.8	−1.0	−0.7	−1.1	−0.6
10	−0.7	−1.0	−0.7	−1.0	−0.8	−1.0	−0.8	−1.0	−1.0	−0.8	−1.0	−0.7
5	−0.8	−1.0	−1.0	−0.9	−1.0	−0.9	−0.8	−1.0	−0.7	−0.4	−0.7	−0.4
0	−1.2	−0.1	−1.3	−0.2	−1.5	−0.5	−1.2	−0.2	−1.0	0.2	−1.0	0.5
5°S	−1.4	−0.1	−1.2	−0.1	−1.3	−0.2	−1.3	0.0	−1.3	−0.3	−1.2	0.3
10	−1.2	−0.2	−1.1	−0.0	−1.1	0.0	−1.2	0.2	−1.1	0.5	−1.1	0.2

Lat.	July		Aug.		Sept.		Oct.		Nov.		Dec.	
	T_x	T_y	T_x	T_y	T_x	T_y	T_x	T_y	T_x	T_y	T_x	T_y
45°N	0.3	0.3	0.4	0.3	0.4	0.2	0.8	0.2	1.0	0.1	0.5	0.2
40	0.1	0.2	0.2	0.2	0.1	−0.0	0.5	0.0	0.7	0.1	0.8	−0.2
35	−0.1	−0.0	−0.1	0.1	−0.1	−0.1	0.2	−0.2	0.5	−0.2	0.8	−0.3
30	−0.2	−0.1	−0.3	0.4	−0.3	−0.2	−0.2	−0.3	0.2	−0.3	0.5	−0.1
25	−0.8	−0.3	−0.6	−0.2	−0.6	−0.4	−0.7	−0.4	−0.5	−0.5	−0.2	−0.4
20	−0.9	−0.3	−0.8	−0.2	−0.8	−0.4	−0.9	−0.5	−1.0	−0.7	−0.7	−0.7
15	−1.3	−0.4	−1.5	−0.4	−1.3	−0.3	−1.1	−0.5	−1.1	−0.8	−0.7	−1.0
10	−1.3	−0.4	−1.1	−0.1	−1.0	−0.1	−1.0	0.4	−1.0	−0.8	−0.9	−0.9
5	−0.7	0.3	−0.8	0.6	−0.6	0.4	−0.6	0.4	−0.8	0.1	−0.9	−0.4
0	−0.3	0.7	−0.4	0.7	−0.3	0.6	−0.4	0.6	−0.7	0·4	−1.3	−0.2
5°S	−0.7	0.7	−0.7	0.4	−0.5	0.5	−0.6	0.4	−1.1	0.2	−1.3	0.1
10	−1.0	0.7	−0.7	0.6	−0.9	0.5	−0.8	0.3	−1.3	0.0	−1.2	−0.0

Table 2. The meridional mean values of wind stresses over the Pacific Ocean.
(dyne/cm², T_x=E Comp., T_y=N Comp.)

Long.	Jan.		Feb.		Mar.		Apr.		May		June	
	T_x	T_y	T_x	T_y	T_x	T_y	T_x	T_y	T_x	T_y	T_x	T_y
130°E	−0.2	−1.0	−0.2	−0.9	−0.3	−0.7	−0.4	−0.2	−0.3	0.2	−0.3	0.2
135	−0.3	−1.0	−0.3	−0.7	−0.2	−0.5	−0.4	−0.4	−0.3	0.2	−0.4	0.3
140	0.0	−1.0	−0.3	−0.8	−0.4	−0.6	−0.4	−0.3	−0.4	−0.0	−0.4	0.1
145	0.0	−1.0	−0.1	−0.7	−0.3	−0.7	−0.4	−0.3	−0.6	0.1	−0.5	0.1
150	0.1	−0.9	0.0	−0.7	−0.2	−0.6	−0.5	−0.2	−0.5	−0.1	−0.6	−0.1
155	0.1	−0.8	0.1	−0.6	−0.2	−0.6	−0.6	−0.3	−0.6	−0.2	−0.6	−0.2
160	0.1	−0.6	0.0	−0.6	−0.1	−0.5	−0.6	−0.5	−0.5	−0.2	−0.5	−0.1
165	0.1	−0.6	0.1	−0.6	0.0	−0.2	−0.4	−0.3	−0.5	−0.1	−0.5	−0.2
170	0.0	−0.4	0.2	−0.4	0.3	−0.2	−0.5	−0.3	−0.4	−0.1	−0.5	0.0
175	−0.0	−0.3	0.1	−0.1	−0.3	−0.3	−0.5	−0.3	−0.6	−0.3	−0.7	−0.2
180	−0.3	0.0	−0.1	−0.3	−0.3	−0.3	−0.6	−0.3	−0.5	−0.2	−0.7	−0.2
175°W	−0.3	−0.4	−0.2	−0.3	−0.7	−0.2	−0.7	−0.3	−0.6	−0.4	−0.7	−0.3
170	−0.5	−0.3	−0.4	−0.3	−0.6	−0.4	−0.7	−0.5	−0.8	−0.2	−0.8	−0.2
165	−0.6	−0.2	−0.5	−0.3	−0.7	−0.3	−0.7	−0.4	−0.7	−0.3	−0.8	−0.3
160	−0.7	−0.1	−0.6	−0.1	−0.8	−0.1	−0.7	−0.5	−0.8	−9.2	−0.8	−0.2
155	−0.7	−0.1	−0.7	−0.0	−0.7	−0.3	−0.8	−0.5	−0.8	−0.1	−0.9	−0.2
150	−0.8	0.0	−0.8	0.0	−0.7	−0.2	−0.8	−0.5	−0.7	−0.2	−0.9	−0.2
145	−0.8	−0.1	−0.9	−0.1	−0.7	−0.2	−0.8	−0.4	−0.7	−0.3	−0.8	−0.4
140	−0.8	−0.4	−0.8	0.1	−0.6	−0.5	−0.7	−0.6	−0.7	−0.4	−0.7	−0.5
135	−0.8	−0.3	−0.7	0.0	−0.7	−0.3	−0.8	−0.1	−0.7	−0.4	−0.6	−0.4
130	−0.7	−0.2	−0.6	0.0	−0.5	−0.4	−0.7	−0.3	−0.5	−0.2	−0.5	−0.4
125	−0.8	−0.3	−0.7	−0.2	−0.7	−0.6	−0.8	−0.4	−0.7	−0.1	−1.0	−0.4
120	−0.8	−0.1	−0.6	−0.5	−0.7	−0.6	−1.0	−0.4	−0.5	−0.0	−0.5	−0.3
115	−1.0	0.3	−0.8	−0.3	−0.6	−0.5	−0.8	−0.4	−0.4	−0.2	−0.4	−0.3

Long.	July		Aug.		Sept.		Oct.		Nov.		Dec.	
	T_x	T_y	T_x	T_y	T_x	T_y	T_x	T_y	T_x	T_y	T_x	T_y
130°E	−0.2	0.5	−0.1	0.4	−0.2	0.2	−0.3	−0.3	−0.3	−0.6	−0.2	−1.0
135	−0.1	0.4	−0.2	0.4	−0.3	0.1	−0.1	−0.4	−0.4	−0.4	−0.4	−1.0
140	−0.2	0.3	−0.3	0.5	−0.3	0.2	−0.3	0.0	0.2	−0.5	−0.2	−0.8
145	−0.3	0.4	−0.5	0.5	−0.5	0.2	−0.4	0.1	0.2	−0.1	0.1	−0.5
150	−0.4	0.3	−0.5	0.5	−0.5	0.3	−0.4	0.1	−0.4	−0.4	−0.1	−0.5
155	−0.6	0.3	−0.6	0.4	−0.5	0.0	−0.3	−0.0	−0.2	−0.4	−0.1	−0.5
160	−0.6	0.3	−0.6	0.3	−0.4	0.0	−0.3	−0.0	−0.1	−0.3	0.0	−0.3
165	−0.7	0.3	−0.6	0.3	−0.5	−0.0	−0.4	−0.1	−0.2	−0.2	0.0	−0.3
170	−0.8	0.4	−0.5	0.3	−0.5	−0.0	−0.3	−0.1	−0.2	−0.1	0.0	−0.1
175	−0.8	0.4	−0.5	0.0	−0.5	0.1	−0.3	−0.2	−0.2	−0.5	−0.0	−0.3
180	−0.9	0.1	−0.8	0.2	−0.5	0.0	−0.4	−0.4	−0.4	−0.3	−0.2	−0.3
175°W	−0.9	−0.1	−0.8	−0.1	−0.6	0.0	−0.4	−0.1	−0.4	−0.3	−0.3	−0.2
170	−0.9	−0.2	−0.9	0.0	−0.7	0.0	−0.5	−0.2	−0.6	−0.4	−0.5	−0.4
165	−0.6	−0.3	−1.0	−0.1	−0.8	0.0	−0.5	0.1	−0.6	−0.4	−0.5	−0.2
160	−1.1	−0.2	−0.9	0.0	−0.8	0.0	−0.6	0.1	−0.7	−0.2	−0.7	−0.2
155	−1.1	−0.1	−0.8	0.0	−0.9	−0.0	−0.6	0.0	−0.7	−0.1	−0.8	−0.1
150	−1.0	−0.2	−0.8	−0.2	−0.9	−0.0	−0.7	0.0	−0.7	−0.1	−0.9	−0.0
145	−0.9	−0.5	−0.8	−0.2	−1.0	−0.1	−0.7	0.0	−0.8	0.1	−1.0	−0.1
140	−0.8	−0.3	−0.7	−0.4	−0.7	−0.1	−0.8	0.0	−0.8	0.1	−0.9	−0.2
135	−0.6	−0.4	−0.7	−0.3	−0.6	−0.1	−0.7	−0.2	−0.6	0.0	−0.8	−0.3
130	−0.4	−0.3	−0.5	−0.2	−0.4	−0.3	−0.7	−0.2	−0.6	−0.1	−0.7	−0.2
125	−0.5	−0.2	−0.4	−0.1	−0.6	−0.3	−0.4	0.3	−0.6	−0.1	−0.8	−0.3
120	−0.3	−0.1	−0.3	0.2	−0.3	0.1	−0.4	0.1	−0.6	−0.1	−0.7	−0.4
115	−0.4	0.6	−0.5	0.4	−0.3	0.5	−0.4	0.4	−0.9	0.2	−1.0	0.1

Table 3. The coefficients of T_i, T_i' determined from the zonal mean values of T_x, T_y by the method of least squares.

($T_x = T_0 + T_1 \cos \pi y/b + T_2 \cos 2\pi y/b$, $T_y = T_0' + T_1' \sin \pi y/b + T_2' \sin 2\pi y/b$.)

	T_1	T_2	T_1'	T_2'		T_1	T_2	T_1'	T_2'
Jan.	−0.94	0.18	−0.60	−0.28	Jul.	−0.66	0.07	−0.09	0.08
Feb.	−0.94	0.09	−0.61	−0.35	Aug.	−0.71	0.00	0.09	0.06
Mar.	−0.99	0.20	−0.66	−0.41	Sept.	−0.60	0.07	−0.11	0.22
Apr.	−0.94	0.44	−0.58	−0.36	Oct.	−0.74	0.21	−0.23	0.18
May	−0.88	0.38	−0.39	−0.23	Nov.	−1.01	0.31	−0.53	−0.03
June	−0.81	0.11	−0.30	−0.11	Dec.	−1.02	0.20	−0.56	−0.11

Table 4. Results of harmonic analysis of the wind stresses.

$$T_x = \left(P_0 + P_1 \cos \frac{2\pi}{b} y + q_1 \sin \frac{2\pi}{b} y + \ldots\right)\left(A_0 + A_1 \cos \frac{2\pi}{a} x + B_1 \sin \frac{2\pi}{a} x + \ldots\right)$$

$$T_y = \left(P_0' + P_1' \cos \frac{2\pi}{b} y + q_1' \sin \frac{2\pi}{b} y + \ldots\right)\left(A_0' + A_1' \cos \frac{2\pi}{a} x + B_1' \sin \frac{2\pi}{a} x + \ldots\right)$$

	A_0P_0	A_0P_1	A_0q_1	A_0P_2	A_0q_2	$A_0'P_0'$	$A_0'P_1'$	$A_0'q_1'$	A_0P_2'	$A_0'q_2'$
Jan.	−0.33	0.65	−0.82	−0.15	−0.09	−0.36	0.42	−0.07	−0.04	0.14
Feb.	−0.30	0.69	−0.84	−0.11	−0.05	−0.34	0.50	−0.10	0.07	0.13
Mar.	−0.40	0.68	−0.78	0.05	−0.06	−0.39	0.53	−0.15	0.05	0.10
Apr.	−0.55	0.77	−0.49	0.02	−0.38	−0.33	0.52	−0.09	−0.00	0.16
May	−0.50	0.58	−0.56	−0.01	−0.28	−0.15	0.45	−0.00	−0.03	0.06
June	−0.54	0.43	−0.54	−0.06	−0.21	−0.10	0.41	0.08	−0.22	0.10
July	−0.56	0.27	−0.30	0.02	−0.46	−0.11	0.40	0.31	−0.18	0·10
Aug.	−0.55	0.21	−0.37	0.06	−0.45	−0.19	0.30	0.26	−0.35	0.02
Sept.	−0.49	0.23	−0.23	0.01	−0.45	−0.07	0.24	0.40	−0.12	0.01
Oct.	−0.40	0.43	−0.31	0.09	−0.49	−0.04	0.30	0.37	−0.17	−0.02
Nov.	−0.41	0.70	−0.56	−0.01	−0.18	−0.20	0.40	0.25	−0.25	−0.04
Dec.	−0.39	0.73	−0.83	−0.09	−0.22	−0.32	0.42	0.03	−0.14	0.10

	P_0A_0	P_0A_1	P_0B_1	P_0A_2	P_0B_2	P_0A_3	P_0B_3	P_0A_4	P_0B_4	$P_0'A_0'$
Jan.	−0.38	0.01	0.50	−0.06	0.04	0.00	0.07	−0.02	0.15	−0.40
Feb.	−0.36	−0.03	0.47	−0.03	−0.05	−0.03	0.04	−0.01	0.04	−0.36
Mar.	−0.45	0.05	0.33	−0.10	−0.06	0.09	0.03	−0.01	0.08	−0.40
Apr.	−0.62	0.06	0.18	0.01	0.04	0.04	0.18	0.01	0.09	−0.33
May	−0.57	0.13	0.10	0.05	−0.06	0.08	0.03	0.03	0.02	−0.14
June	−0.62	0.17	0.11	0.04	0.00	0.06	0.06	0.06	0.06	−0.16
July	−0.63	0.36	0.09	0.07	−0.01	−0.04	0.01	0.02	0.07	0.07
Aug.	−0.60	0.28	0.08	0.00	−0.06	0.06	0.02	0.00	0.00	0.13
Sept.	−0.50	0.21	0.14	0.00	−0.11	0.10	0.00	−0.06	0.02	0.04
Oct.	−0.46	0.08	0.19	0.11	−0.02	0.01	−0.01	0.01	0.01	−0.04
Nov.	−0.43	0.08	0.34	−0.01	0.04	−0.02	0.10	−0.05	0.08	−0.18
Dec.	−0.44	−0.01	0.48	−0.02	0.00	0.00	0.05	−0.01	0.07	−0.33

	$P_0'A_1'$	$P_0'B_1$	$P_0'A_2'$	$P_0'B_2'$	$P_0'A_3'$	$P_0'B_3'$	$P_0'A_4'$	$P_0'B_4'$
Jan.	−0.25	−0.29	0.02	−0.17	0.05	−0.12	−0.25	−0.11
Feb.	−0.22	−0.29	−0.03	−0.13	0.00	0.03	−0.10	−0.00
Mar.	−0.21	−0.05	−0.03	−0.03	−0.03	0.02	0.00	0.04
Apr.	−0.04	0.06	0.00	−0.01	0.01	0.06	−0.03	0.02
May	0.12	0.07	0.08	0.06	0.04	−0.08	−0.04	−0.03
June	0.08	0.17	0.10	0.09	0.11	0.16	0.07	−0.02
July	0.15	0.35	0.10	0.00	0.16	−0.02	−0.03	0.00
Aug.	0.17	0.28	0.09	0.08	0.04	−0.05	0.04	−0.04
Sept.	0.03	0.10	0.09	0.06	0.02	0.03	0.01	−0.06
Oct.	−0.01	−0.04	−0.04	0.03	0.00	−0.12	−0.06	−0.05
Nov.	0.06	−0.15	−0.19	−0.03	0.01	−0.03	0.02	−0.07
Dec.	−0.13	−0.13	−0.13	−0.09	0.15	−0.04	−0.07	−0.10

Table 5. Coefficients of $\partial T_y/\partial x - \partial T_x/\partial y$.

$$\partial T_y/\partial x - \partial T_x/\partial y = \frac{\pi}{b}\sin\frac{\pi y}{b}\Sigma\left(P_{1n}\cos\frac{2n\pi}{a}x + Q_{1n}\sin\frac{2n\pi}{a}\right) + \sin\frac{2\pi y}{p}\Sigma\left(P_{2n}\cos\frac{2n\pi}{a}x + Q_{2n}\sin\frac{2n\pi}{a}x\right)$$

	P_{11}	Q_{11}	P_{12}	Q_{12}	P_{13}	Q_{13}	P_{14}	Q_{14}
Jan.	−0.24	1.55	−0.48	0.07	−0.33	0.04	−0.45	0.56
Feb.	−0.38	1.56	−0.35	−0.08	0.00	0.11	−0.03	0.51
Mar.	0.07	0.92	−0.29	−0.08	0.27	0.16	0.10	0.19
Apr.	0.16	0.33	−0.01	0.06	0.34	0.26	0.10	0.26
May	0.32	−0.02	0.26	−0.36	0.26	−0.13	−0.15	0.21
June	0.47	0.04	0.30	−0.26	0.74	−0.37	−0.04	−0.28
July	0.60	0.01	0.08	−0.13	−0.07	−0.26	0.02	0.00
Aug.	0.44	0.04	0.04	−0.13	0.01	−0.01	0.04	−0.04
Sept.	0.12	0.21	−0.16	0.11	0.00	0.06	0.25	0.10
Oct.	0.01	0.37	0.39	0.23	−0.28	−0.02	−0.22	0.42
Nov.	−0.05	0.72	−0.12	0.72	−0.20	0.18	−0.30	−0.03
Dec.	−0.15	1.31	−0.23	0.26	−0.12	−0.32	−0.42	0.45
	P_{21}	Q_{21}	P_{22}	Q_{22}	P_{23}	Q_{23}	P_{24}	Q_{24}
Jan.	−0.13	−0.39	−0.08	−0.06	−0.15	−0.14	−0.18	0.26
Feb.	−0.16	−0.07	−0.15	0.06	0.07	−0.02	0.00	0.22
Mar.	−0.07	−0.19	0.06	0.10	−0.05	0.04	0.09	−0.08
Apr.	−0.06	−0.26	−0.04	−0.06	0.06	−0.31	0.02	−0.07
May	−0.12	−0.25	0.04	−0.08	−0.36	−0.15	−0.16	0.12
June	0.02	−0.08	0.08	−0.10	−0.22	−0.17	−0.06	−0.16
July	0.10	−0.10	0.00	−0.10	−0.02	−0.24	−0.01	−0.06
Aug.	0.06	0.04	0.04	−0.04	−0.03	−0.03	−0.03	−0.02
Sept.	0.17	−0.11	0.24	−0.28	0.19	−0.15	−0.24	−0.05
Oct.	0.03	−0.21	−0.26	−0.20	0.32	0.01	0.20	−0.25
Nov.	−0.13	−0.55	0.01	−0.02	0.04	−0.14	0.04	−0.12
Dec.	−0.01	−0.48	−0.02	0.04	−0.03	−0.13	−0.07	−0.02

are more convenient, we take $A_{10}=T_1$ and $A_{20}=T_2$, where T_1 and T_2 are given in Table 2, and then we obtain Aj_n and $Bj_n(n\neq 0)$ from Table 3. Further, in the same manner A'_{10} and A'_{20} are obtained from the meridional mean values of T_y shown in Table 2 by the method of least squares, and the results are shown also in Table 3 as T_1' and T_2', and the coefficients A'_{jn}, and $B'_{jn}(n\neq 0)$ are calculated from the harmonic components of Table 4. For the purpose of computing the current velocity, the rotation of the wind stress vector should be calculated, and putting

$$\partial T_y/\partial x-\partial T_x/\partial y=\frac{\pi}{b}\sum_{j=1,2}\sin\frac{j\pi y}{b}\left(\sum P_{jn}\cos\frac{2n\pi x}{a}+Q_{jn}\sin\frac{2n\pi x}{a}\right),$$

$$P_{j_0}=T_j,\quad P_{jn}=jA_{jn}+\frac{2nb}{a}B'_{jn},\quad Q_{jn}=jB_{jn}-\frac{2nb}{a}A'_{jn},$$

the coefficients P_{jn} and Q_{jn} are shown in Table 5. The current velocity and stream function corresponding to such wind system are

$$\psi=\frac{\pi}{\beta b}\sum_{j=1,2}j\sin j\left(\frac{\pi}{b}y\right)\left[\frac{a}{2n\pi}\left(P_n\sin\frac{2n\pi}{a}x-Q_n\cos\frac{2n\pi}{a}x\right)\right.$$
$$+\left(\frac{1}{\alpha_2}P_n+\frac{a}{2n\pi}Q_n\right)e^{\alpha_1 j(x-a)}-\frac{1}{\alpha_2}P_n\left\{e^{\alpha_2(x-a)}\right.$$
$$\left.\left.+\frac{2}{\sqrt{3}}e^{-\frac{\alpha_2}{2}x}\left(\sin\frac{\sqrt{3}\alpha_2}{2}x+\cos\frac{\sqrt{3}}{2}\alpha_2 x-\frac{\pi}{6}\right)\right\}\right]. \qquad (1)$$

$$u=-\frac{a\pi}{2\beta b^2 D}\sum j^2\sin j\frac{\pi y}{b}\left[\frac{1}{n}\left(P_n\sin\frac{2n\pi}{a}x-Q_n\cos\frac{2n\pi}{a}x\right)\right.$$
$$+\left(\frac{1}{n}Q_n+\frac{2\pi}{\alpha_2 a}P_n\right)e^{\alpha_1 j(x-a)}-\frac{2\pi}{\alpha_2 a}P_n\left\{e^{\alpha_2(x-a)}\right.$$
$$\left.\left.+\frac{2}{\sqrt{3}}e^{-\frac{\alpha_2}{2}x}\left(\sin\frac{\sqrt{3}\alpha_2}{2}x+\cos\frac{\sqrt{3}\alpha_2}{2}x-\frac{\pi}{6}\right)\right\}\right], \qquad (2)$$

$$v=\frac{\pi}{\beta bD}\sum j\sin j\frac{\pi y}{b}\left[P_n\cos\frac{2n\pi}{a}x+Q_n\sin\frac{2n\pi}{a}x\right.$$
$$\left.-P_n\left\{e^{\alpha_2(x-\gamma)}+\frac{2}{\sqrt{3}}e^{-\frac{\alpha_2}{2}x}\left(\cos\frac{\sqrt{3}\alpha_2 x}{2}+\frac{\pi}{6}-\sin\frac{\sqrt{3}\alpha_2}{2}x\right)\right\}\right] \qquad (3)$$

$$\alpha_1 j=\frac{K}{\beta}\left(\frac{j\pi}{b}\right),$$

As seen from the above equations, the equations u and v are represented by $u=-\frac{a\pi}{2\beta b^2 D}u(x,y)$ and $v=\frac{\pi}{\beta bD}v(x,y)$, where $u(x,y)$ and $v(x,y)$ are of the order 1, and the factors are 3.85, 2.14 (cm/sec), thus the effect of the zonal variation of wind stresses are not so large for the variation of the meridional current velocity v, since its annual variation due to the variation of the meridional mean value of T_x has an amplitude of about 50~100 (cm/sec) as shown in Fig. 1. In Fig. 2 the variation of v near the western and eastern boundaries are shown for each month, where $y=b/4$, $b/2$ and $3b/4$. These curves show that the maximum velocity due to the zonal variation of the wind stresses is only about 13 cm/sec and generally it flows from January to March to the south and from April to August to the north in the western boundary, and it is intensified in

the same region as in the case of meridional distribution of the wind stress, the maximum current of which occurs at about 150 km off the western coast and the velocity is large at the southern section, i. e., at $y=b/4$ and $b/2$. From

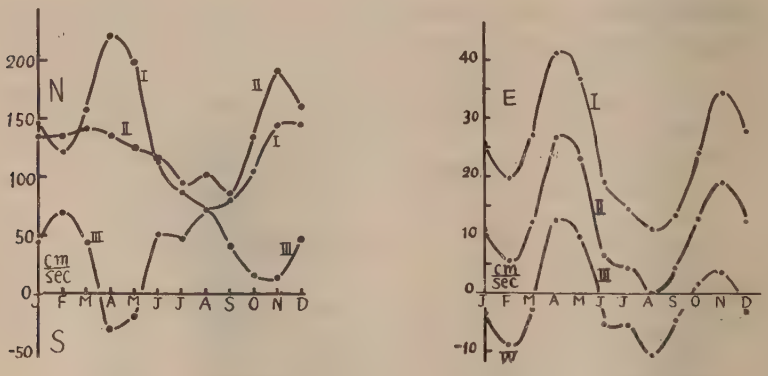

(A) N–S Component (B) E–W Component

Fig. 1. The annual variation of the maximum current velocity due to the wind stress $T_x=T_0+T_1\cos\frac{\pi}{b}y+T_2\cos\frac{2\pi}{b}y$ near the western boundary. (The numbers of the curves indicate the latitudes as follows:
For N–S component, I, $y=b/4$; II, $y=b/2$; III, $y=3b/4$.
For E–W component, I, $y=0$; II, $y=b/2$; III, $y=b$.

September to November such western current flows to the north at the northern section $y=3b/4$ and to the south at $y=b/4$ and westward intensification is somewhat indistinct at $y=3b/4$ or $b/2$ and in December the western current again flows to the south. The current near the eastern boundary flows almost in the same direction as the western current, although its velocity is less, and therefore it flows to the south in winter and to the north in spring and summer, and its direction is different in latitudes in autumn. The resultant current of Fig. 1 and Fig. 2 does not undergo a substantial change from the curves in Fig. 1, provided the winter or early spring maximum is a little weakened and the summer minimum current is somewhat intensified.

When we express the zonal distribution of the wind stress in the usual Fourier series as shown in Table 4 the rotation of the wind stress $\partial T_y/\partial x-\partial T_x/\partial y$ has its terms proportional to $\cos\frac{2n\pi}{b}y$, and especially for the terms $A_0q_n\cos\frac{2n\pi}{b}y$ which correspond to T_1, T_2 in Table 3 the current volocity is given by

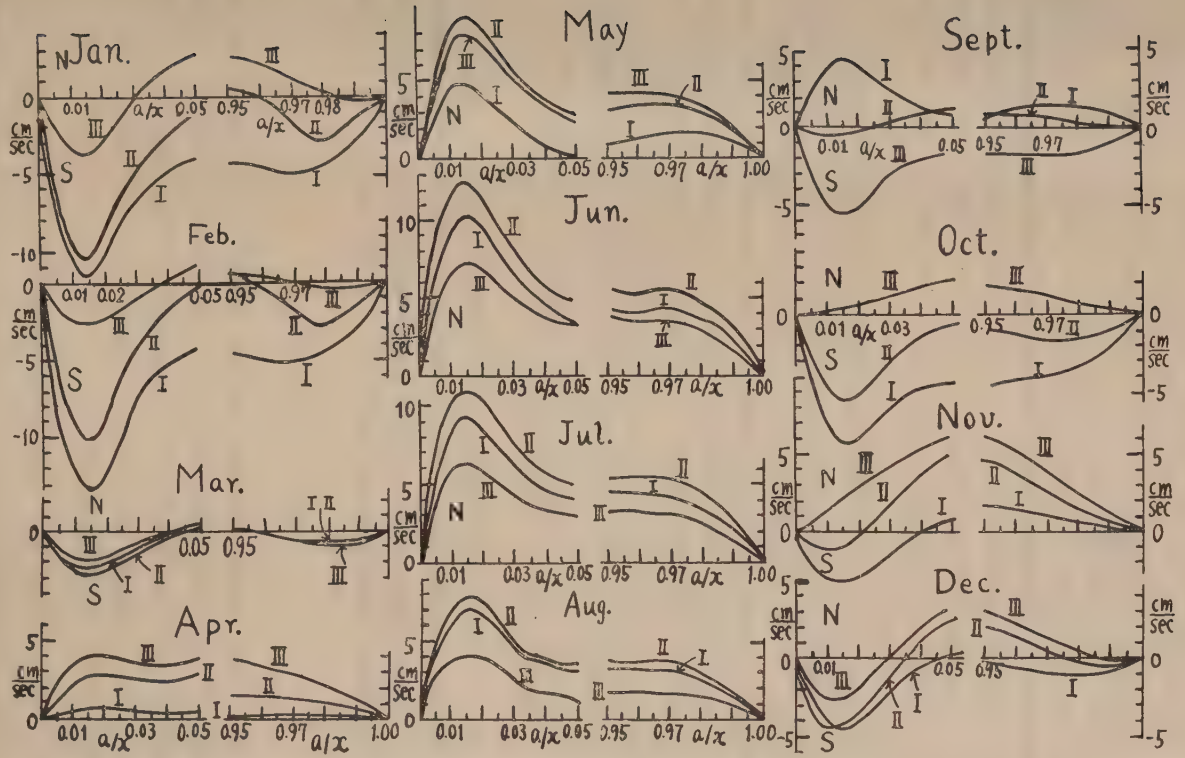

Fig. 2. Monthly distributions of the N-S component of the current near the western and eastern boundaries due to the terms of the rotation of the wind stress $\sum_{j=1,2} \sin \frac{j\pi}{b} y \left(\sum_{n=1}^{4} P_{jn} \cos \frac{2n\pi}{a} x + Q_{jn} \sin \frac{2n\pi}{a} x \right)$
(The numbers of the curves indicate the latitude as follows; I, $y=b/4$; II, $y=b/2$; III, $y=3b/4$.

$$u=\frac{a}{\beta D}\left(\frac{2\pi}{b}\right)^2\left(A_0q_1\sin\frac{2\pi}{b}y+4A_0q_2\sin\frac{4\pi}{b}y+\dots\right)f(x),$$

$$v=\frac{2}{\sqrt{3}}\beta^{-2/3}K^{-1/3}\frac{2\pi a}{bD}\left(A_0q_1\cos\frac{2\pi y}{b}+2A_0q_2\cos\frac{4\pi y}{b}+\dots\right)g(x),$$

where the factors dependent on x are the same as the equations in § 1. The velocity distributions above indicate that the meridional current flux exists at the northern and southern boundaries $y=0$ and $y=b$. Since the current at these boundaries is proportinal to $A_0q_1+2A_0q_2$, it flows to the south and its velocity is large in April, August and October, and small in February, Junuary and November as seen in Table 4.

§ 3. The variation of the lateral mixing coefficient K also should be taken into account but a complete theory for this problem is not yet given. An approximate estimation of K is obtained as follows: Since the oceanic circulation of large scale is almost governed by the meridional distribution of the zonal wind stress, the deviations of the wind stress from the zonal mean values may be considered as the irregular disturbing forces which given the energy to the oceanic turbulence. Therefore when we consider the energy supply by the irregular forces is dissipated by the turbulence, the following relation is obtained[5]:

$$\sum_{m=0}^{n}(u_mX_m+v_mY_m)=\eta_n\sum_{m=0}^{n}\left(\frac{\partial u_m}{\partial x}\right)^2+\left(\frac{\partial v_m}{\partial y}\right)^2, \qquad (4)$$

where X_m and Y_m are disturbing forces with the wave number m, u_m and v_m turbulence velocity components, η_m turbulent viscosity with the wave number m, and L_m the length corresponding to the wave length. When we assume the horizontal isotropy of turbulence and similarity, then the equation (4) becomes

$$\sum_{m=0}^{n}(X_m+Y_m)u_m\sim\frac{u_m^3}{L_m},$$

and when we in the first approximation take the spectral distribution of u_m as proportional to $L_m^{1/3}$, then the eddy viscosity $K_m\sim L_m^{1/3}[\sum(X_m+Y_m)L_m^{1/3}]^{1/3}$. In the present case the amplitude of the Fourier components of wind stresses $(A_m^2+B_m^2)^{1/2}$ and $(A_m'^2+B_m'^2)^{1/2}$ can be taken as X_m and Y_m, and the wave length $a/2m\pi$ as L_m, then the value of K is proportional to

$$[\sum\{(A_m^2+B_m^2)^{1/2}+(A_m'^2+B_m'^2)^{1/2}\}m^{-1/3}]^{1/3}.$$

In the table below the annual variation of K is given, where the mean value is K_0.

	Jan.	Feb.	Mar.	Apr.	May	June	July	Aug.	Sept.	Oct.	Nov.	Dec.
K/K_0	1.20	1.09	1.00	0.83	0.90	0.96	1.10	1.07	0.92	0.85	1.00	1.08.

From these figures we can see that the turbulence intensity is vigorous in winter and summer, and such condition seems to contribute to the variation of oceanic circulation.

In conclusion, the author expresses his hearty thanks to Miss Chiyoko Nagao for her assistance.

Literatures

(1) Takashi Ichiye: On the variation of Oceanic Circulation (I). *Ocean. Mag.* Vol. 3, No. 2, 1951.

(2) Takashi Ichiye: On the Variation of Oceanic Circulation (II). *Ocean. Mag.* Vol. 3, No. 3, 1951.

(3) R. O. Reid: The Equatorial Currents of the Eastern Pacific as Maintained by the Stress of the Wind. *Journ. Mar. Res.* Vol. VIII, 2, 1948.

(4) Takashi Ichiye: On the Effect of Lateral Mixing in the Ocean Current. *Ocean. Mag.* Vol. 2, No. 3, 1950.

(5) Weizsäcker: Das Spektrum der Turbulenz bei grossen Reynoldsschenzahlen. *Zeit. f. Physik* Bd. 124, Heft 7/12, 1948.

(6) Takashi Ichiye: Theory of Oceanic Turbulence. *Ocean. Mag.* Vol. 3, No. 3, 1951.

昭和27年10月23日　印刷
昭和27年10月28日　發行

編集兼發行人　中央氣象臺
東京都千代田區大手町一の七

印刷人　笠井康賴
東京都千代田區富士見町一の十

印刷所　國際文献印刷社
東京都千代田區富士見町一の十

With the Author's Compliments

On the Variation of Oceanographical Elements due to the Tidal Currents

T. ICHIYE

Reprinted from the *Oceanographical Magazine* Vol. 4 No. 3
December 1952

On the Variation of Oceanographical Elements due to the Tidal Currents

By

Takashi ICHIYE

(Kobe Marine Observatory)

§1. In bays or coastal region the oceanographical conditions are most variable and the observed results even with only a several hours interval show sometimes quite a different features. The most important factors for such fluctuations are considered to be the effect of tidal currents, the inflow of the land waters, the diurnal variations of heating and cooling at the surface, etc. Recently Dr. H. STOMMEL[1] has proposed a theory of tidal flushing for explanation of chlorinity distributions in estuaries and previously the author[2] also discussed the annual variations of water temperatures in the Osaka Bay by considering the tidal currents as turbulence elements for horizontal diffusion. Further Dr. A. DEFANT[3] has indicated the importancy of the effect of temperature variation with tidal period for the correction of the observed data in oceanographical survey. Therefore it seems to be of some use to show the observed facts and theoretical discussions about the effect of tidal currents to the variation of oceanographical elements.

§2. First the most simple case is that there is no diffusion and the tidal currents have only an advection effect. In such case the variation of elements is expressed by

$$\partial S/\partial t+u\,\partial S/\partial x+v\,\partial S/\partial y=0$$

and the solution is given by

$$S=f_1\left(x-\int udt\right)+g_1\left(y-\int vdt\right)+f_2\left(x-\int udt\right)g_2\left(y-\int vdt\right)$$

Further when the gradient is almost constant,

$$S=\alpha\int udt+\beta\int vdt$$

where $\alpha=-\partial S/\partial x$, $\beta=-\partial S/\partial y$.

Generally only the vertical mixing has an effect on the variation of elements from the scale effect of turbulence when the considered time interval is only a day or so and therefore the mean values of elements with the depth seems to

change as the above equation when the exchange at the surface and bottom is negligible, as seen from the integration of the diffusion equation with the depth

$$\frac{\partial \bar{S}}{\partial x}+\overline{u\frac{\partial S}{\partial x}}=\frac{1}{h}\left(K\frac{\partial S}{\partial z}\Big|_{z=\text{surface}}-K\frac{\partial S}{\partial z}\Big|_{z=\text{bottom}}\right)$$

where bar means $\frac{1}{h}\int dz$, h is the depth. When the right hand side is negligible and $\overline{u\frac{\partial S}{\partial x}}\sim\bar{u}\frac{\partial \bar{S}}{\partial x}$, the effect of vertical mixing vanishes. One example for such case is shown in Fig. 1, where the mean water temperatures and mean current velocity in the maximum current direction are shown from the data at St, 48 in Mar. 11–12, 1932.[4] Their harmonic components are as follows: (Time origin is taken at 13h.)

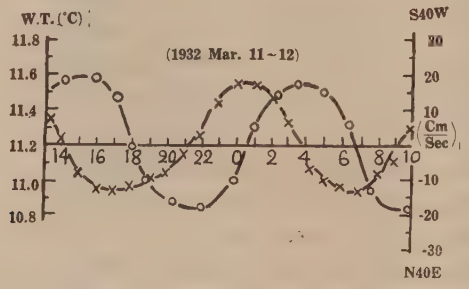

Fig. 1. Daily change of water temperatures and current velocities at St. 48 in the Inland Sea.

Both are means of observed values at 10, 20, 30 m depth and the bottom layer.

×——× Water temperatures.

○——○ Velocity components parallel to the direction from N 40° E to S 40° W.

	Mean	Diurnal		Semi-diurnal	
$\bar{u}$ (cm/sec)	0	1.6	316.°4	19.9	73.°6
$\bar{S}$ (°C)	11.20	0.08	194.°2	0.27	333.°7

and when we put the current velocity of one harmonic component as $U_0\cos(\sigma t-\mu)$, then the corresponding temperature variation is given by

$$S=\left|\frac{\partial T}{\partial x}\right|\frac{U_0}{\sigma}\cos\left(\sigma t-\mu^{+90°}_{-270°}\right),$$

thus the order of horizontal gradients of elements can be determined by

$$\sigma S_0/U_0 \quad (S_0=\text{amplitude of } S)$$

which gives the value 1.96×10^{-7} t.i. the difference of about 0.2°C at two stations 10 km distance apart, which seems to be reasonable. Further the difference of phase lag of the semi-diurnal components is 260.1°, which agrees with the theoretical value 270°. In this example the ellipse of semi-diurnal tidal current is almost a rectilinear line running from N 40° E to S 40° W and only the gradient of elements of this direction has an effect on the variation of semi-diurnal period. In general tidal currents are analysed in N and E direction and it is more convenient to express the variation of elements by N and E direction gradient. When we put

$$u=U_0\cos(\sigma t-\mu),\qquad v=V_0\cos(\sigma t-\mu)$$

for the E and N component of currents, then the variation of the elements is given by

$$\left.\begin{aligned} &S=S_0\cos(\sigma t-k),\qquad S_0^2=p^2+q^2+2pq\cos(\mu-\nu)\\ &\tan k=\frac{p\cos\mu+q\cos\nu}{-(p\sin\mu+q\sin\nu)},\quad p=-\frac{\partial S}{\partial x}\frac{U_0}{\sigma},\quad q=-\frac{\partial S}{\partial y}\frac{V_0}{\sigma}\end{aligned}\right\}\cdots\cdots(1)$$

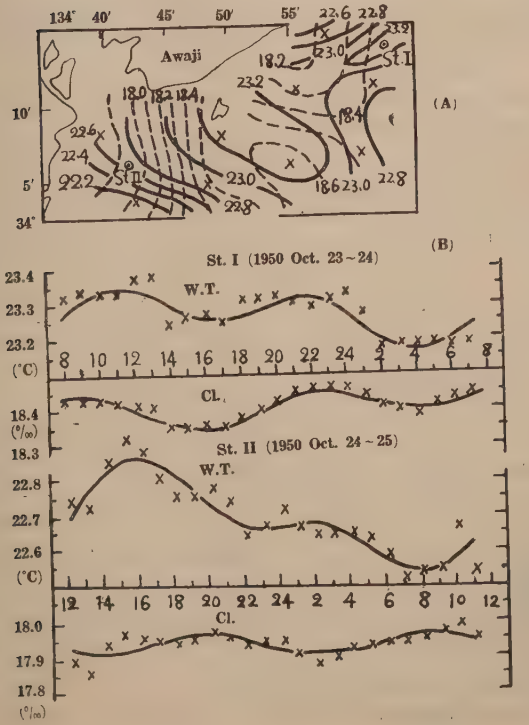

Fig. 2. Horizontal distributions of temperatures and chlorinities in the northern region of Kii-Suido and daily changes of temperatures and chlorinities at two anchored stations.

(A) Each value is obtained from the mean of 5, 10, 20 and 30 m depth. The observation were carried out from 22nd to 28th on Oct., 1950.

— Water temperatures in °C.
- - - Chlorinities in ‰.
× Observation station.
⊙ Anchored station.

(B)

× Observed values.
—— Resultant curves calculated from the harmonic components.

and from this relation the comparison between the above theory and observed change of elements is possible. In Fig. 2A the horizontal distributions of the mean values of water temperatures and chlorinities between 5 m depth and 30 m depth observed on Oct. 22 to 28 in 1950 are shown and their change in 24 hrs. at two stations are plotted in Fig. 2B. The results of harmonic analysis of mean tidal currents at these stations observed at the same time at the same depths are shown in Table 1, and from Fig. 2A the approximate values of $\partial T/\partial x$ and $\partial T/\partial y$ are determined and in Table 2 the theoretical values of semi-diurnal components of temperature and chlorinity variation by use of the above relation and the

Table 1. The harmonic components of the mean current velocities with the depth (U, μ amplitude (cm/sec) and phase lag (degrees) for E-components, V, ν for N-components.)

	Diurnal				Semi-diurnal			
St.	U	μ	V	ν	U	μ	V	ν
I	8	172	10	314	25	96	33	245
II	7	126	6	103	22	343	31	218

Table 2.

Semi-diurnal components							
St.		p	q	S cal.	k cal.	S obs.	k obs.
I	W.T.	−0.147	−0.085	0.086	36.1	0.062	18.5
	Cl.	−0.045	−0.015	0.033	19.6	0.039	34.6
II	W.T.	−0.066	−0.105	0.089	352.4	0.071	353.6
	Cl.	−0.078	0.013	0.090	258.0	0.025	209.3
Diurnal components							
St.		p	q	S cal.	k cal.	S obs.	k obs.
I	W.T.	−0.094	−0.052	0.057	113	0.051	342.8
	Cl.	−0.028	−0.010	0.023	100	0.027	160.5
II	W.T.	−0.042	−0.041	0.082	24	0.122	4.9
	Cl.	−0.050	0.005	0.049	17	0.008	40.8

S: The amplitude (W.T. in °C, Cl in ‰)
k: The phase lag (degrees).
Subscript (cal.): means the results obtained from the eqs. (1).
Subscript (obs.): means the results obtained by harmonic analysis of the data.

results from the harmonic analysis of the data in Fig. 2B are shown. The agreement between these two values is satisfactory, considering the rough determination of horizontal gradients.

In the above discussions only the semi-diurnal components are treated, since the diurnal ones are not only influenced by tidal currents but also by heating, cooling, evaporation, condensation etc., especially in water temperatures. The same calculations are practised for the diurnal components and the results are indicated also in Table 2. The agreement between the observed values and theoretical ones is not so remarkable as in the case of semi-diurnal components and the effect of heating is clearly seen in water temperatures at St. II in Fig. 2B but it is not so easy to determine such effect quantitatively from the above data, since the numerical constants have involved not so exact factors such as horizontal gradients of elements and temperatures used in the above analysis are integrated values with the depth. However such effect is expected to be most important at the surface layer in summer season and it is necessary to study the relation between the diurnal variation due to heating and semi-diurnal one due to the tidal currents. For this purpose from the diffusion equation

$$\frac{\partial S}{\partial t}+u\frac{\partial S}{\partial x}=K\frac{\partial^2 S}{\partial z^2}$$

we obtain the simple equation

$$\frac{\partial S}{\partial t}=K\frac{\partial^2 S}{\partial z^2}+u\alpha S$$

by assuming

$$\partial S/\partial x=-\alpha S$$

The boundary conditions are assumed as follows:

$z=h$ (surface) $\quad S=p_0+p_1\cos\sigma t+q_1\sin\sigma t$

$z=0$ (bottom) $\quad \partial S/\partial z=0$

then taking $\quad u=U\cos 2\sigma t$

$$S=-P_0+\sum P_j\cos j\sigma t+Q_j\sin j\sigma t$$

we obtain

$$P_1=\Re\left[\left\{\frac{p_1(K\beta^2-\gamma)/\sigma-q_1}{\cos\beta h}\cos\beta z+\frac{p_1(K\beta^2+\gamma)/\sigma+q_1}{\cosh\beta h}\cosh\beta z\right\}\Big/2\frac{K\beta^2}{\sigma}\right] \quad (2)$$

$$Q_1=\Re\left[\left\{\frac{\{q_1-p_1(K\beta^2-\gamma)/\sigma\}(K\beta^2+\gamma)/\sigma}{\cos\beta h}\cos\beta z+\frac{\{q_1+p_1(K\beta^2+\gamma)/\sigma\}(K\beta^2-\gamma)/\sigma}{\cosh\beta h}\cosh\beta z\right\}\Big/2\frac{K\beta^2}{\sigma}\right]$$

$$P_2+Q_2 i=\frac{\gamma P_0}{2\sigma} i\left(\frac{\cosh \mu z}{\cosh \mu h}-1\right) \quad \cdots\cdots (3)$$

$$\gamma=U\alpha/2\,, \qquad \beta^2=i\sqrt{\frac{\sigma^2-\gamma^2}{K^2}}\,, \qquad \mu^2=-\frac{2\sigma}{K}i$$

by taking the approximation to the second harmonics. In the usual case $\sigma^2 \gg \gamma^2$, since $\sigma=7.27\times10^{-5}$ and for temperature difference of 4°C for the distance of 10 km at the meam temperature 20°C and for $U=10^2$(cm/sec), $\gamma=10^{-5}$ and such horizontal gradient of water temperatures is probably the upper limit even in the coastal water region.

Thus the effect to the diurnal component of changes of elements due to the semi-diurnal currents is almost negligible, and the comparison between the case $\gamma=0$ and $\gamma=10^{-5}$ are shown in Fig. 3A by taking $K=10^2$ and $h=10$(m) for

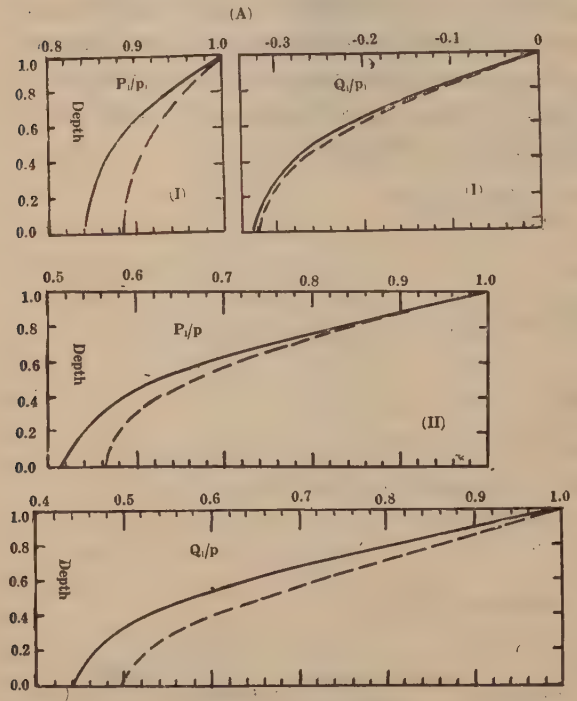

Fig. 3. Vertical distributions of diurnal and semi-diurnal components of elements given by the equations (2) and (3).
(A) Diurnal components.
(I) $q_1=0$
(II) $p_1=q_1=p$
—— $\gamma=10^{-5}$
····· $\gamma=0$
When $p_1 \fallingdotseq 0$, the effect of the semi-diurnal current is almost negligible and
$P_1 \fallingdotseq Q_1$ (in case I)
$Q_1 \fallingdotseq P_1$ (in case I)
(B) —— Amplitude
····· Phase lag.

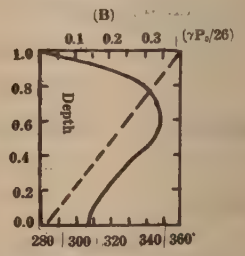

three case $q_1=0$, $p_1=q_1$, and $p_1=0$. Further the vertical distributions of amplitude and phase lag for semi-diurnal component given by the equation are also shown in Fig. 3B for $K=10$ and the same depth as the diurnal component, from which the amplitude attains to the maximum at the mid-depth due to the

surface condition but in the practical case the surface temperature has also semi-diurnal component and thus such distribution is only an ideal case. The phase lag decreases almost linearly from the top layer and reaches almost that of no vertical diffusion only at the bottom layer.

Next some remarks are given to the conception of the tidal current as turbulent elements in the horizontal mixing from the above observed facts and theoretical discussions. The above examples that the changes of water temperatures and chlorinities are in good agreement with the advection equation indicate that the water masses of different type are not completely mixed with the surrounding waters within only one or two tidal periods. In the ordinary conception of mixing length, the water masses should lose their property after the advance of this length, thus the total distance of the water masses in one tidal period is not always equal to the mixing length in the usual sense. When we consider the mixing of the different water mass with the surrounding homogeneous waters, we take the simplified equation

$$\partial S/\partial t + u\,\partial S/\partial x = -k(S-S_0)\ ,$$

where the right hand side represents all mixing processes such as vertical diffusion, horizontal mixing due to irregular motions etc. and u is assumed to express only the periodic motion of tidal character. Then the solution for the initial distribution $S=f(x)$ is given by $S=f(x-\int u dt)\,e^{-kt}+S_0$. When T is half period of diurnal or semi-diurnal tide and $T_0 < T$, $kT_0 \gg 1$, the mixing length becomes

$$\int_0^{T_0} u_m \sin \sigma t\, dt\ ,$$

where u_m is the amplitude of tidal currents and thus the mixing length is shorter than the distance of water mass within one tidal period. When $kT \ll 1$, the tidal currents only transport the water mass to and fro even at the average of relatively large time interval. Thus it is only when k has an adequate value and the water mass is completely mixed just after the elapse of about T that the tidal currents act as the most effective turbulence elements for the horizontal diffusion. From such considerations it seems to be more reasonable to put the horizontal mixing coefficient A as $A \sim u_m^2\, T(k_1 T)\, e^{-k_1 T}$, where k_1 is considered to be proportional to k and this proposition indicates that the horizontal mixing reaches maximum at the suitable mixing conditions of the individual water mass as stated above. However the determination of k_1 should be possible only after the accumulation of many observed results and further discussions will be published later.

Literatures.

1) H. STOMMEL and A.B. ARONS: A mixing length theory of tidal flushing. *Trans. Amer. Geophys. Union.* 32, 1951.

2) Takashi ICHIYE: On the heat exchange between the bay waters and off-shore waters. *Mem. Kobe Mar. Obs.* Vol. VIII, 1950.

3) A. DEFANT: Reality and illusion in oceanographic survey. *Journ. Mar. Res.* IX, 2, 1950.

4) Report of the oceanographical observations on board R.M.S. "Syumpu Maru" in the western half of the Seto-Naikai in winters 1930, 1932, 1933. *Journ. Oceano.* Vol. IX, No. 3, 1936.

昭和28年3月11日印刷
昭和28年3月16日發行

編集兼發行人　中央氣象臺
東京都千代田區大手町一ノ七

印刷人　花崎實
東京都中央區新富町二ノ十九

印刷所　大東印刷工藝株式會社
東京都中央區新富町二ノ十九

With the Author's Compliments

A Short Note on Energy Transfer from Wind to Waves and Currents

T. ICHIYE

Reprinted from the *Oceanographical Magazine* Vol. 4 No. 3
December 1952

A Short Note on Energy Transfer from Wind to Waves and Currents

By

Takashi ICHIYE

(Kobe Marine Observatory)

§1. Wind waves and drift currents are generated both as results of energy transfer from the wind and heretofore the process of these two phenomena has been theoretically treated independently with each other. However the basic idea about the relation of these different phenomena seems to remain somewhat obscure. Recently K. YOSHIDA has published a schematical treaties on this problem and called the attention of oceanographers.[1] The author has been also interested in such proplem and here some remarks are proposed.

§2. First it is necessary to give a clear notion about the conditions for validity of the customary theories of the drift currents and waves. As for the former the most simple equation of motion are

$$\frac{\partial u}{\partial t}-\lambda v=\frac{\partial}{\partial z}\left(k\frac{\partial u}{\partial z}\right) \quad \text{etc.}$$

and for obtaining them from the basic equations of motion

$$\frac{\partial u}{\partial t}-\lambda v=\frac{\partial}{\partial x}\left(\frac{1}{\rho}p_{xx}-u^2\right)+\frac{\partial}{\partial y}\left(\frac{1}{\rho}p_{xy}-uv\right)+\frac{\partial}{\partial z}\left(\frac{1}{\rho}p_{xz}-uw\right) \quad \text{etc.}$$

it is necessary to assume that the current is homogeneous in horizontal directions and no slope of the surface exists, etc. or in other words we should adopt some averaging process and all the difficulties and obscurities arised from the surface conditions and internal movements of fluid are forced to be involved in the eddy viscosity K. However the friction term is

$$\frac{\partial}{\partial z}\left(K\frac{\partial u}{\partial z}\right)=\nu\frac{\partial^2 u}{\partial z^2}-\frac{\partial\overline{u'w'}}{\partial z}$$

in the exact expression, where ν is the molecular viscosity coefficient and u' and w' are turbulent velocity and energy balance between the turbulent velocity and mean current should be existent for validity of such relation in the friction terms, therefore the averaging time or space for obtaining the mean motion must be

sufficiently large compared with the scale of turbulent motion. When discussing the energy transfer at the surface, it is more convenient to use the vertically integrated energy equation

$$\frac{dE_c}{dt}=-\left(u\,\overline{u'w'}+v\,\overline{v'w'}\right)_0+\int_{-\infty}^{0}\left(\overline{u'w'}\frac{\partial u}{\partial z}+\overline{v'w'}\frac{\partial v}{\partial z}\right)dz\,,$$

where in the right hand side only the terms having relation to the surface condition are retained and all other terms due to the horizontal convection effect are considered to be involved in $\frac{d}{dt}$. The first term represent the energy transfer by the surface stress and form drag of the wind and the second integral means the dissipation of energy due to the internal turbulent motion. When the turbulence motion is expressed by $-\overline{u'w'}=K\frac{\partial u}{\partial z}$, the equation becomes

$$\frac{dE_c}{dt}=\left(Ku\frac{\partial u}{\partial z}-Kv\frac{\partial v}{\partial z}\right)_0-\int_{-\infty}^{0}K\left\{\left(\frac{\partial u}{\partial z}\right)^2+\left(\frac{\partial v}{\partial z}\right)^2\right\}dz$$

as usual equation of viscous fluid. Thus the energy transfered to the current from the wind is influenced by the condition of turbulence at the surface layer and at the development stage of the currents it is not always possible to put simply $-\overline{u'w'}=\tau$, where τ is the wind stress. In this respect we can show two simple examples, one of which is the case when the surface is suddenly set in motion with constant velocity, the other is the drift current caused by the constant stress given suddenly as treated by EKMAN.[2] In these cases the energy transfer at the surface is

$$\frac{{u_0}^2}{\sqrt{\pi t}}\sqrt{K}\sim\sqrt{K}\ \text{and}\ \sqrt{\frac{2}{\lambda K}}\tau^2\,C(\lambda t)\sim\frac{1}{\sqrt{K}}\,,$$

respectively, which illustrate that the energy transfer should be large when the turbulence is well developed in the former, whereas it is reverse in the latter, if the variation with time is not taken into account of.

As for waves, it is also necessary to consider the averaging process and the effect of viscosity for explanation of their growth. When we take only x and z component, then energy equation obtained from the fundamental equations of motion is

$$\frac{\partial E_{wk}}{\partial t}=\int_{-\infty}^{\zeta}\left\{u\frac{\partial}{\partial x}(p_{xx}-\rho u^2)+w\frac{\partial}{\partial z}(p_{zx}-\rho uw)-\rho gw-(p_{xx}-\rho uw)\frac{\partial u}{\partial z}\right.$$
$$\left.-(p_{zz}-\rho w^2)\frac{\partial w}{\partial z}\right\}dz+u\,(p_{zx}-\rho uw)\Big|_{z=\zeta}+w\,(p_{zz}-\rho w^2)\Big|_{z=\zeta}\,,$$

where ζ is the surface elevation from mean level, E_{wk} means kinetic energy, and when we consider only the problem of energy transfer at the surface, this equation can be put simply

$$\frac{dE_w}{dt} = u(p_{xz} - \rho uw) + w(p_{zz} - \rho w^2)\Big|_{z=\zeta},$$

where E_w is total energy of waves and all the processes about the energy transport in x direction are considered to be involved in the total differential d/dt. Further when we discuss the growth of waves, we must take the average of each quantity in the above equation over the distance of one wave length and assume

$$p_{xz} = 2\mu\left(\frac{\partial u}{\partial z} + \frac{\partial w}{\partial x}\right) = \tau \quad \text{and} \quad p_{zz} = -p + \mu\frac{\partial w}{\partial z} \fallingdotseq -p - \Delta p,$$

where Δp is the wind pressure against the different portion of the wave according to JEFFREYS and it is also necessary to introduce the mass transport of STOKES' finite amplitude wave as the surface velocity for the energy transfer to the wave by the tangential stress.[3)]

In short it is the property of the problem to take a statistical method for the discussion of energy transfer from the wind to waves and currents, since in the nature there is no wind having the constant speed and direction in regard to time and space, waves caused by the wind are also of various type and the drift currents are not uniform in any respect.

§ 3. In the present paper only the qualitative analysis of energy transfer is given by the energy spectrum of both waves and currents. First we put the energy distribution function of waves between the wave age β and $\beta+d\beta$ as $E(\beta, t)$, where the wave length L is given by $\frac{2\pi}{g}U^2\beta^2$. Then the variation of $E(\beta, t)$ is

$$\frac{\partial E}{\partial t} = R_T \pm R_N + R_{ta} - R_{tw}$$

where R_T, R_N is the energy transfer due to the tangential stress and normal pressure of the mean wind and R_{ta} means that given to various parts of the energy spectrum due to the turbulent fluctuations of the wind and R_{tw} is dissipation of wave energy to the turbulent motion of currents. Further $\frac{dE}{dt} = \frac{\partial F}{\partial t} + \frac{\partial F}{\partial \beta}\frac{d\beta}{dt}$ and for the significant wave $R_T \sim E\beta^{-3}$, $R_N \sim E(1-\beta)^2\beta^{-3}$ as given by SVERDRUP and MUNK.[3)] The functional form of R_{ta} and R_{tw} is unknown but if we can analyse the wind fluctuations and obtain the turbulent

energy spectrum of the wind about the period as $f(T)$ then it is rational to put $R_{ta} \sim f\left(U\beta \cdot \frac{2\pi}{g}\right)$ and since the breaking of the waves is the most important factor for the increase of turbulence in the currents, we can put $R_{tw} \sim F(\beta_0, t)$, where $\frac{1}{\pi}\sqrt{\frac{2g}{\rho}}\frac{F^{\frac{1}{2}}}{\beta^2 U^2} < \delta_c$ and δ_c is the critical wave steepnees at which the breaking of the most waves occurs. Generally the function $F(\beta, t)$ has maximum value at the wave age corresponding to the significant wave and since $\frac{d\beta}{dt} > 0$ in such wave region, the important part of the energy spectrum shifts to the larger wave length. Thus the stages of the growth of the waves seems to be separate in three stages, the first of which is the development of the first significant wave due to R_{ta} and the second stage is the increasement of the energy maximum at the range of the significant wave and its shifting to the region of the larger wave length and the last stage is the decrease of this maximum below the critical value due to R_{tw} as the results of wave breaking. Such processes are shown schematically in Fig. 1.

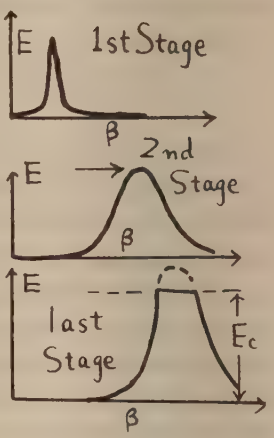

Fig. 1.

As for the drift current, it is more complicated to obtain the energy spectrum, since the definition of the drift currents itself is vague and obscure, but if we can define them as the region of larger wave length of the energy spectrum after the spectrum theory of turbulence, the variation of energy spectrum $F(k, t)$ is given by [4]

$$\frac{\partial F}{\partial t} = \int_0^k F^{\frac{1}{2}}\, kdk \int_k^\infty F \cdot kdk - \text{dissipation term}$$

where k means the wave number and the first term of this equation indicates the transfer of surface energy and its effect is to prevent the break up of the larger turbulent element into smaller one. In the early stage of development of drift currents or in the later stage of the growth of waves we can put

$$\int_k^\infty F \cdot kdk \sim R_{tw}$$

which shows that the turbulent energy of the surface layer is supplied by the wave action. The further discussions of the functional form of $F(k, t)$ are

impossible, since we have any knowledge about R_{tw} but if we can determine it by observations the general character of the solution of the above equation will be easily explained.

Literatures.

1) K. YOSHIDA: Dynamics on the Co-existent system of Waves and Currents in the Ocean. Part 1. *Journ. of Ocean. Soc. of Japan.* Vol. 7, No. 3-4, 1951.

2) V.W. EKMAN: *Arkiv för Mat. och Fysik.* 2, 1905.

3) H.U. SVERDRUP and W.H. MUNK: Wind, Sea and Swell. *H. O. Pub.* No. 601, 1947.

4) HEISENBERG: On the Theory of Statistical and Isotropic Turbulence. *Proc. Roy. Soc.* 1948.

昭和28年3月11日印刷
昭和28年3月16日發行

編集兼發行人 中央氣象臺
東京都千代田區大手町一ノ七

印刷人 花崎實
東京都中央區新富町二ノ十九

印刷所 大東印刷工藝株式會社
東京都中央區新富町二ノ十九

Some Remarks on the Non-linear Theory of Shallow Water Waves on a Sloping Beach

By

Takashi Ichiye

(Kobe Marine Observatory)

§1. Practical and theoretical researches on the non-linear theory of water waves have been much developed by American oceanographers[1] and mathematicians,[2] and important results have been obtained both in fundamental principles and practical applications. Here the author will add some considerations to the above works, especially for the case of variable depth, principally from the mathematical point of view. He does not intend to give a complete theory or a useful method for the forecasting of the breaker conditions, but only to show some complements to the theory.

§2. The equations of non-linear shallow water waves were deduced by K. O. Friedrichs[3] as the relations between the lowest-order terms of the perturbation equations for a motion of two-dimensions in the case of uniform depth (to be referred to as (F) hereafter in this paper). In this section we use his notations and the same process shall be applied to the waves on a uniformly sloping beach. When we put the bottom $y=\tan\theta\cdot x$, the condition at the bottom (A. 05) in (F) becomes

$$v=\tan\theta\cdot u \qquad \text{at} \qquad y=\tan\theta\cdot x, \tag{1}$$

and its dimensionless form corresponding to the eq. (A. 05) is

$$\bar{v}=\sqrt{\sigma}\tan\theta\cdot\bar{u} \qquad \text{at} \qquad \beta=\tan\theta\cdot\alpha/\sqrt{\sigma}\,. \tag{2}$$

Therefore, essential difficulties arise in the development of perturbation equations by the power series of σ, since the boundary condition contains $\sqrt{\sigma}$. It is necessary to take a different procedure for the order of slope $\tan\theta$. When $\tan\theta=k\sigma^{3/2+n}$ $(n\geq 0)$ and k is not far from 1, then the eq. (2) becomes

$$\bar{v}=k\sigma^{2+n}\bar{u} \qquad \text{at} \qquad \beta=k\sigma^{1+n}\alpha,$$

and since the lowest-order relation becomes

$$\bar{v}=0 \qquad \text{at} \qquad \beta=0,$$

the resultant equations are the same as in the case of uniform depth. When $\tan\theta=k\sigma^{1/2}$, the bottom condition is

$$\bar{v}=k\sigma\,\bar{u} \qquad \text{at} \qquad \beta=k\alpha,$$

and therefore the eq. (A. 28) in (F) is replaced by

$$\bar{v}^{(1)} = -(\beta - k\alpha)\bar{u}_\alpha^{(0)} + k\bar{u}^{(0)},$$

and (A. 29) is

$$\bar{v}^{(1)}(\alpha, Y^{(0)}, \tau) = -(Y^{(0)} - k\alpha)\bar{u}_\alpha^{(0)} + k\bar{u}^{(0)},$$

and (A. 31) is

$$Y_\tau^{(0)} + (Y^{(0)} \cdot \bar{u}^{(0)})_\alpha = k(\alpha \bar{u}_\alpha^{(0)} + \bar{u}^{(0)}).$$

Reintroducing the conventional variables, the eqs. (A. 33) are

$$\left.\begin{aligned} &\zeta_t + \{u(\zeta + h)\}_x = \tan\theta(xu_x + u) \\ &u_t + uu_x + g\zeta_x = -gh_x, \end{aligned}\right\} \tag{3}$$

where $h = h_0(1 - \tan\theta \cdot x)$ and ζ is the elevation from the mean level.

In the ordinary shallow water equations the right-hand side terms vanish. Further discussions about these equations shall be given later, and now we proceed to the case of $\tan\theta = k$. For such bottom slope we should expand all terms in powers of $\sigma^{1/2} = \lambda$ instead of σ, since the bottom condition becomes

$$\bar{v} = k\lambda\bar{u} \quad \text{at} \quad \alpha = \lambda\beta/k. \tag{4}$$

When we put $\bar{u} = \bar{u}^{(0)} + \lambda\bar{u}^{(1)} + \lambda^2\bar{u}^{(2)} + \cdots\cdots$ for example, all the relations deduced from the eqs. (A. 01) ~ (A. 04) in (F) are

$$\bar{v}_\beta^{(0)} = \bar{v}_\beta^{(1)} = 0, \quad \bar{v}_\beta^{(2)} = -\bar{u}_\alpha^{(0)}, \quad \bar{v}_\beta^{(3)} = -\bar{u}_\alpha^{(1)}, \cdots\cdots \tag{5}$$

$$\bar{u}_\beta^{(0)} = \bar{v}_\alpha^{(0)}, \quad \bar{u}_\beta^{(1)} = \bar{v}_\alpha^{(1)}, \quad \bar{u}_\beta^{(2)} = \bar{v}_\alpha^{(2)}, \cdots\cdots \tag{6}$$

$$\bar{v}^{(0)}\bar{u}_\beta^{(0)} = 0, \quad \bar{v}^{(1)}\bar{u}_\beta^{(0)} + \bar{v}^{(0)}u_\beta^{(1)} = 0,$$
$$\bar{u}_\tau^{(0)} + \bar{u}^{(0)}\bar{u}_\alpha^{(0)} + \pi_\alpha^{(0)} = \bar{v}^{(0)}\bar{v}_\beta^{(2)} + \bar{v}^{(1)}\bar{u}_\beta^{(1)} + \bar{v}^{(2)}\bar{u}_\beta^{(0)}, \tag{7}$$

$$\bar{v}^{(0)}\bar{v}_\beta^{(0)} = 0, \quad \bar{v}^{(0)}\bar{v}_\beta^{(1)} + \bar{v}^{(1)}\bar{v}_\beta^{(0)} = 0,$$
$$\bar{v}_\tau^{(0)} + \bar{u}^{(0)}\bar{v}_\alpha^{(0)} + \pi_\beta^{(0)} + 1 = \bar{v}^{(0)}\bar{v}_\beta^{(2)} + \bar{v}^{(1)}\bar{v}_\beta^{(1)} + \bar{v}^{(2)}\bar{v}_\beta^{(0)}, \tag{8}$$

and from the boundary conditions (4) (A. 06) and (A. 07) we get

$$\alpha = 0, \quad \bar{v}^{(0)} = 0, \quad \bar{v}^{(1)} = k\bar{u}^{(0)}, \quad \bar{v}^{(2)} = k\bar{u}^{(1)}, \tag{9}$$

$$\beta = Y^{(0)}, \quad \bar{v}^{(0)} = \bar{v}^{(1)} = 0, \quad \bar{v}^{(2)} = Y_\tau^{(0)} + \bar{u}^{(0)}Y_\alpha^{(0)}, \tag{10}$$

$$\beta = Y^{(0)}, \quad \pi^{(0)} = 0, \tag{11}$$

as the relations between the lowest-order terms.

From eqs. (5) and (10) we obtain

$$\bar{v}^{(0)} = \bar{v}^{(1)} = 0, \tag{12}$$

and thus the pressure obeys the hydrostatic law automatically at the first approximation as in the case of uniform depth, whereas the bottom condition (9) demands that

$$\bar{u}^{(0)} = 0 \quad \text{at} \quad \alpha = 0, \tag{13}$$

and further, from the second-order condition $\bar{v}^{(2)} = k\bar{u}^{(1)}$ at $\alpha = 0$ we obtain

$$\bar{u}_\alpha^{(0)} = 0 \quad \text{at} \quad \alpha = 0, \tag{14}$$

since $\overline{v}^{(2)}=-\beta\overline{u}_\alpha^{(0)}+f(\alpha)$ and $\overline{u}^{(1)}$ is merely the function of the eq. (6). Thus the resultant equations are

$$\overline{u}_\tau^{(0)}+\overline{u}^{(0)}\overline{u}_\alpha^{(0)}=-\pi_\alpha^{(0)}, \qquad Y_\tau^{(0)}+(\overline{u}^{(0)}Y^{(0)})_\alpha=k\overline{u}^{(1)}, \qquad \pi^{(0)}=Y^{(0)}-\beta$$

with the boundary conditions

$$\overline{u}^{(0)}=\overline{v}_\alpha^{(0)}=0 \qquad \text{at} \qquad \alpha=0,$$

and it is necessary to take further approximation for determining $\overline{u}^{(1)}$, whereas the boundary condition at $\alpha=0$ means that the reflection of waves should occur at $\alpha=0$. When $\tan\theta=k\sigma$, all the quantities should also be expanded in powers of λ, but in this case $\overline{v}^{(0)}=\overline{v}^{(1)}=\overline{v}^{(2)}=0$ for $\beta=0$, thus the same equations as in the case of uniform depth are obtained between the lowest-order terms. When $\tan\theta=k\sigma^{-1/2-n}$ $(n>0)$ the bottom condition becomes $\overline{v}=k\sigma^{-n}\overline{u}$ at $\alpha=\sigma^{1+n}\beta/k$ or $\overline{v}^{(0)}=0$ for $\alpha=0$, which indicates that the motion is of vertical type or the reflexion of waves occurs at $\alpha=0$ when the motion is of shallow water type.

Summarizing the above results, we can get the following criteria for the waves on a sloping beach:

(i) $\tan\theta\sim\sigma^{1/2+n}$ pure shallow water theory,

(ii) $\tan\theta\sim\sigma$,, (by expanding in powers of $\sigma^{1/2}$)

(iii) $\tan\theta\sim\sigma^{1/2}$ corrected shallow water theory,

(iv) $\tan\theta\sim1$,, (reflexion at $x=0$),

(v) $\tan\theta\sim\sigma^{-1/2-n}$ reflexion at $x=0$, or vertical motion.

If the initial waves are assumed to be of oscillating type, then the dimensionless number σ can be expressed by the amplitude A and wave length L of the initial waves and by the depth h at $x=0$ as $\sigma=\left(\frac{2\pi}{L}\right)^2Ah$. For example, when we take $L=20(m)$, $h=5(m)$, $A=1(m)$, the above criteria are

(i) $\theta\leq19.^\circ1$, (ii) $19.^\circ1\leq\theta\leq26.^\circ2$, (iii) $26.^\circ2\leq\theta\leq35.^\circ1$,

(iv) $35.^\circ1\leq\theta\leq55^\circ$, (v) $\theta\geq55^\circ$.

and when σ decreases corresponding to the decrease of initial wave steepness A/L and depth, the range of bottom slope for the validity of shallow water theory decreases, but the general convergency of the series in the expansion with λ or σ increases.

§3. In this section we discuss the approximative solution for the shallow water wave equations $u_t+uu_x=-g\zeta_x$, $\{u(h+\zeta)\}_x=-\zeta_t$. For the sake of convenience, we assume that the depth h_0 at $x<0$ is uniform and the linear shallow water waves such as $\zeta=A\cos\frac{2\pi}{L}(x-\sqrt{gh_0}\,t)$ proceed to the positive x-direction to the region $x<0$. In order to transform all quantities into dimensionless ones, we put

$$U=u/\sqrt{gh_0}, \quad \alpha=2\pi x/L, \quad \tau=2\pi\sqrt{gh_0}\,t/L, \quad Y=\zeta/h_0 \quad \text{and} \quad H=h/h_0,$$

then the fundamental equations become

$$U_\tau+UU_\alpha=-Y_\alpha, \qquad \{U(H+Y)\}_\alpha=-Y_\tau, \tag{1}$$

and the boundary conditions at $\alpha=0$ are $U=Y=p\cos\tau\,(p=A/h_0)$. The most elementary method for the approximative solution can be given by putting $U=\sum_{n=1}^{\infty}\alpha^n U_n$, $Y=\sum_{n=1}^{\infty}\alpha^n U_n$, $H=\sum_{n=1}^{\infty}\alpha^n H_n$ (where $H_0=1$ by definition), and determining U_{n+1}, Y_{n+1} successively by equating the coefficients of α^n. The general equations for U_{n+1}, Y_{n+1} are

$$\begin{aligned}
U_{n+1}(X_0-U_0^2) &= -(Y_n'/(n+1)+U_nX_1+U_{n-1}X_2+\cdots\cdots+U_1X_n \\
&\quad +U_0H_{n+1})+U_0(U_n'/(n+1)+U_1U_n+U_2U_{n-2}+\cdots\cdots), \\
Y_{n+1}(X_0-U_0^2) &= -X_0(U_n'/(n+1)+U_1U_n+\cdots\cdots) \\
&\quad +U_0(Y_n'/(n+1)+U_nX_1+\cdots\cdots+U_1X_n+U_0H_{n+1}),
\end{aligned} \tag{2}$$

where $X_n=Y_n+H_n$ and $Y_n'=\partial Y_n/\partial\tau$. Thus, if all terms $Y_0, Y_1\cdots\cdots Y_n$, $U_0, U_1\cdots\cdots$, U_n are known, Y_{n+1} and U_{n+1} can be determined from the above relations successively. However, the formal computations of the coefficients U_n, Y_n are so complicated even for the simplest boundary conditions given above, that only a general discussion about the convergence of the solution expressed by the power series of α and its physical meaning can be given here. First, when the depth is uniform and the non-linear terms are neglected, then

$$U_{n+1}=-\frac{Y_n'}{n+1}, \qquad Y_{n+1}=-\frac{U_n'}{n+1},$$

therefore the radius of convergence of power series in α of U and Y is infinite, since $|Y_n/Y_{n+1}|\sim|U_n/U_{n+1}|\sim(n+1)$, corresponding to the fact that the radius of convergence of the expansion of the exact solutions of $Y=p\cos(\alpha-\tau)$ and $U=p\cos(\alpha-\tau)$ in powers of α is infinite. Further, for a uniformly sloping beach $H=1-\alpha H_1$, $H_2=H_3=\cdots\cdots=0$ and $U_{n+1}=-\left(\frac{Y_n'}{n+1}-U_nH_1\right)$, $Y_{n+1}=-\frac{U_n'}{n+1}$, or $\lim|U_n/U_{n+1}|=1/H_1$, $\lim|Y_n/Y_{n+1}|\sim|U_n'/U_{n+1}'|\sim1/H_1$, thus the convergence radius becomes finite and is given by $1/H_1$, even if the non-linear terms are neglected, which also corresponds to the fact that the solutions of linear shallow water equations can be expressed by the combination of the 1st and 2nd kinds of Bessel functions, and the latter diverges at $\alpha=1/H_1$ as will be shown later. When we retain the non-linear terms, the radius of convergence may decrease further, corresponding to the breaking of the waves, since, for example, $X_0-U_0^2$ should necessarily vanish for some τ, and the radius of convergence of the solutions becomes zero, when $p\geq0.617$ for the boundary conditions given above, which shows that the waves whose amplitude is larger than 0.617 h_0 should inevitably break down.

Thus, it is reasonable to consider that the radius of convergence of the solutions expressed in power series of α gives the limit of the breaking of the

waves, since at this point U, Y, U_α and Y_α become infinite. If we retain only the initial term of non-linear property and assume a uniform slope, then the radius of convergence is

$$l(1+p\cos\tau-p^2\cos^2\tau), \tag{3}$$

where $l=1/H_1$ or the distance from $\alpha=0$ to the shore line. When we further retain the non-linear terms such as U_1 and Y_1, we have

$$U_{n+1}(X_0-U_0^2)\sim-\{U_n(Y_1-H_1)+U_1Y_n\}+U_0U_1U_n,$$
$$Y_{n+1}(X_0-U_0^2)\sim-X_0U_nU_1+U_0\{U_n(Y_1-H_1)+U_1Y_n\},$$

and the breaking point is given by

$$\mathrm{Min}\left\{\frac{|X_0-U_0^2|}{|U_0U_1-Y_1+H_1-U_1|},\ \frac{|X_0-U_0^2|}{|U_0U_1+(Y_1-H_1)U_0-X_0U_1|}\right\}, \tag{4}$$

where

$$U_1=\frac{p\sin\tau-p^2\cos\tau\sin\tau+H_1p\cos\tau}{1+p\cos\tau-p^2\cos^2\tau},$$

$$Y_1=\frac{p\sin\tau-H_1p^2\cos^2\tau}{1+p\cos\tau-p^2\cos^2\tau}.$$

For several values of p the numerical examples of breaking point given by the eqs. (3) and (4) are shown on the next table, where the equation (4) can be expressed approximately by

$$\mathrm{Min}\left\{\frac{1-p-p^2}{H_1(1+p^2)+2p+2p^2+p^3},\ \frac{1-p-p^2}{H_1p(2+p^2)+p^3}\right\}. \tag{4}'$$

Table 1.

p	0.1	0.2	0.3	0.4	0.5	0.6	
From (3)	0.89	0.76	0.61	0.44	0.25	0.04	$\times l$
From (4)′	0.420	0.218	0.119	0.062	0.027	0.003	$\times l\,(l=5)$
	0.276	0.128	0.067	0.034	0.014	0.002	$\times l\,(l=10)$
	4.02	1.56	0.76	0.37	0.15	0.02	$(l\sim\infty)$

The above results have no practical meaning and only explain that the breaking of the waves is caused by the non-linearity of fundamental equations which has also more effect on a sloping beach, owing to the increase of the amplitude.

The general criteria for the convergence of the solutions given by power series of α can be deduced from Cauchy's existence theorem of the differential equations. If we transform the initial equations (1) into the following forms:

$$\left.\begin{aligned} U_{\tau\tau}&=F(U,Y,U_\tau,Y_\tau)=(UU_\tau-Y_\tau-UH_\alpha)/(H+Y-U^2),\\ Y_\alpha&=G(U,Y,U_\tau,Y_\tau)=\{U(Y_\tau+UH_\alpha)-U_\tau(H+Y)\}/(H+Y-U^2),\end{aligned}\right\} \tag{5}$$

then F and G are regular for $|\alpha|<r$, $|U-p\cos\tau|<\rho$, $|Y-p\cos\tau|<\rho$, where $H_m>P+P^2$, $H_m=\mathrm{Min}(H)$ for $|\alpha|<r$ and $P=p+\rho$. Further, when we assume

that Y_τ and U_τ are of the same order as Y and U, which is possible by comparing the coefficients of U_n, Y_n as given by (2) with their derivatives about τ, U_n' and Y_n', then Cauchy's existence theorem shows, by considering the eqs, (5) as the system of ordinary differential equations of variable α, that the solutions of (5) satisfying the initial condition,

$$\text{at} \quad \alpha=0, \quad U=Y=p\cos\tau,$$

exist uniquely and they are regular for

$$|\alpha|<r(1-e^{-\rho/3Mr}), \tag{6}$$

or, in other words, the minimum of the radius of convergence of the expansions in powers of α of the solutions of (5) is given by the right-hand side of (6). Here, $M=\mathrm{Max}(F, G)$ for $|\alpha|<r$, $|U-p|<\rho$, $|Y-p|<\rho$. Thus, the breaking of waves does not occur in the region of α shown by the eq. (6), and it is reasonable to consider the breaking point is given by the value of r, for which the right-hand side of (6) becomes maximum, though practical determination of such r is not so simple. The limit of convergence of the solutions can be more extended, when we take the limit of existence theorem as $|\alpha'|<r'=\mathrm{Min}(r, \rho/M)$ and if we consider that the maximum value of r' as proportional to the distance of breaking point from $\alpha=0$, then the change of such distance with the initial value p is as follows:

for $p=0.1$, 0.2, 0.3, 0.4 ratio of $r'=0.275$, 0.128, 0.62, 0.26

for the uniform depth. M can generally be expressed by

$$M\sim\mathrm{Max}\left\{\frac{P^2+P+|H_\alpha|P}{H_m-P-P^2}, \frac{2P^2+P+|H_\alpha|P}{H_m-P-P^2}\right\}$$

and in the case of uniform depth r can take ∞ and $|H_\alpha|=0$, $H_m=1$, whereas in the case of sloping beach r should be taken as satisfying the condition $H_m>P+P^2$ and $\rho<\rho_0$, $M>M_0$ where ρ_0 and M_0 mean the values in the case of uniform depth; thus, it is concluded qualitatively that the breaking should occur at an earlier point on sloping beach than in uniform depth.

§4. Another successive approximation of the solutions of eqs. (1) in §3 for the boundary condition given there is obtained by expanding in powers of p such as

$$U=\sum_{n=0}^{\infty}U_np^n, \qquad Y=\sum_{n=0}^{\infty}Y_np^n, \tag{1}$$

where U_n and Y_n are the functions of variables α and τ satisfying the equations

$$\left.\begin{aligned} &U_{n,\tau}+Y_{n,\alpha}+U_0U_{n,\alpha}+U_nU_{0,\alpha}=-(U_1U_{(n-1),\alpha}+U_2U_{(n-2),\alpha}+\cdots\cdots+U_{n-1}U_{2,\alpha}),\\ &(U_nH+U_nU_0+U_0Y_n)_\alpha+Y_{n,\tau}=(U_1Y_{n-1}+U_2Y_{n-2}+\cdots\cdots+U_{n-1}Y_1)_\alpha \end{aligned}\right\} \tag{2}$$

under the boundary conditions $\alpha=0$, $U_1=Y_1=\cos\tau$, $U_n=Y_n=0$ $(n\neq1)$[4]. From

the boundary condition, immediately $U_0=Y_0=0$, and assuming the uniform slope $H=1-\alpha/a$, we have[5]

$$\left.\begin{aligned} U_1&=a\pi y^{-1/2}\{(Y_0^{(1)}J_0-J_0^{(1)}Y_0)\cos\tau+(Y_1^{(1)}J_0-J_1^{(1)}Y_0)\sin\tau\},\\ Z_1&=a\pi\{(J_1^{(1)}Y_0-Y_1^{(1)}J_0)\cos\tau-(J_0^{(1)}Y_0-Y_0^{(1)}J_0)\sin\tau\},\end{aligned}\right\} \tag{3}$$

where Z is taken instead of Y, and J, Y are the 1st and 2nd kinds of Bessel functions, the argument of which is, for examples,

$$J_0=J_0(2ay^{1/2}),\qquad J_0^{(1)}=J_0(2a),\qquad y=1-\alpha/a. \tag{4}$$

The second approximation is obtained from the solutions of the equations

$$\left.\begin{aligned} (HZ_{,\alpha})_\alpha+4Z_2&=\left(3iU_1Z_1-\frac{1}{a}U_1^2\right)_\alpha,\\ iU_2&=-\left(Z_2+\frac{1}{2}U_1^2\right)_\alpha\end{aligned}\right\} \tag{5}$$

by taking the real part, where the boundary condition becomes $U_2=Z_2=0$ at $\alpha=0$.

The expressions for U_2 and Z_2 are much complicated and here the explicit form of Z_2 only is given

$$\begin{aligned} Z_2=&3\pi\{J_0^{(2)}Y_0(2Z)-Y_0^{(2)}J_0(2Z)\}\cos 2\tau\\ &+5a\pi\{J_0^{(2)}Y_0(2Z)-Y_0^{(2)}J_0(2Z)\}\sin 2\tau\\ &+(a\pi)^3\left\{J_0(2Z)\int_{4a}^{2Z}Y_1(2w)P(w)\,dw-Y_0(2Z)\int_1^{2Z}J_1(2w)P(w)\,dw\right\}\cos 2\tau\\ &+(a\pi)^3\left\{J_0(2Z)\int_{4a}^{2Z}Y_1(2w)Q(w)\,dw-Y_0(2Z)\int_1^{2Z}J_1(2w)Q(w)\,dw\right\}\sin 2\tau,\end{aligned} \tag{6}$$

where $Z=4ay^{1/2}$, $J_0^{(2)}=J_0(4a)$,

$$\begin{aligned} P(w)=&\{(Y_1^{(1)})^2-(Y_0^{(1)})^2\}\left\{J_1^2(w)-\frac{6a}{w}J_1(w)J_0(w)\right\}\\ &+\{(J_1^{(1)})^2-(J_0^{(1)})^2\}\left\{Y_1^2(w)-\frac{6a}{w}Y_1(w)Y_0(w)\right\}\\ &+(Y_0^{(1)}J_0^{(1)}-Y_1^{(1)}J_1^{(1)})\left\{2J_1(w)Y_1(w)-\frac{6a}{w}J_1(w)Y_0(w)-\frac{6a}{w}Y_1(w)J_0(w)\right\},\\ Q(w)=&-2Y_1^{(1)}Y_0^{(1)}\left\{J_1^2(w)-\frac{6a}{w}J_1(w)J_0(w)\right\}\\ &-2J_0^{(1)}J_1^{(1)}\left\{Y_1^2(w)-\frac{6a}{w}Y_1(w)Y_0(w)\right\}\\ &+(Y_1^{(1)}J_1^{(1)}+Y_0^{(1)}J_0^{(1)})\left\{2J_1(w)Y_1(w)-\frac{6a}{w}J_1(w)Y_0(w)-\frac{6a}{w}Y_1(w)J_0(w)\right\}.\end{aligned}$$

The numerical computation of this solution is quite difficult in the general case and here we assume that $a\gg 1$ for the case of a gentle slope, and further, if we

take the assymptotic expansion of Bessel functions and retain only the term proportional to $(ay^{1/2})^{-1/2}$, then $Z_1 \sim y^{-1/4}$. From physical consideration, $|Z| < H(=y)$, where $|Z|$ means the amplitude of the elevation. Thus, it is reasonable to consider that the breaking point of the solution (1) is given by the value of α, where $Z=H$. The positions of the breaking point α_b determined by such method are shown on Table 2, where α_b is expressed with the fraction of a (or l in § 3) for different p's for the cases of the 1st and 2nd approximations shown by eqs. (3) and (6).

Table 2.

p	0.1	0.2	0.3	0.4	0.5	
1st Appr. (3)	0.842	0.724	0.618	0.520	0.426	$(\times a)$
2nd Appr. (6)	0.812	0.648	0.500	0.386	0.309	$(\times a)$ $(a=10)$

As seen from the table, the breaking distance (α_b) decreases as the degree of the approximation increases. Further, comparing it with the result shown on Table 2, we can see that the present method of approximation gives larger values of α_b than those shown in § 3, though it is unsatisfactory to discuss the details from only the 2nd approximation.

(To be continued)

Literatures.

(1) MUNK, W. H.: The solitary wave theory and its applications to surf problems. *Ann. N.Y. Acad. Sci.* 51, 1949.

(2) STOKER, J. J.: On the formation of breakers and bores. *Comm. Appl. Math.* 1, 1948.

(3) FRIEDRICHS, K. O.: On the derivation of the shallow water theory. Appendix to (2).

(4) $U_0=Y_0=0$ means that there is no stationary current, nor stationary elevation corresponding to the initially travelling waves. In this respect, Mr. M. MIYAZAKI (Oceano. Mag. Vol. 3, No. 2 and Vol. 4, No. 1, 1952) has made a mistake, since his equations (3·1) are the same as the present ones of the zero-th order by putting $U_{0,\tau}=Y_{0,\tau}=0$, $\left(\frac{1}{2}U_0^2\right)_\alpha=-Y_{0,\alpha}$, $(U_0H)_\alpha=0$. The solutions of them are simply given by $\frac{1}{2}U_0^2+Y_0=\text{const}$, $U_0H=\text{const}$, and if $U_0=Y_0=0$, at $\alpha=0$ or any point, U_0 and Y_0 always vanish. Though U_0 and Y_0 can be determined from the above relations when $U_0\neq 0$, $Y_0\neq 0$ and $\alpha=0$, it is out of the problem of the wave motion, and therefore, the breaking point or other wave characteristics should not be determined from the conditions of U_0 and Y_0, since the point where U_0 or Y_0 has a large value indicates only the singular point accompanying with the incomplete dynamical equations for stationary flow. Thus, his subsequent argument seem to be inadequate.

(5) The first and second approximations for the waves on a uniformly sloping beach are given by Mr. T. HIRONO (Geophys. Mag. Vol. XIV No. 1, 1946), but the boundary value problem and the solutions, which we treat in this paper, are different from his results.

Tidal Variations of Oceanographical Elements

By

Masamori MIYAZAKI

(Kobe Marine Observatory)

Introduction.

In general, various waters of various origin co-exist near the coast. Roughly speaking, the temperature, chlorinity, and other characteristic elements are invariable for each part of water areas, while, in their boundary regions, we often observe large, conservative gradients of these quantities.

If the periodic flow intersects the isometric lines of such a field, these isometric lines will oscillate with the same period. Therefore, under such circumstances there will be seen in the tidal currents the tidal variations of these quantities, which are, of course, significant and of larger amplitude in the boundary regions.

In the present days we have but few investigations on these tidal variations. SAITO (1952) clarified the theoretical distribution of the tidal salinity variation for a special case. PROUDMAN (1938) carried out the tidal analysis of the water temperature observations made at several stations in the Irish Sea. These results are of course very important, but too small to know the general features of the tidal variation.

In this paper the author intends to propose simple models of the tidal variation in a boundary region of two different water masses, and to compare the results with the actual observations. We may find from these results some of the most elementary features of the tidal variation.

Theory.

Let us now consider the tidal variation in a boundary region, where two different water masses meet and mix with each other. In this region the quantities are supposed to be variable only along a horizontal coordinate x. The diffusion equation in this case will become

$$\frac{\partial \theta}{\partial t} + u\frac{\partial \theta}{\partial x} = \mu\frac{\partial^2 \theta}{\partial x^2}, \tag{1}$$

where the tidal current u is assumed to vary in the form of $u_0 \cos \sigma t$, and other

notations for it are customary.

For the sake of simplification, we take that $\theta_{x=-r}$ and $\theta_{x=r}$ are constants and equal to the proper values of two water masses θ_1 and θ_2, respectively. Then, the boundary conditions for the intermediate region are

$$\left.\begin{aligned} &\theta=\theta_1 \quad \text{at} \quad x=-r, \\ \text{and} \quad &\theta=\theta_2 \quad \text{at} \quad x=r. \end{aligned}\right\} \quad (\theta_2>\theta_1) \tag{2}$$

Next, instead of the initial condition, we assume that the periodic variation is conserved and its fundamental period is $2\pi/\sigma$.

If we transform the coordinates (t, x) to (t', x') by using the relations

$$t'=t \quad \text{and} \quad x'=x-\int u dt=x-\frac{u_0}{\sigma}\sin\sigma t,$$

the equation (1) will become

$$\frac{\partial\theta}{\partial t'}=\mu\frac{\partial^2\theta}{\partial x'^2}. \tag{3}$$

Therefore, the tidal variation will be given by*

$$\left.\begin{aligned} \theta=&A+B\left(x-\frac{u_0}{\sigma}\sin\sigma t\right)+ \\ &+\sum_{n=1}^{\infty}\Big[\exp.\left(\alpha_n x-\frac{\alpha_n u_0}{\sigma}\sin\sigma t\right)\left\{C_n\cos\left(n\sigma t+\alpha_n x-\frac{\alpha_n u_0}{\sigma}\sin\sigma t\right)+\right. \\ &\left.+D_n\sin\left(n\sigma t+\alpha_n x-\frac{\alpha_n u_0}{\sigma}\sin\sigma t\right)\right\}+ \\ &+\exp.\left(-\alpha_n x+\frac{\alpha_n u_0}{\sigma}\sin\sigma t\right)\left\{E_n\cos\left(n\sigma t-\alpha_n x+\frac{\alpha_n u_0}{\sigma}\sin\sigma t\right)+\right. \\ &\left.+F_n\sin\left(n\sigma t-\alpha_n x+\frac{\alpha_n u_0}{\sigma}\sin\sigma t\right)\right\}\Big], \end{aligned}\right\} \tag{4}$$

where $\alpha_n=\sqrt{\frac{n\sigma}{2\mu}}$, and A, B, C_n, D_n, E_n and F_n are all integral constants.

In order to determine the integral constants, we rewrite the expression (4) in the Fourier series of the form

$$\theta=\sum_{n=0}^{\infty}\{a_n(x)\cos n\sigma t+b_{n+1}(x)\sin(n+1)\sigma t\}, \tag{5}$$

by taking the relation

$$\left.\begin{aligned} \exp.\{\pm(i)^{1/2}Z\sin\delta\}=\sum_{k=0}^{\infty}(-1)^k\{&(\mathrm{ber}_{2k}Z+i\,\mathrm{bei}_{2k}Z)\cos 2kZ\pm \\ &\pm 2(\mathrm{ber}_{2k+1}Z+i\,\mathrm{bei}_{k+1}Z)\sin(2k+1)Z\} \end{aligned}\right\} \tag{6}$$

into account. Then, the boundary conditions (2) become

* An analogous general solution was already given by McEwen (1919).

$$\left.\begin{aligned} &a_0(-r)=\theta_1, \quad a_0(r)=\theta_2, \\ \text{and}\quad &a_n(-r)=b_n(-r)=a_n(r)=b_n(r)=0. \end{aligned}\right\} \quad (n=1,\ 2,\ 3,\ \ldots\ldots) \tag{7}$$

Therefore, the integral constants are determined as the roots of infinite simultaneous equations (7). In the process of practical approximate calculations, we shall only retain the finite low-order terms and neglect the higher order terms corresponding to n, $k \geqq N$ (N being a positive integer).

When we take $N=2$, (7) become

$$\left.\begin{aligned}
&A-Br-\mathrm{ber}_1\beta\,(Ce^{-\alpha r}\sin\alpha r+Ee^{\alpha r}\sin\alpha r+De^{-\alpha r}\cos\alpha r-Fe^{\alpha r}\cos\alpha r)+\\
&\quad+\mathrm{bei}_1\beta\,(Ce^{-\alpha r}\cos\alpha r-Ee^{\alpha r}\cos\alpha r-De^{-\alpha r}\sin\alpha r-Fe^{\alpha r}\sin\alpha r)=\theta_1,\\
&A+Br+\mathrm{ber}_1\beta\,(Ce^{\alpha r}\sin\alpha r+Ee^{-\alpha r}\sin\alpha r-De^{\alpha r}\cos\alpha r+Fe^{-\alpha r}\cos\alpha r)+\\
&\quad+\mathrm{bei}_1\beta\,(Ce^{\alpha r}\cos\alpha r-Ee^{-\alpha r}\cos\alpha r+De^{\alpha r}\sin\alpha r+Fe^{-\alpha r}\sin\alpha r)=\theta_2,\\
&\left(\mathrm{ber}_0\beta-\frac{\mathrm{ber}_2\beta}{2}\right)(Ce^{-\alpha r}\cos\alpha r+Ee^{\alpha r}\cos\alpha r-De^{-\alpha r}\sin\alpha r+Fe^{\alpha r}\sin\alpha r)+\\
&\quad+\left(\mathrm{bei}_0\beta-\frac{\mathrm{bei}_2\beta}{2}\right)(Ce^{-\alpha r}\sin\alpha r-Ee^{\alpha r}\sin\alpha r+De^{-\alpha r}\cos\alpha r+Fe^{\alpha r}\cos\alpha r)=0,\\
&\left(\mathrm{ber}_0\beta-\frac{\mathrm{ber}_2\beta}{2}\right)(Ce^{\alpha r}\cos\alpha r+Ee^{-\alpha r}\cos\alpha r+De^{\alpha r}\sin\alpha r-Fe^{-\alpha r}\sin\alpha r)-\\
&\quad-\left(\mathrm{bei}_0\beta-\frac{\mathrm{bei}_2\beta}{2}\right)(Ce^{\alpha r}\sin\alpha r-Ee^{-\alpha r}\sin\alpha r-De^{\alpha r}\cos\alpha r-Fe^{-\alpha r}\cos\alpha r)=0,\\
&-\frac{Bu_0}{\sigma}+\left(\mathrm{ber}_0\beta+\frac{\mathrm{ber}_2\beta}{2}\right)(Ce^{-\alpha r}\sin\alpha r-Ee^{\alpha r}\sin\alpha r+De^{-\alpha r}\cos\alpha r+Fe^{\alpha r}\cos\alpha r)-\\
&\quad-\left(\mathrm{bei}_0\beta+\frac{\mathrm{bei}_2\beta}{2}\right)(Ce^{-\alpha r}\cos\alpha r+Ee^{\alpha r}\cos\alpha r-De^{-\alpha r}\sin\alpha r+Fe^{\alpha r}\sin\alpha r)=0,\\
&-\frac{Bu_0}{\sigma}-\left(\mathrm{ber}_0\beta+\frac{\mathrm{ber}_2\beta}{2}\right)(Ce^{\alpha r}\sin\alpha r-Ee^{-\alpha r}\sin\alpha r-De^{\alpha r}\cos\alpha r-Fe^{-\alpha r}\cos\alpha r)-\\
&\quad-\left(\mathrm{bei}_0\beta+\frac{\mathrm{bei}_2\beta}{2}\right)(Ce^{\alpha r}\cos\alpha r+Ee^{-\alpha r}\cos\alpha r+De^{\alpha r}\sin\alpha r-Fe^{-\alpha r}\sin\alpha r)=0,
\end{aligned}\right\} \tag{8}$$

where $\beta=\sqrt{\dfrac{u_0}{\sigma\mu}}$ and the suffix 1 is omitted from C_1, D_1, E_1, F_1 and α_1. Solving (8), we easily obtain

$$\left.\begin{aligned}
&A=(\theta_1+\theta_2)/2\\
&B=I(\theta_2-\theta_1)/2\Big[rI-\sinh 2\alpha r\left\{\left(\mathrm{ber}_0\beta-\frac{\mathrm{ber}_2\beta}{2}\right)\mathrm{ber}_1\beta+\left(\mathrm{bei}_0\beta-\frac{\mathrm{bei}_2\beta}{2}\right)\mathrm{bei}_1\beta\right\}-\\
&\qquad-\sin 2\alpha r\left\{\left(\mathrm{ber}_0\beta-\frac{\mathrm{ber}_2\beta}{2}\right)\mathrm{bei}_1\beta+\left(\mathrm{bei}_0\beta-\frac{\mathrm{bei}_2\beta}{2}\right)\mathrm{ber}_1\beta\right\}\Big],\\
&C=E=-B\left\{\left(\mathrm{ber}_0\beta-\frac{\mathrm{ber}_2\beta}{2}\right)\sin\alpha r\sinh\alpha r+\left(\mathrm{bei}_0\beta-\frac{\mathrm{bei}_2\beta}{2}\right)\cos\alpha r\cosh\alpha r\right\}/I,\\
&D=F=-B\left\{\left(\mathrm{bei}_0\beta-\frac{\mathrm{bei}_2\beta}{2}\right)\sin\alpha r\sinh\alpha r-\left(\mathrm{ber}_0\beta-\frac{\mathrm{ber}_2\beta}{2}\right)\cos\alpha r\cosh\alpha r\right\}/I,
\end{aligned}\right\} \tag{9}$$

where $I=\frac{2\sigma}{u_0}(\cos^2\alpha r-\cosh^2\alpha r-1)\left(\mathrm{ber}_0{}^2\beta+\mathrm{bei}_0{}^2\beta-\frac{\mathrm{ber}_2{}^2\beta}{4}-\frac{\mathrm{bei}_2{}^2\beta}{4}\right)$. The final solution will be, in the first approximation, given by the substitution of (9) into (4).

Theoretical patterns of the tidal variation in several cases.

If the numerical values of αr and β are given, those of the integral constants can be easily calculated from (9). Therefore, the harmonic constants of the tidal variation a_0, a_1 and b_1 will be determined for every point of the boundary region.

Figs. 1~3 represent the space variations of the time mean value a_0, the amplitude of the tidal variation $\Theta=\sqrt{a_1{}^2+b_1{}^2}$, and its phase lag $\varepsilon=\mathrm{tg}^{-1}\frac{b_1}{a_1}$, where we take $\alpha r=\pi$. Fig. 1 shows that a_0 varies more slowly in the inner region, which is of course the effect of the inertia term. This feature is somewhat strengthened by the increase of β. Θ and ε (Fig. 2 and 3) decrease symmetrically and with the increasing rate on both sides of $x=0$. At $x=0$, Θ attains its

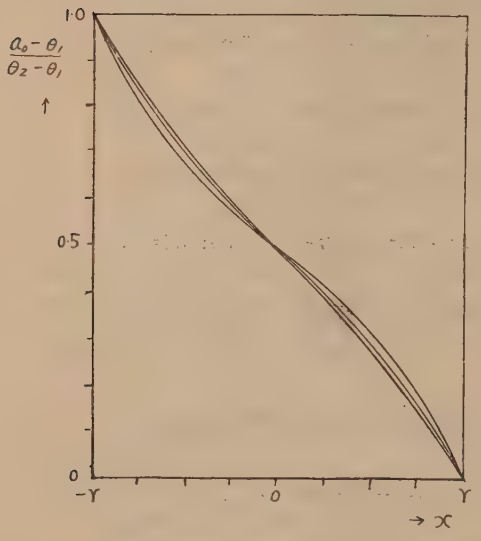

Fig. 1. Space distributions of a_0 for $\alpha r=\pi$.

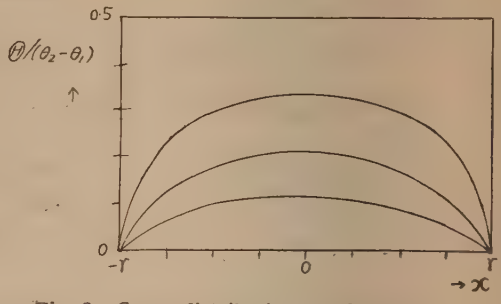

Fig. 2. Space distributions of Θ for $\alpha r=\pi$.

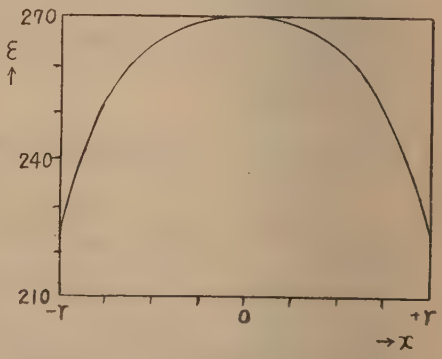

Fig. 3. Space distributions of ε for $\alpha r=\pi$.

maximum value which is nearly proportional to β, while ε is a constant and equals to $3\pi/2$. At $x=\pm r$, Θ vanishes, and ε tends to about $5\pi/4$. The qualitative characteristics of these conclusions will be also applicable to other αr-values.

The variations of the maximum amplitude Θ_m and the corresponding phase lag ε_m at the center $x=0$ are illustrated in Figs. 4 and 5. Accordingly, as the

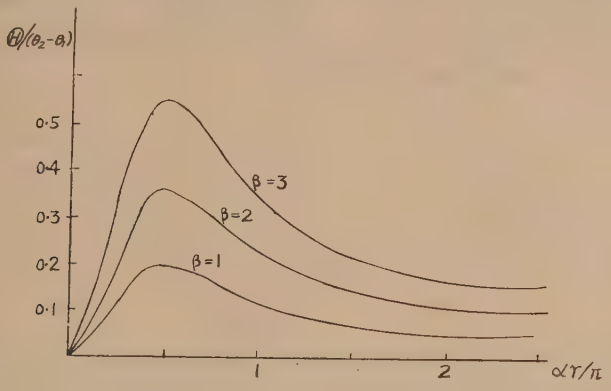

Fig. 4 Variations of the maximum amplitude Θ_m.

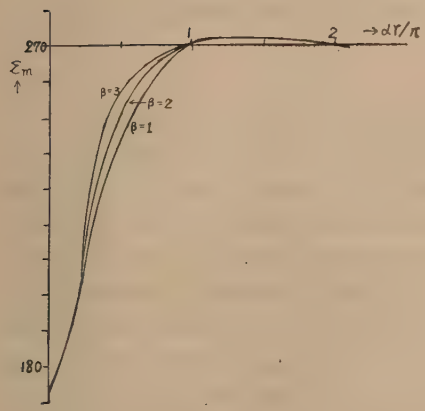

Fig. 5. Variations of the phase ε_m corresponding to Θ_m.

parameter αr increases, Θ_m first increases from zero, reachs a maximum at about $\alpha r=\pi/2$, and then gradually decreases. With respect to β, the variations are nearly proportional. Θ_m slightly exceeds the value $(\theta_2-\theta_1)/2$ in the neighbourhood of $\alpha r=\pi/2$ when β is larger than about 2.8. Then, for a small part of a periodic cycle, θ does not fall in the interval of θ_1 and θ_2. This incompletion will be modified by the higher approximation of the solution.

ε_m is nearly equal to π at $\alpha r=0$, and for small αr-values rapidly increases with αr. The rate of increase gradually decreases near $\alpha r=\pi$, and when $\alpha r>\pi$, ε_m is nearly a constant and equals to about $3\pi/2$.

In the above sentences, we have used the non-dimensional parameters dr and β instead of the dimensional parameters r and u_0. Therefore, it will be necessary to obtain the mutual relations of these quantities.

Now, when we take, for instance,

$$\left.\begin{aligned} &\sigma = 1.4052\times10^{-4} \text{ sec} \quad \text{(frequency of } M_2 \text{ tide)}, \\ \text{and} \quad &\mu = (2r)^{4/3}\times10^{-2} \text{ c.g.s.} \quad \text{(cf. INOUE, 1951)}, \end{aligned}\right\} \tag{10}$$

r varies a $(\alpha r)^3$, and u_0 as $\beta(\alpha r)^2$. Corresponding values are shown in Figs. 6 and 7. These figures denote that the practical interest will be concentrated to the right-hand sides of Figs. 4 and 5, where θ_m gradually decreases with αr, and θ varies in the neighbourhood of $3\pi/2$.

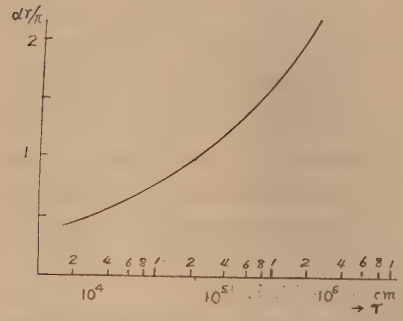

Fig. 6. Relation between αr and r.

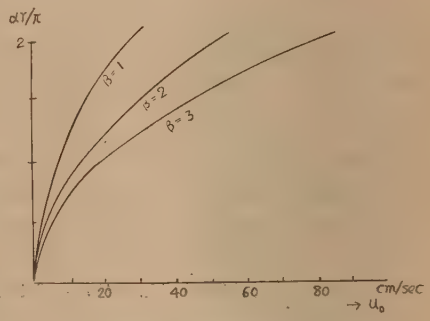

Fig. 7. Relation among u_0, αr, and β.

Comparison with the observations.

In this paragraph, we shall compare our theoretical patterns of the tidal variation with the actual observations. Unfortunately, at least until now, the number of available data is very small, since it has been difficult to obtain continuous and simultaneous observations of the tidal current and diffusible quantities. Two sets of observations are quoted here from these data.

Fig. 8 represents the variations of the water temperature, chlorinity and tidal currents at the center of the Misaki Strait during 28~29th August 1947 (MIYAKE, 1948). It seems that two different water masses exist to the east and west of the strait, which are originated in Tokyo Bay and Sagami Bay, respectively. Fig. 8 evidently shows that the water temperature (chlorinity) of the eastern water mass is higher (lower) than that of the western. By the aid of the $T-Cl$ diagram, we can presume that

$$T=25.8°, \quad Cl=18.20\,‰,$$

and

$$=24.6°, \quad =18.80\,‰,$$

for each of the water masses. Of course, the effects of the diurnal variation are deducted from the latter values.

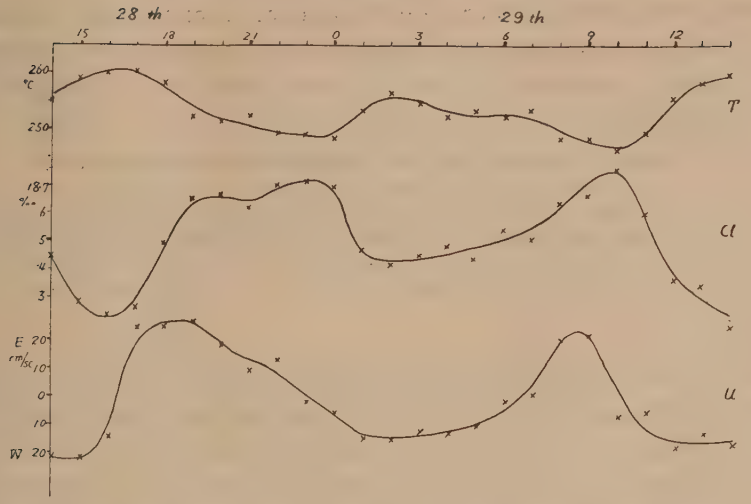

Fig. 8. Diurnal variations of the water temperature and the chlorinity at the depth 2 m, and the surface tidal current (Misaki, Strait, observed by Miyake on August, 1947).

Now, the semi-diurnal components of tidal variations (of 12.5-hour period) are:

	Amplitude	Phase (counted from the upper transit of the moon)
T	0.41 °	169°
Cl	0.181 ‰	343
u	16.2 cm/sec	283

where u is taken positive in the direction to the east. Therefore, on the average, we obtain

$$\Theta/(\theta_2-\theta_1)=0.30 \quad \text{and} \quad \varepsilon/\sigma=8.4 \text{ (hour)}.$$

These values are considered to represent the maximum amplitude and the corresponding phase, since the variations of these quantities are very little near the center. Then from u_0 and $\Theta_m/(\theta_2-\theta_1)$, we obtain

$$\varepsilon_m/\sigma=9.3 \text{ (hour)} \quad \text{and} \quad r=1.95 \text{ km}$$

by using Figs. 4~7.

For all limitations of theory and observation, the former value is in good agreement with the prior result of harmonic analysis. The latter value will be also regarded to be agreeable, since the length of the above-mentioned strait is about 2.5 km.

Other data, more inclusive, were obtained by PROUDMAN (1938). He analysed the results of the surface water temperature observations made on board the light-vessels (to be abbreviated as L.V.) in the Irish Sea, and calculated the phases and amplitudes of M_2 and MSf constituents for every month.

Table 1. M_2 constituents of the water temperature variations at the Morecambe Bay L.V. (Proudman, 1938).

	Jan.	Feb.	Mar.	Apr.	May	June	July	Aug.	Sept.	Oct.	Nov.	Dec.
Amplitude H in °C	0.11	0.22	0.18	0.42	—	—	—	0.31	0.22	0.18	0.22	0.16
Phase-lag g in deg.	89	340	48	44	—	—	—	191	24	350	6	349

Now, in the eastern part of the Irish Sea, the water temperature gradually varies from the west coast of England to the Isle of Man. It increases towards the land in summer, and towards the sea in winter. There is likely to exist two different water masses, the coastal water and the offsea water originated in the middle of the Sea. The temperature differences between these two water masses are, on the monthly average,

February	August	November	
3.0	−2.8	3.5	C°

for the southern half of this area (PROUDMAN, LEWIS and DENNIS, 1937).

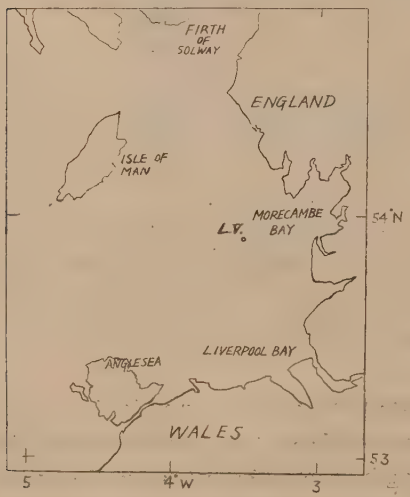

Fig. 9. Eastern part of the Irish Sea.

Fortunately, the monthy mean isotherms are nearly parallel to the eastern coast, and the tidal current runs almost perpendicularly to them. The time of turn and the maximum speed in spring are also constant, roughly speaking. Therefore, the underlying conditions of our theory are approximately satisfied in this region.

For instance, at the Morecambe Bay L.V. (see Fig. 9), the tidal current runs to ESE or to WNW, and the amplitude and phase of its M_2 constituent are estimated to be 1.5 knots and 272°, where the axis is taken positive to ESE.

By using these results, we have

	February	August	November
$\theta/(\theta_2-\theta_1)$	0.073	0.111	0.063
ε/σ (hour)	8.5	9.6	9.4

at the Morecambe Bay L.V. Combining the first row of this table and the value $u_0=1.5$ knots, we finally obtain

	February	August	November	
ε/σ	9.2	9.0	9.2	(hour)
r	71	49	79	(km)

where we take that the L.V. is 31 km distant from the coast.

The first row of this table is nearly equal to the former results of harmonic analysis, and the errors are within 0.7 hours. The second row also shows agreeable values, since the distance $2r$ is supposed to be of the order of 120 km —the distance between the Anglesea—Man line and the west coast of England. It seems that the distance is somewhat smaller in summer, but we cannot ascertain its significance from the above values. In spring, the temperature difference between two water masses is too small to conserve significant tidal variations.

Summary.

1) The tidal variations of the oceanographic elements will take place in the boundary regions of different water masses. A theory is proposed in this paper in order to explain the variations of their phases and amplitudes. Here, the quantities are supposed to be variable only along a horizontal direction, and invariable outside a finite range $-r\leq x\leq r$.

2) According to our theory, the amplitude and the phase lag of the tidal variation are largest at the center $x=0$, and gradually decreases on its both sides.

3) These elements also vary with the length of the boundary region and with the amplitude of tidal currents, as shown in Figs. 4~7. When the distance r is sufficiently large, the phase lag is nearly equal to $3\pi/2$, and the amplitude slightly decreases with r.

4) Our theoretical patterns are compared with two data of observation, i.e.,

(i) With the 24-hourly observations of oceanographic elements at a fixed station in the Misaki Strait, which were made on April 1947 by Dr. Miyake and his staff, and

(ii) With the M_2-variations of the surface water temperature at the Morecambe Bay Light-Vessel in the Irish Sea, which are analysed by PROUDMAN.

The agreement between theory and observation is fair.

Acknowledgements.

The author wishes to express his hearty thanks to Dr. Masito NAKANO, who kindly read this paper before printing. The author also expresses his hearty thanks to Dr. Yasuo MIYAKE, who kindly lent him his precious data.

References.

1) MCEWEN, G. F.: Ocean temperatures, their relation to solar radiation, and oceanic circulation. *Semicent. Publ., Univ. Calif.*, 1919.
2) MIYAKE, Y.: The diurnal variation of dissolved oxygen in sea water consisting of different water masses. *Geophys. Mag.*, 16, 66—70, 1948.
3) PROUDMAN, J.: On tidal variations of temperature in the Irish Sea, *M. N. R. S. A. Geophys. Suppl.* 4, 373—386, 1938.
4) PROUDMAN, J., H. M. LEWIS, and A. L. DENNIS: On the temperature of the surface waters of the Irish Sea. *Phil. Trans.* A 236, 261—302, 1937.
5) SAITO, Yasukazu: On the diffusion of salinity in a horizontal current field, *Jour. Tokyo Univ. Fish.*, 38, 351—361, 1952.

Wiht the Author's Compliments

On the Variation of Oceanic Circulation. (IV)

By

Takashi ICHIYE

Reprinted from the *Oceanographical Magazine* Vol. 5, No. 1.

June 1953

On the Variation of Oceanic Circulation. (IV)

By Takashi ICHIYE

Kobe Marine Observatory

§ 1. The ocean current has been considered to show short-period fluctuations as well as the other geophysical phenomena do, but until now it has been not so easy to obtain oceanographical data at short intervals, and the observed facts about this problem are quite poor. In 1950, the daily oceanographical conditions of the Gulf Stream were observed, and the meandering of the current and the change of isolated water mass discharged from the main stream were discovered[1]. Unfortunately such observations have not been carried out in the Kuroshio region and the detailed discussions about short-period fluctuations are impossible. However, oceanographical observations have been continued usually twice a month along the "C" line (extending from 38°N, 142°E to 38°N, 150°E) since 1947 and sometimes quite an abrupt change of water temperature has been observed in such successive observations. In this paper some examples are shown and the mechanism of short-period variation of the ocean current is explained.

§ 2. The examples are almost all limited to the winter season, since in this season the horizontal gradients of the water temperature and chlorinity are largest off the Sanriku district, owing to the penetration of the Oyashio from north, and the slight change of the current has large effects on the distributions of oceanographical elements.

The three examples of such fluctuations are found and they are discussed individually in the following. For simplification, these observations are indicated as follows: IA (Dec. 10～12, 1949), IB (Dec. 24, 1949), IIA (Feb. 4～5, 1950), IIB (Feb. 18～20, 1950), IIIA (Dec. 10～12, 1950), IIIB (Dec. 23～25, 1950). In fig. 1 temperature and chlorinity distributions in each case are shown and in fig. 2 the difference between these values of two successive observations (B—A) are indicated. In IA a water mass with highest temperatures above 20°C was found between 144°E and 145°E in the layer more than 100 m deep, the chlorinities of which are also higher than $19.1^0/_{00}$ and this water mass separates the colder and less haline water of the Oyashio type, and near 143°E the cold water with tem-

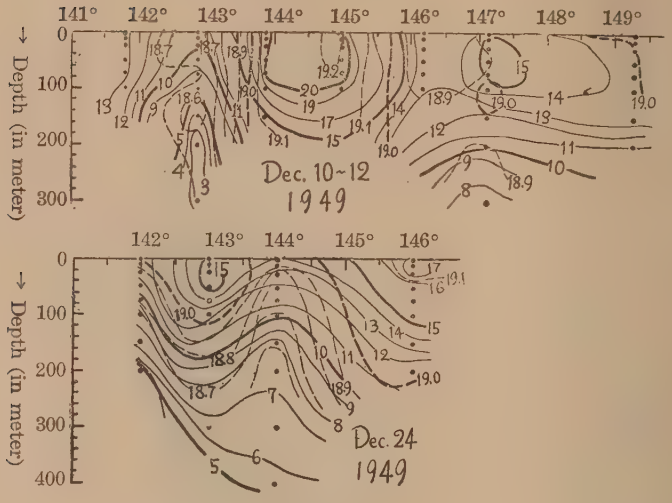

Fig. 1. (a)

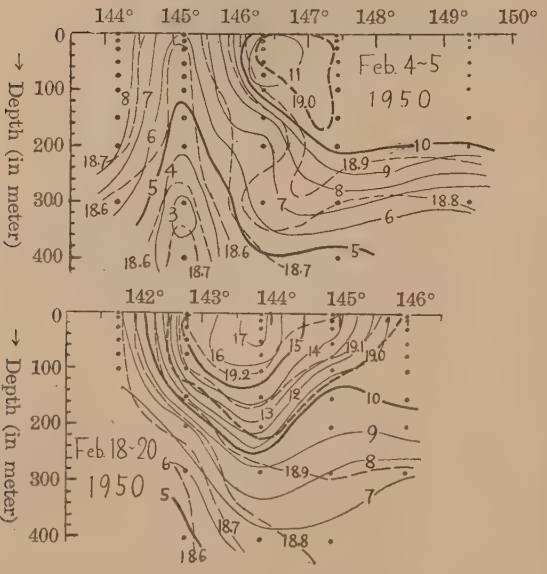

Fig. 1. (b)

Fig. 1. Distributions of water temperature and chlorinity in the vertical sections along the "C" line (38°N).
(——— Water temperature, — — — chlorinity)

peratures below 5°C was met with until the depth of about 100 m. In IB the warm water seems to be displaced to the east of 146°E and the upwelling of the colder water also shifted eastward by about 1 degree of longitude, although the water below 5°C was not found above the 300-m depth. Somewhat warmer aud more haline water appeared near 143°E in the top layer and thus the penetration of the southern water is expected. From the difference charts we can see that the temperature increase is accompanied with that of chlorinity and that the maximum values are found at about 100-m depth. Further, the decrease was largest between 144°E and 145°E, due to the displacement of the warmer and more haline water mass. Positive difference near 143°E seems to be caused by the penetration of the southern water. As for the observations of IIA, water temperatures are generally low and only at the top layer east of 147°E the water with temperatures above 10°C was found and near 145°E the upwelling of the bottom water was seen. In IIB the water considered as of Kuroshio origin appeared above the 100-m layer between 143°E and 144°E and caused the temperature increase of about 9°C. From fig. 2 we can observe that the difference of tempera-

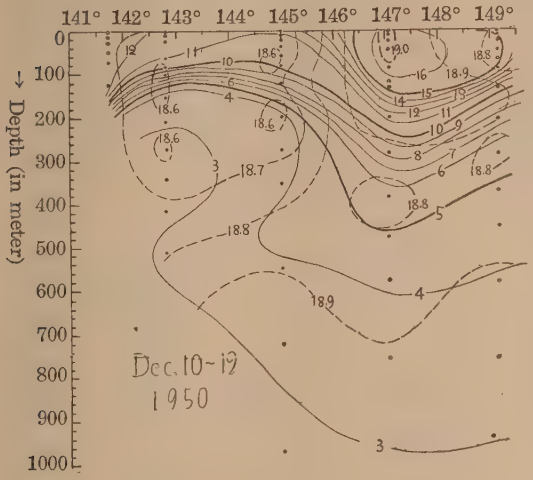

Fig. 1. (c)

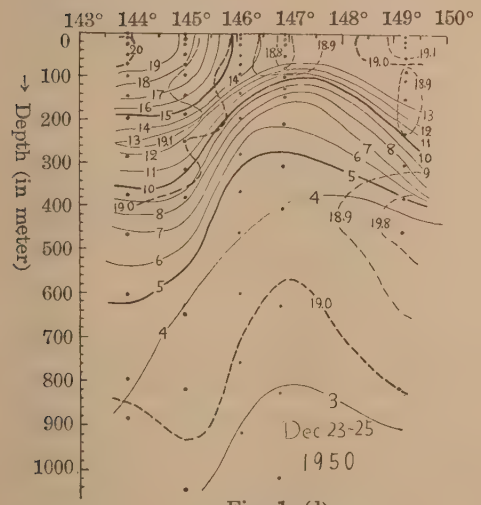

Fig. 1. (d)

Fig. 1—Continued

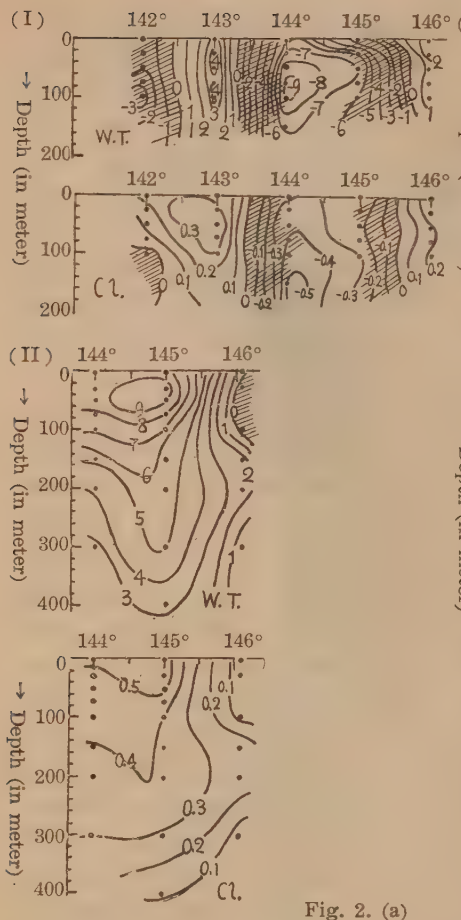

Fig. 2. (a)

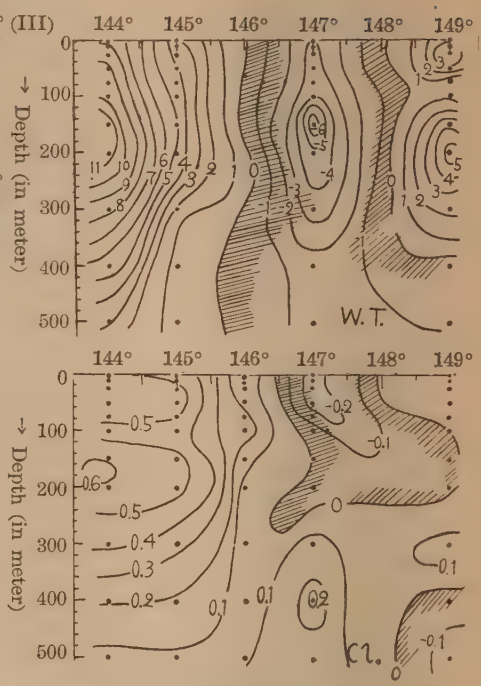

Fig. 2. (b)

Fig. 2. Differences in water temperature and chlorinity for the three cases as shown in Fig. 1. (*Plus* sign indicates an increase in elements at the later observation.)

tures in these two cruises reaches a maximum at about 50-m depth and seems to vanish at about 500-m depth. In IIIA the water mass stratification was different in the regions divided by 146°E, and in the region from 142°E to 146°E the cold water below 5°C was present even in the 200-m depth and formed a conspicuous thermocline layer in contrast to the surface water with temperatures above 10°C at the depths between 100 m and 200 m, whereas in the region from 146°E to 149°E the warmer water with temperatures more than 15°C and chlorinities more than 18.9‰ was found above the 200-m layer and the cold water below 5°C sunk to the depth of 500 m, and therefore the

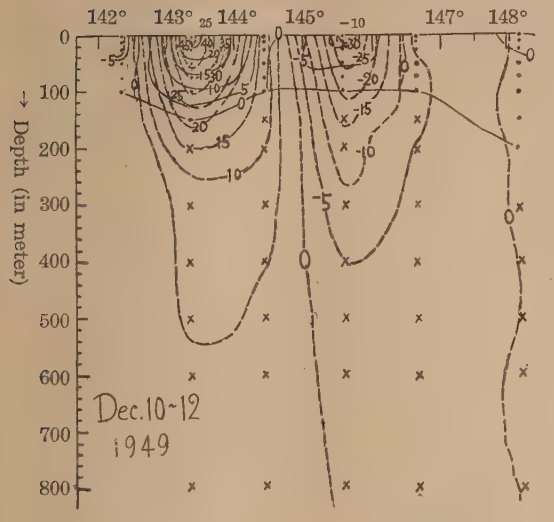

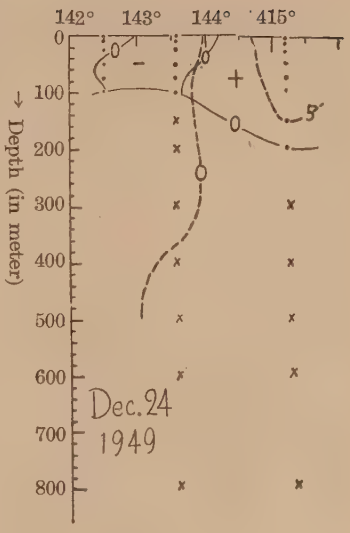

Fig. 3. (a)

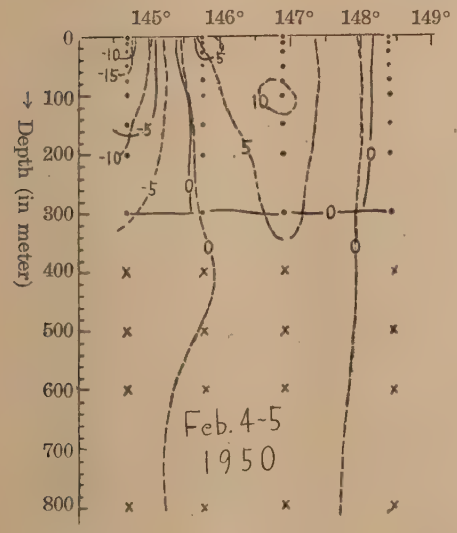

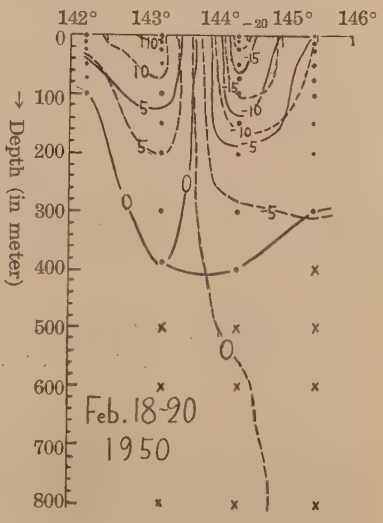

Fig. 3. (b)

Fig. 3. Distribution of the velocity of current for the three cases as shown in Fig. 1. (Numerals indicate the velocity of current in cm/sec. obtained by dynamical calculation, assuming the 1000 m layer to be the motionless layer. Positive sign corresponds to the northerly current.)

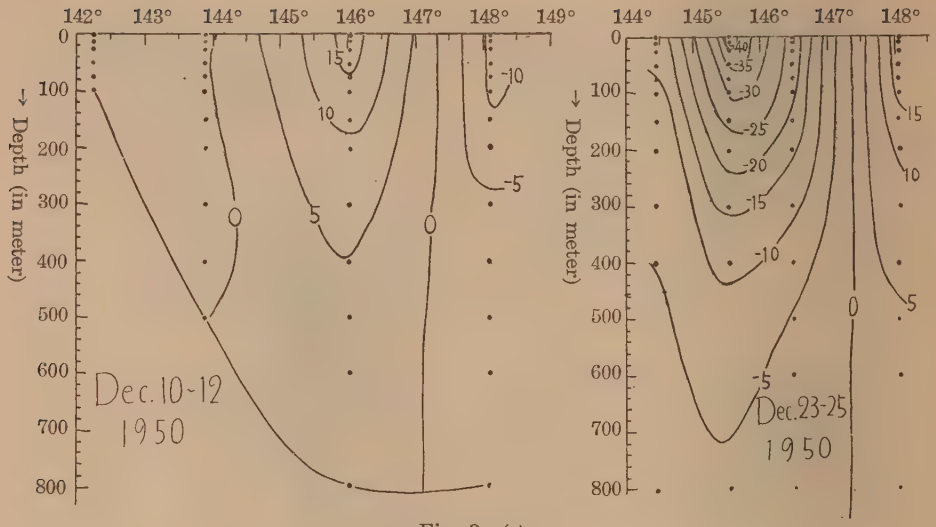

Fig. 3. (c)

Fig. 3—Continued.

temperature gradient became rather small in this region. The chlorinity distribution was somewhat different from that of temperature, unlike the above two cases, and it shows lower values in the region 142°E to 146°E and higher values in the top layer of the warmer water and below the depth of 600 m, which shows that the water of the Oyashio origin in the top layer of the western region was not thoroughly mixed with that of Kuroshio origin. In IIIB, the warmer and more haline water which was found in the region 146°E to 149°E by the previous observation was moved to the east of 148°E and in its stead a new water mass of Kuroshio origin appeared in the west of 146°E. From fig. 2 we can see that the domain of the water of Oyashio origin was much reduced, and thus that the chlorinity was generally increased. The increases in temperature and chlorinity was remarkable in the neighbourhood of 144°E, due to the appearance of the new warmer water mass and in the region 146°E to 148°E the negative difference of these elements was met with, such increase and decrease being probably due to the movement of the water mass, whereas the increase of chlorinity in the layer below 300 m in the region 146°E to 148°E seems to be due to the mixing of the Kuroshio water rather than due to the effect of the water mass movement. Further, the difference was maximum at about 200-m depth, deeper than in the above two cases.

The current distributions obtained by dynamical calculation are shown in fig. 3. The next method was applied to the estimation of the velocity, when we are lacking in the data below-200-m depth. Plotting $\log(D_z - D_b)$ against the depth, where D_z is density in situ at the depth z below 100 m and D_b is that at the 1000-m depth from the data at 8 stations in IIIA and IIIB, we obtain fig. 4, which

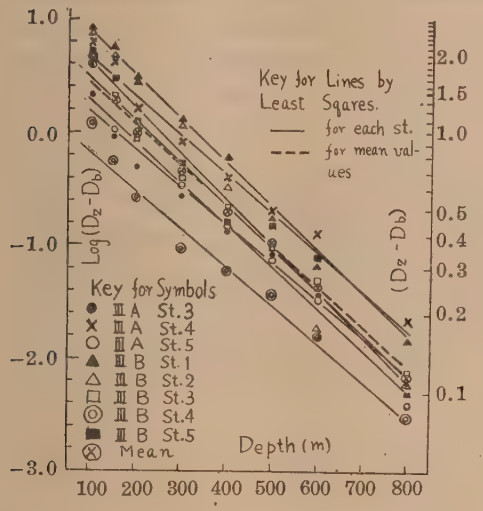

Fig. 4. The relation between $D_z - D_b$ and the depth obtained from the data of 8 stations in the observations IIIA and IIIB. (D_z is density in situ at the deepth z, and D_b is that at the 1000 m layer. The station number shown in the figure is counted from the west in each section shown in fig. 1. The straight lines are determined by the method of least squres for each station.)

shows that points of each station lie nearly on one of the straight lines which are almost parallel to each other. Therefore, assuming that $D_z = Ae^{-\alpha z} + D_b$, where α and D_b are nearly constant for each station and only A is variable, we can estimate the values of D_z at depth between 200 m and 800 m, knowing D_z at 100 m or 200 m. The mean value of D_b for 8 stations is 27.40 and the mean of eight values of α determined from each set of points by the method of least squares is $0.368 \times 10^{-2}(\mathrm{m}^{-1})$. Further, the mean values of $\log(D_z - D_b)$ at each depth for the above 8 stations are

Depth (m)	100	150	200	300	400
$\log(D_z - D_b)$	0.68 (0.18)	0.32 (0.32)	0.05 (0.35)	−0.32 (0.31)	−0.67 (0.25)

Depth (m)	500	600	800
$\log(D_z - D_b)$	−0.98 (0.24)	−1.35 (0.24)	−2.16 (0.24),

where the values in parentheses indicate the confidence limit of 95% significance. The value of α obtained from these mean values by the method of least squares

is $0.387\times10^{-2}(m^{-1})$, which is almost the same as the above α. Thus, taking α as $0.378\times10^{-2}(m^{-1})$, the mean of the above two values, and estimating the density in situ below the 200-m depth, the current velocity is obtained, and the results are shown in fig. 3 with broken lines. The comparison of the velocity distribution calculated by the observed density in situ with the shallower zero layer shows that the general characteristics are consiatent but the absolute value of estimated

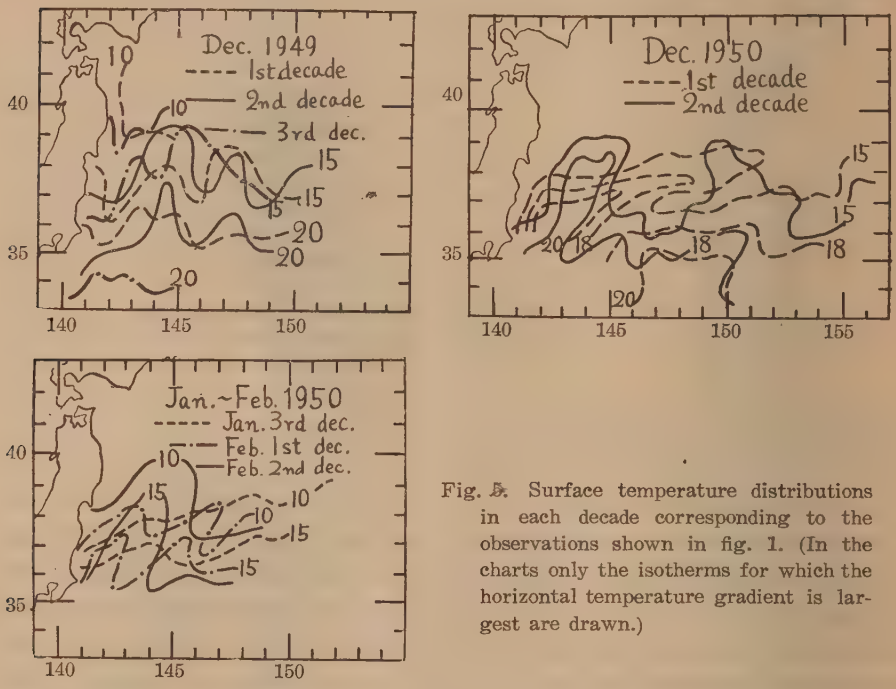

Fig. 5. Surface temperature distributions in each decade corresponding to the observations shown in fig. 1. (In the charts only the isotherms for which the horizontal temperature gradient is largest are drawn.)

velocity becomes larger, especially in IA, where the horizontal gradient of the density in situ at the top layer is large. From fig. 3, the strong northerly current was found between 142°E and 145°E and the southerly ones between 145°E and 148°E in IA, whereas in IB the northerly current was met with in the east of 144°E and the magnitude of the velocity is slight, which indicates that the strong northerly current accompanies the strong southerly one. Such characteristics are seen also in II and III, although the velocity is weaker in A of these cases. In IIIA the northern, relatively weak current was found between 144°E and 147°E, whereas in IIIB the strong northerly current replaced it in this region.

In fig. 5 the surface temperature distributions in each decade of the month corresponding to the above three cases are shown by 10°C, 5°C and 20°C isotherms, where the horizontal gradient of temperature is largest between these lines. By comparing the current distribution shown in fig. 3 with these charts, we can see that in the case IA the northerly strong current corresponds to a tongue-like protrusion of the 15°C isotherm to ward north and the southerly one corresponds to the southward protrusion and in IB the weak current accompanies the slight meandering of the isotherms in the 3rd decade. In II and III also the rough consistency of the surface isotherms and the current distribution shown in fig. 3 is seen and the large amplitude of the meandering of the isotherms accompanies the great southerly and northerly currents and the tongue of warmer or colder water corresponds to the northerly or southerly current.

By comparing the velocity distributions with those of temperature and chlorinity in fig. 1, we can see that the warm and haline water mass of Kuroshio origin was found on the right hand of the maximum northerly current, since the velocity obtained by dynamical calculation represents only the geostrophic component, given by $v=1/\lambda\cdot\partial p/\partial x$, when we take as the x-axis the east direction. The pressure at the depth z is

$$p(z)=g\left(\int_z^0 \rho dz+\zeta\rho_0\right),$$

where ρ is the density of sea water, ρ_0 its surface value, and ζ the elevation of the surface from the mean level $z=0$. When we take $z=-h$ as a constant zero layer, $(\partial p/\partial x)_{z=-h}=0$, and therefore $v=-\frac{g}{\lambda}\frac{\partial}{\partial x}\int_{-h}^{z}\rho dz$. When the difference of the density in situ is more affected by temperature than by chlorinity as in the present case of the northing of the Kuroshio water by the wind current or the meandering of the current, the maximum northerly velocity is found at the western edge of the warmer water and the maximum southerly one at the eastern edge. Thus the warm water is transported to the western side and the cold water to the eastern, and the initial warm water region is shifted to the left but then the lateral velocity is produced, and when $\partial^2 u/\partial t^2$ and $\partial p/\partial y$ are neglected, it is given by $u=-1/\lambda\cdot\partial^2 p/\partial x\partial t$, and since $v=1/\lambda\cdot\partial p/\partial x$, it decreases on the both edges of the warm water mass, $u>0$, and easterly current appears. Therefore the warm water region seems be be maintained stable at the initial position.

Summarizing the above results,

(1) short-period fluctuations of temperature and chlorinity occurred almost until the depth of 500 m and its magnitude reaches 10°C or more in temperature, and since the temperature change is consistent with that of chlorinity, such fluctuation is due to the variation of the current;

(2) the meandering of the surface isotherms is also changed, and the northerly or southerly current varies with its amplitude.[2)]

As for the cause of such fluctuations we can point out the travelling of a cyclone as shown in each case of fig. 6, where the weather charts are inserted,

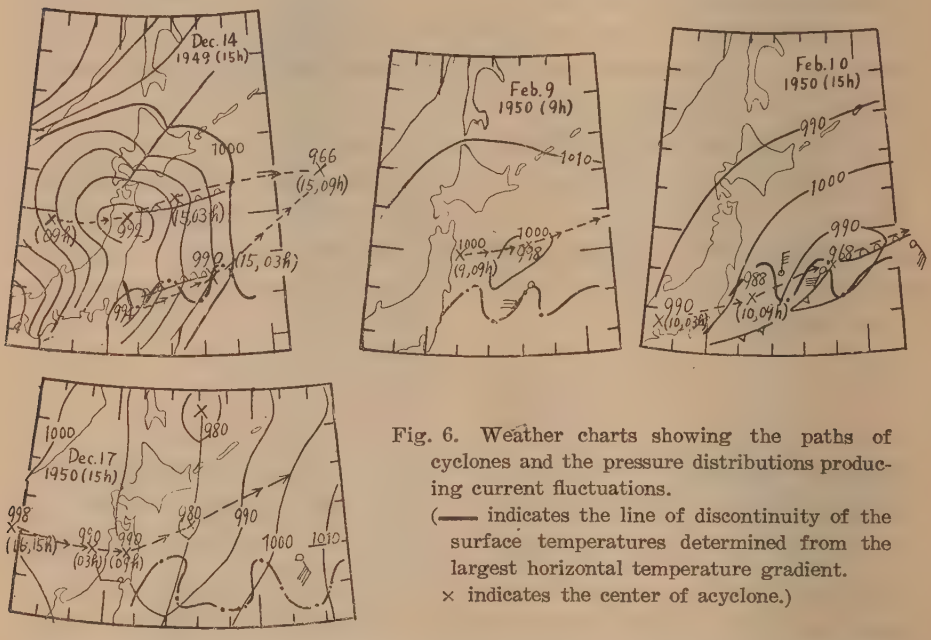

Fig. 6. Weather charts showing the paths of cyclones and the pressure distributions producing current fluctuations.
(—— indicates the line of discontinuity of the surface temperatures determined from the largest horizontal temperature gradient.
× indicates the center of acyclone.)

showing the paths of cyclones and a general isobaric condition. By comparing them with the surface temperatures in fig. 5, it is clearly seen that the development of the meandering of isotherms always occurred after the passage of a cyclone. Further, the boundary of the warm and cold water masses, where the temperature gradient is largest, is also shown in these charts and we can see that a cyclone or a front is apt to be generated at such boundary as shown by the cyclone and from appearing at 15h. Dec. 14 in I at 37°N and those at 09h. Feb. 10 in II at 37°N 143°E and a front generated at 09h. Dec. 17 in III along 38°N (not shown in the chart), such tendency being possible, judging from the

heating and cooling of the air by the sea surface.

§3. In this section the drift current caused by the travelling disturbance such as a cyclone is theoretically discussed. First, when the disturbance propagates over the ocean current with a vertically uniform velocity, the equations of motion are

$$\left.\begin{aligned}\frac{\partial u}{\partial t}+U\frac{\partial u}{\partial x}-\lambda v&=\frac{\partial}{\partial z}\left(K\frac{\partial u}{\partial z}\right),\\ \frac{\partial v}{\partial t}+U\frac{\partial v}{\partial x}+\lambda u&=\frac{\partial}{\partial z}\left(K\frac{\partial v}{\partial z}\right).\end{aligned}\right\}\qquad(1)$$

Assuming that the depth is infinite, the boundary conditions are as follows:

at the surface $\quad z=0\,,\quad \nu\dfrac{\partial u}{\partial z}=T_x(x,y,t)\,,\quad \nu\dfrac{\partial v}{\partial z}=T_y(x,y,t),$

at the bottom $\quad z=-\infty\,,\quad u=v=0\,.$

Then by some calculations, we obtain the solution as follows:

$$\left.\begin{aligned}u=&\frac{1}{\sqrt{\pi K}}\int_0^t\Big\{T_y(x-U(t-\tau),y,\tau)\sin\lambda(t-\tau)\\ &+T_x(x-U(t-\tau),y,\tau)\cos\lambda(t-\tau)\Big\}\exp\left\{-\frac{z^2}{4K(t-\tau)}\right\}d\tau/\sqrt{t-\tau}\,,\\ v=&\frac{1}{\sqrt{\pi K}}\int_0^t\Big\{T_y(x-U(t-\tau),y,\tau)\cos\lambda(t-\tau)\\ &-T_x(x-U(t-\tau),y,\tau)\sin\lambda(t-\tau)\Big\}\exp\left\{-\frac{z^2}{4K(t-\tau)}\right\}d\tau/\sqrt{t-\tau}\,.\end{aligned}\right\}\qquad(2)$$

When the disturbance travels with a constant velocity c, T_x and T_y are expressed by the function $f(x-ct,y)$ and the integrands of (2) include the terms $f(x-U(t-\tau)-c\tau,y)$. Therefore, assuming the isolated disturbance such as $f(p,y)\fallingdotseq 0$ only in the interval $a>p>-a$ and $U\fallingdotseq 0$ for simplification, the surface current is produced only when $t>(x-a)/c$, and after the passage of the disturbance it is given by $(t\gg(x+a)/c)$,

$$u,v\sim\frac{1}{\sqrt{t}}\left\{\cos\lambda t\int_{(x-a)/c}^{(x+a)/c}f(x-c\tau,y)\cos\lambda\tau d\tau+\dots\right\}.$$

Thus the surface current velocity diminishes with time and it varies with the period of the inertia oscillation.

In order to obtain the functional form of T_x, T_y (T_x being the E-component

of wind stress), we calculate them, by using Rossby's formula[3], from the observed wind at the fixed point 39°N, 153°E) and plot their variation with time in fig. 7.

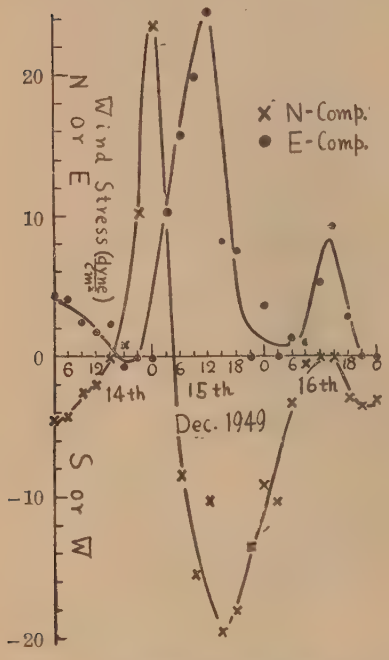

Fig. 7. Variation of wind stress at the fixed point (39°N, 153°E) on the occasion of the passage of a cyclone from Dec. 14 to Dec. 16, 1949. (Wind stress is calculated by Rossby's formula from the observed wind and is shown in dyne/cm².)

For knowing the general features of the drift current caused by the stationary cyclone travelling with the constant velocity, we assume that

$$T_y=\frac{2}{\sqrt{\pi}}T\alpha\left(\frac{x}{c}-t\right)e^{-\alpha^2(t-\frac{x}{c})^2},$$

and putting this in (2), we have

$$v+iu=\frac{2T}{\pi\sqrt{K}}\int_0^\infty\alpha\left(\frac{x}{c}-t-\gamma\mu\right)\times e^{-\alpha^2(\frac{x}{c}-t-\gamma\mu)^2+i\lambda\mu}d\mu/\sqrt{\mu} \qquad (3)$$

for $z=0$, where $\gamma=1-U/c$. When we apply the method of saddle point to the integration of (3), we have

$$v+iu=i\frac{T}{\sqrt{\pi K}}\frac{\lambda}{\alpha^3\gamma^{3/2}}\cdot e^{-\frac{1}{2}(\frac{\lambda}{\alpha\gamma})^2+i\frac{\lambda}{\gamma}(t-\frac{x}{c})}\cdot\left(t-\frac{x}{c}+\frac{i\lambda}{\alpha^2\gamma}\right)^{-1/2}. \qquad (4)$$

Thus the surface velocity decreases with $t^{-1/2}$ when the main part of the disturbance is far away from the considered station. For practical application, taking

$U=1$ m/sec, $C=10$ m/sec (36 km/hr),
$T=4.3$ (dyne/cm²), $\alpha=0.2$ (hr^{-1}),
$K=200$ (cm²/sec),

corresponding to the observed wind stress shown in fig. 7, we plot the velocity variation at $x=0$ in fig. 8. The variation of T_y is also inserted in this figure and it is almost negligible at $t>10$ hr. and $t<-10$ hr., whereas the velocity is about 30 cm/sec at 48 hours before and after the arrival of the centre of the disturbance, since the current is the integral effect of wind stress. Further, the maximum current occurs at $t=0$ with NE direction and velocity of 113 cm/sec, owing to the fact that the integrated S-component of the wind stress reaches its maximum at

this instant. The wave length of the current fluctuation is given by $2\pi\gamma c/\lambda$ and it is 678 km in the present case. Although this wave length is roughly consistent with the observed length of meandering, the velocity of the current fluctuation is too large in eq. (3) to be applied to the practical case.

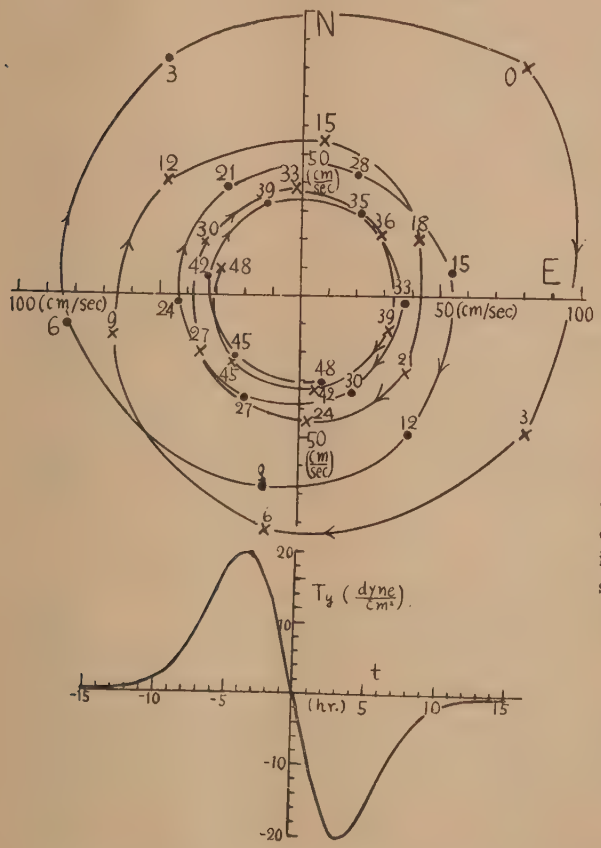

Fig. 8.

The theoretical surface drift current produced by a travelling disturbance with a constant velocity.

Upper figure: The hodograph of the current velocity at 3 hours' interval at the point $x=0$. (●···for $t<0$. ×···for $t>0$)

Lower figure: The variation with time of the wind stress at $x=0$.

Another theory for the occurrence of the meandering of the current is given by the analogy the planetary wave in the atmosphere, where the variation of Coriolis' parameter plays an important role. In the ocean current the external force which produces such wave is explicitly given by the rotation of the wind stress as shown in fhe following discussion. First, the perturbation equations of motion are

$$\left.\begin{aligned}&\frac{\partial u}{\partial t}+U\frac{\partial u}{\partial x}+v\frac{\partial U}{\partial y}-\lambda v=-\frac{\partial P}{\partial x}+T_x\,,\\&\frac{\partial v}{\partial t}+U\frac{\partial v}{\partial y}+\lambda u=-\frac{\partial P}{\partial y}+T_y\,,\end{aligned}\right\}\qquad(5)$$

where the axes x, y are taken in the directions E and N and u, v and P are the integrated velocity and pressure with respect to z-axis respectively. Eliminating P by the equation of continuity, we have

$$\frac{\partial \Delta\phi}{\partial t}+U\frac{\partial \Delta\phi}{\partial x}-\frac{\partial\phi}{\partial x}\frac{\partial^2 U}{\partial y^2}-\frac{\partial^2\phi}{\partial x\partial y}\frac{\partial U}{\partial y}+\beta\frac{\partial\phi}{\partial x}=\frac{\partial T_x}{\partial y}-\frac{\partial T_y}{\partial x}\,,\qquad(6)$$

where U is assumed to be a function variable only with y and $u=\partial\phi/\partial y$, $v=-\partial\phi/\partial x$, $\beta=\partial\lambda/\partial y$.

For simplification, we assume that the perturbation velocity has only a y-component and neglect $\partial\phi/\partial y$. Then we have

$$\frac{\partial^3\phi}{\partial t\partial x^2}+U\frac{\partial^3\phi}{\partial x^3}+\left(\beta-\frac{\partial^2 U}{\partial y^2}\right)\frac{\partial\phi}{\partial x}=\frac{\partial T_x}{\partial y}-\frac{\partial T_y}{\partial x}\,.\qquad(7)$$

When the external force travels with a constant velocity c, we put

$$\partial T_x/\partial y-\partial T_y/\partial x=F\quad\text{and}\quad F=\int_{-\infty}^{\infty}f(\mu)e^{i\mu(x-ct)}d\mu\,.$$

Then solution ϕ is given by

$$\phi=\int_{-\infty}^{\infty}\frac{f(\mu)\exp\{i\mu(x-ct)\}}{i\mu\{\beta'+\mu^2(c-U)\}}d\mu\,,\qquad(8)$$

where $\beta'=\beta-\partial^2U/\partial y^2$ or latitudinal gradient of the absolute vorticity of the main current U. As seen from the equation (8), the wave caused by the travelling disturbance is quite different according to the circumstance $\beta'/(c-U)<0$ or >0, and in the former case the current perturbation has a term proportional to $\exp\left\{i\sqrt{\frac{-\beta'}{c-U}}(x-ct)\right\}$, which shows that a simple harmonic train of waves proceed beyond and behind the passage of the disturbance, and in the latter this is given by $\exp\left\{-\sqrt{\frac{\beta'}{c-U}}|x-ct|\right\}$, indicating that the current is insensible beyond a certain distance from the seat of travelling disturbance. Further, when we take into account the friction terms such as $-ku$ and $-kv$ in the equation (5), the numerator of the integral (8) becomes $i\{\mu^2(c-U)+ik\mu+\beta'\}$, and thus the periodic term in the former case vanishes at $x-ct>0$ when $c-U>0$, and at $x-ct<0$ when

$c-U<0$. Therefore, a train of waves proceed behind the disturbance when $c-U>0$ and they go in advance of it when $c-U<0$.

For the practical application of the above equation we estimate the value of β' in a hypothetical mean current

$$\alpha>y>0,\quad U=U_0\left(1-\cos\frac{2\pi}{\alpha}y\right);\quad y>\alpha,\ y<0,\quad U=0\,. \tag{9}$$

When we take $U_0=10$ (cm/sec), the values of β' becomes as follows:

y \ α (100 km)	2	4	6	
0, α	−7.99	−0.59	0.78	$\times10^{-13}$,
$\alpha/2$	11.75	4.35	2.98	$\times10^{-13}$,

where the latitude is taken at 35°N. Therefore, a wave train is apt to be produced after the passage of the disturbance at the boundaries of the current when the breadth of the current is below 400 km and the maximum velocity (mean value with the depth) is above 20 cm/sec or so, since in the travelling cyclone usually $c>U$. However, their wave length $2\pi/b$ is quite large, compared with the present meandering of the current, as seen from the following table.

$-\beta'$ (sec^{-1}cm^{-1})		10^{-12}	5×10^{-13}	10^{-13}	
$c-U$ (m/sec)	5	1.40	1.99	4.44	
	10	1.99	2.81	6.28	($\times10^3$km)

As an example we take a form of disturbance as $F(x)=F_0e^{-\alpha|x|}$, then

(i) $b^2=\dfrac{\beta'}{c-U}>0$,

$$v=-\partial\psi/\partial x=\frac{F_0}{(c-U)(a^2-b^2)}\left\{e^{-a|ct-x|}-\frac{a}{b}e^{-b|ct-x|}\right\}, \tag{10}$$

(ii) $b^2=\dfrac{-\beta'}{c-U}>0$, $c>U$,

$$\left.\begin{aligned} v&=\frac{F_0e^{-a(x-ct)}}{(c-U)(a^2+b^2)}, \quad (\text{when } x>ct)\\ v&=\frac{F_0}{(c-U)(a^2+b^2)}\left\{e^{-a(ct-x)}-\frac{2a}{b}\sin b(ct-x)\right\} \quad (\text{when } ct>x), \end{aligned}\right\} \tag{11}$$

when we determine F_0 and a from the observed value of $\partial T_x/\partial y-\partial T_y/\partial x$ shown

in fig. 9, we obtain $F_0 = -0.925 \times 10^{-6}$ (cm sec^{-2}) $a = 4.63 \times 10^{-8}$ (cm^{-1}) as a probable value, since T_y decreases by about 40 (cm^{2}sec^{-2}) in 12 hours at the passage of cyclone center and the velocity of the cyclone is about 36 km/hr and

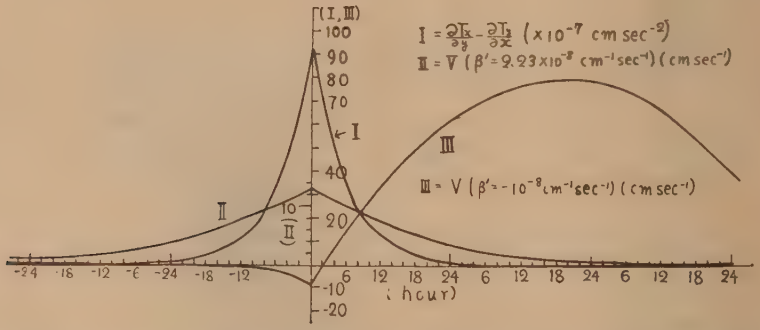

Fig. 9. Variation of the rotation of the wind stress and the current velocity for a travelling disturbance with a constant velocity. (Time origin is taken at the time of passage of the center of disturbance. Positive velocity means northern current.)

the region of negative F is considered to be about $40 \times 12 = 480$ (km), Further we put $c = 10$ (m/sec) and $\beta' = 2.23 \times 10^{-8}$ (at the center of the current) or $\beta' = -10^{-8}$ (at the boundaries), which corresponds approximately to the model shown by (9) with the breadth about 300 km and we take the depth of the perturbation current as 500 m (v in (10) and (11), indicating the current flux). The variation of F and V (the current velocity v/500 m) at one station with time obtained from (10) or (11) by use of the above numerical values are shown in fig. 9. From these figures we can see that the northerly current occurs both at the boundaries and center of the zonal cnrrent system after the passage of a cyclone, that its maximum velocity reaches about 80 cm/sec at the boundaries and that it changes to the southerly current after 87.3 hours. (The period of the perturbation current at the boundaries is twice as much as this value.) The general increase of temperatures along "C" line and the northing of the isotherms experienced after the passage of a cyclone as stated in § 2 are probably due to such northerly current caused by a cyclone at the boundary of the Kuroshio[4].

Heretofore only the effect of a disturbance travelling without a change is considered. In the practical case a cyclone or other meteorological disturbing force always develops or is weakend over the ocean, and it is necessary to discuss such effect. However, complete mathematical treatment of the problem for the current

perturbation due to the travelling disturbance variable with time is extremely complicated, and as a step we take a model for the disturbance such as

$$F(x,t)=P(t)Q(x)=\iint p(\sigma)q(\mu)e^{i(\sigma t+\mu x)}d\sigma d\mu\ .$$

Then the solution of the equation (6) is

$$\phi=\iint\frac{p(\sigma)q(\mu)e^{i(\sigma t+\mu x)}}{i\mu(\beta'+ik\mu-\sigma\mu-U\mu^2)}d\sigma d\mu\ , \tag{12}$$

where the friction terms are taken into account when the integration about σ is performed at first, there exists a term due to a pole $\sigma=\beta'/\mu+ik-U\mu$ for $t>0$ which is of a form as

$$\phi_1=\int q_1(\mu)\,e^{i\{(\frac{\beta'}{\mu}-U\mu)t+\mu x\}-kt}d\mu\ . \tag{13}$$

Other terms obtained by the first integration represent a forced motion due to the disturbance. For understanding the property of the motion expressed by (13), we make use of the method of stationary phase, then

$$\begin{aligned}\phi_1\sim&\exp i2\sqrt{\beta' t(x-Ut)}\ (x>Ut)\quad\sim\exp(-2\sqrt{\beta' t(Ut-x)})\ (x<Ut)\ \text{for}\ \beta'>0\\ &\exp(-i2\sqrt{\beta' t(Ut-x)})\ (x<Ut)\ \sim\exp(-2\sqrt{\beta' t(x-Ut)})\ (x>Ut)\ \text{for}\ \beta'<0\ .\end{aligned} \tag{14}$$

Therefore a train of waves are generated in the east of the disturbance when $\beta'>0$, and in the west of it when $\beta'<0$.[5] The wave length determined by the above circular function is given by

x (100 km) \ β'	10^{-13}	5×10^{-13}	10^{-12}	
10	30.69	11.27	7.57	
5	23.90	8.85	5.85	($\times$100 km),

where $t=10^6$ (sec) (about 11.5 days) $U=10$ (cm/sec). Thus, when the breadth of the zonal current is less than 300 km, the central portion of the current may show the meandering of about 600~800 km wave length due to the change of cyclone near the coast, whereas at the boundaries of the zonal current such meandering in the west of the cyclone has a wave length slightly larger than the observed one. The present case seems to correspond to the meandering of the west wind drift or the eastern end of the kuroshio or the Gulf Stream stated by some authors[6].

When we take account of the variation of U and F in y-direction, the solution of (6) becomes so complicated that a complete analytical representation seems to be impossible. Only a simplified treatment is permissible and we assume U, U', U'' to be constant. Then, for a travelling disturbance

$$\psi=\iint \frac{f(\mu,\nu)e^{i\mu(x-ct)+i\nu y}}{i\mu\{\beta'-i\nu\gamma+(\mu^2+\nu^2)(c-U)\}}\,d\mu d\nu\,,$$
$$(\gamma=\partial U/\partial y)$$

and when we consider the neighbourhood of $y=0$, then the periodic term due to poles about μ is expressed by

$$\psi_1\sim\int p(\nu)\exp\{i\sqrt{\nu\gamma i/c'-\nu^2-\beta'/c'}\,(ct-x)\}d\nu\,.$$
$$(c'=c-U)$$

The wave train given by this equation is

$$\psi_2\sim\exp i\sqrt{-\frac{\beta'}{c'}-\frac{1}{4}\left(\frac{\gamma}{c'}\right)^2}(ct-x)\,.$$

But the correction term $\frac{1}{4}(\gamma/c')^2$ is negligible in the ordinary condition, since it is 3×10^{-15} $-\beta'/c'=10^{-15}$ when we assume the zonal current expressed by (9) and $c'=10$ (m/sec), $-\beta'=10^{-12}$, $\gamma^2=1.19\times10^{-11}$.

The solution of the equation of two dimensions corresponding to (12) has predominate terms such as

$$\exp\left\{\frac{\mu_0 t(i\beta'+\nu_0\gamma)}{-\beta' t}-i\mu_0\right\}(Ut-x)\,, \tag{15}$$

where
$$\nu_0=\frac{1}{2}\left(-\frac{\beta'}{\gamma}i\pm\sqrt{-\frac{\beta'^2}{\gamma^2}-\frac{2\beta' t}{Ut-x}}\right)$$

$$\mu_0^2=\frac{-\beta' t}{2(Ut-x)}+\frac{\beta'\nu_0}{\gamma}i\,.$$

When
$$\frac{\beta'}{\gamma}\gg\left(-\frac{2\beta' t}{Ut-x}\right)^{1/2},\quad \nu_0=0\quad\text{or}\quad -\frac{\beta'}{\gamma}i$$

and one term of (15) becomes

$$\exp\left\{\pm i\,\frac{\beta'}{\gamma}(Ut-x)\right\}.$$

The wave length of the train expressed by this term is 2.1, 7.4, 11.0 ($\times$100 km)

for $-\beta'=10^{-13}$, 5×10^{-13}, 10^{-2} with the current model given by (9) for the conditions that $t<10^6$ (sec), $x>10^8$ (cm). When $\beta'>0$, the wave length is 0.65, 1.07, 5.59 ($\times100$ km) for $\beta'=10^{-13}$, 5×10^{-13}, 10×10^{-13}, and this term represents a wave train in both directions to the disturbance with contrast to the wave given by (14). When

$$\beta'\gamma\ll\left(\frac{-2\beta't}{Ut-x}\right)^{1/2} \quad \text{and} \quad \mu_0\approx\nu_0\,,$$

the term (15) becomes

$$\exp i\sqrt{-2\beta't(Ut-x)}\ (x<Ut)\ (\beta'<0)$$

or the corresponding terms to (14). Thus the wave length is $\sqrt{2}$ times as long as that of (14). The conclusion from the above estimation is:

(i) the disturbance finite in y-direction causes a wave train of a length comparable with the meandering of isotherms at the initial stage of the change of its intensity;

(ii) and in the distant region from its center it also causes a wave train in the east of its center ($\beta'>0$) and in the west ($\beta'<0$) with a longer wave length in later stages.

The rigorous treatment of the solution for the disturbance finite in y-direction is possible only when we assume the discontinuous distribution of the general current. For example, we take the current system such as $U=0$ at $y>0$, $U=$ const. at $y<0$, and the disturbance is supposed to exist only at $y<0$. Then at

$$y>0,\quad \frac{\partial\Delta\phi}{\partial t}+\beta\frac{\partial\phi}{\partial x}=0\,,\quad \text{and at}\quad y<0,\quad \frac{\partial\Delta\phi}{\partial t}+U\frac{\partial\Delta\phi}{\partial x}+\beta\frac{\partial\phi}{\partial x}=F.$$

Further, when F, $\phi\sim e^{i\sigma t+i\mu\lambda}$, then

$$\phi=Ae^{-py}\ (y>0),\quad \phi=Be^{qy}+\frac{1}{iq(\sigma+\mu U)}\int_{-\infty}^{y}F(\xi)\sinh q(y-\xi)d\xi,$$

$$p=\left(\mu^2-\frac{\mu}{\sigma}\beta\right)^{1/2},\qquad q=\left(\mu^2-\frac{\mu}{\sigma+\mu U}\beta\right)^{1/2}.$$

From the continuity of the pressure and the kinematical conditions at $y=0$, we can determine A and B as a function of the given value of $F(y)$, and

$$\psi(y=0)=\frac{i(\sigma+U\mu)}{q(\sigma+U\mu)^2+p\sigma^2+\lambda\mu^2U}\cdot\int_{-\infty}^{0}F(\xi)e^{q\xi}d\xi\,. \tag{16}$$

The complete form of ψ is obtained by Fourier integration of (16) about σ and μ.

However, its numerator has no zero for any real value of μ, σ when $U>0$, thus there exists no stable wave, which indicates that the meandering of stationary type is not produced at the northern boundary of the eastward ocean current, even when we take account of β.[3] When we assume the current has a breadth, such stationary wave is possible[2]. Here the effect of U' and U'' to the wave at the boundary of the general current shall be discussed approximately. The disturbance is not taken into account, since, as seen from the equation (16), the wave is determined by the zeros of the numerator which is obtained as a mode of free oscillation. Further we take a model for the general current such that

$$U=0 \ (y>a, \ y<-a), \quad U=U(y) \ (a>y>-a)$$

and in the region $a>y>-a$ we take mean values of $U(y)$, $\partial U/\partial y$, $\partial^2 U/\partial y^2$, and assume these values are constant. The result which gives the modes of free oscillation is

$$\begin{aligned}&[(\sigma+\mu U)\{\mu(\lambda-\gamma_1)-(\sigma+\mu U)p\}-\mu\sigma(\lambda-\sigma)][(\sigma+\mu U)\{\mu(\lambda-\gamma_2)\\&+(\sigma+\mu U)p\}-\mu\sigma(\lambda+\sigma)]e^{-2ap}=[(\sigma+\mu U)\{\mu(\lambda-\gamma_1)+p(\sigma+\mu U)\}\\&-\mu\sigma(\lambda-\sigma)][(\sigma+\mu U)\{\mu(\lambda-\gamma_2)-p(\sigma+\mu U)\}-\mu\sigma(\lambda+\sigma)]e^{2ap}\,,\end{aligned} \tag{17}$$

where

$$(\sigma+U\mu)p^2-\lambda U'p-\mu(\sigma\mu+U\mu^2+U'')=0\,, \tag{18}$$

$$\gamma_1=(\partial U/\partial y)_{y=a}\,, \quad \gamma_2=(\partial U/\partial y)_{y=-a}\,,$$

and U, U', U'' in (18) show the mean values over the region $a>y>-a$. The wave length of the stationary wave can be obtained by putting $\sigma=0$ in (17) and (18), and further when the wave length is larger than the breadth of the general current $2a$, we have $e^{2ap}\sim 2ap$, $e^{-2ap}\sim -2ap$, and thus

$$p^2=(\lambda-\gamma_1)(\lambda-\gamma_2)/U^2\,. \tag{19}$$

When we consider the current given by (9),

$$\overline{U'}=0 \quad \text{and} \quad \gamma_1=\gamma_2=0, \quad \overline{U''}=U_0\pi^2/a^2, \quad \text{and} \quad \mu=\sqrt{(\lambda/U_0)^2-(\pi/a)^2}$$

which indicates that the mean velocity should be larger than $a\lambda/\pi$, in order that the stationary wave may exist. When $U_0=50$ (cm/sec) and $a=100$ (km), the wave length given by the above relation is 2.3×10^3(km). In general the effect of $\partial^2 U/\partial y^2$ increases the wave length of the internal wave of the jet-like current, whereas the effect of shear decreases it, since $-\gamma_1>0$, $\gamma_2>0$ and $-\gamma_1\gg\gamma_2$ in the usual ocean current. Further discussions on the property of the boundary wave given by (19) will be published later.

When we only discuss the stationary wave in the variable general current in y-direction, we should solve

$$U\Delta\psi+\psi\left(\beta-\frac{d^2U}{dy^2}\right)-\frac{\partial\psi}{\partial y}\frac{dU}{dy}=0\,,$$

and by putting $$\psi=e^{i\mu x}f(y)\,,$$

we have

$$\frac{d^2f}{dy^2}-\frac{d\log U}{dy}\frac{df}{dy}-\left(\mu^2+\frac{\frac{d^2U}{dy^2}-\beta}{U}\right)f=0\,.$$

The stationary wave exist only when real value of μ can be determined by the equation given by the two suitable boundary conditions for $f(y)$. When $\beta=0$, the stationary wave does not exist in the continuous general current as seen for the case $U=U_0(y/a)^k$, where the solution of $f(y)$ is given by

$$f(y)=A_yI_1(\mu y)+B_yK_1(\mu y)\,,$$

and from the property of the modified Bessel function K_1, I_1 it can be concluded that more than one zero of $f(y)$ do not exist for the real value of μ and thus when we consider one or two solid boundaries parallel to y-axis we cannot obtain real values of μ which satisfy the boundary conditions. Another example for this problem is given by the general current

$$U=U_0(ay)e^{-a^2y^2}$$

In this case the general current is assumed to extend from $y=-\infty$ to $y=\infty$ and we consider the region of infinite space. The equation for $f(y)$ is given by

$$f''+2a^2yf'-(\mu^2-2a^2+4a^4y^2)f=0$$

and no continuous solution exists which converges to a finite value at $y=\infty$ and $y=-\infty$, since from the theory of linear differential equation of the second order the function $f(y)$ has no normal solution near the points as seen by the transformation $y=1/\zeta$

$$\frac{d^2f}{d\zeta^2}+2(\zeta^{-1}+a\zeta^{-5})\frac{df}{d\zeta}-\{\mu^2-2a^2)\zeta^{-4}+4a^4\zeta^{-8}\}f=0\,.$$

Thus, generally speaking, the stationary wave does not originate in the continuous current system when we neglect the effect of β. The observed meandering of the surface isotherms is probably due to the boundary wave of planetary type.

In the end the author expresses his cordial thanks to Dr. K. Hidaka, Dr. M.

Nakano, Dr. M. Uda and Dr. Y. Takenouchi for their constant kind advice and encouragement. Further he is grateful to Mr. J. Fukuoka for taking the trouble of sending various data to the author.

(To be continued)

Literatures.

1) Fuglister, F. C. and Worthington, L. V: Some Results of a Multiple Ship Survey of the Gulf Stream. *Tellus*, Vol. 3, No. 1, 1951.
2) Ichiye, T.: On the Variation of Ocean Current. (In Japanese.) *Umi to Sora*, Vol. 28, No. 4, 1950.
3) Sverdrup et al.: *The Oceans*, p. 491.
4) Ichiye, T.: On the Hydrography of the Kii Suido (1951) *Oceano. Rep. of the C.*M.O., Vol. 2. No. 3, 1952.
5) Yeh, Tu-cheng.: On the Energy Dispersion in the Atmosphere. *J. Met.* Vol. 6, No. 1, 1949.
6) Iselin, O. D.: A Study of the Circulation of the Western North Atlantic. *Pap. in phys. Oceano. and Met.*, Vol. 6, No. 4, 1936.

With the Author's Compliments

On the Abnormal High Waters in Rivers

By

Takashi ICHIYE

Reprinted from the *Oceanographical Magazine* Vol. 5, No. 1.

June 1953

On the Abnormal High Waters in Rivers

By Takashi Ichiye

Kobe Marine Observatory

§ 1. The rivers and estuaries in the City of Osaka often overflow, chiefly due to the meteorological high waters caused by typhoons, and give serious damages to the constructions and other facilities. Therefore it is demanded from the authorities of civil engineering to investigate the property of flood waves of meteorological tides progressing up the rivers, and some discussions about this problem are presented in this paper.

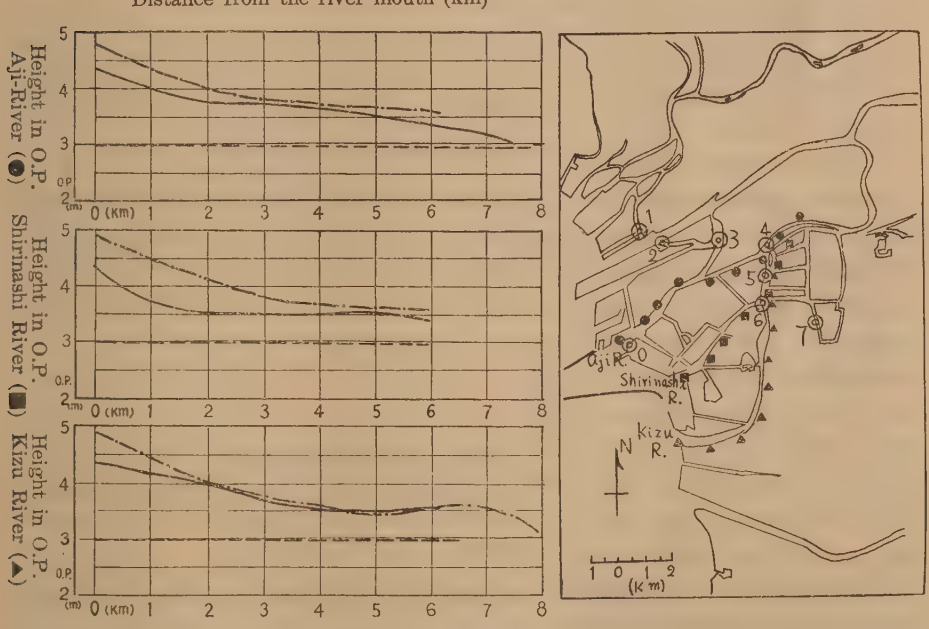
Distance from the river mouth (km)
Height in O.P. Aji-River (●)
Height in O.P. Shirinashi River (■)
Height in O.P. Kizu River (▲)
O.P.
0 (km) 1 2 3 4 5 6 7 8
Aji R.
Shirinashi R.
Kizu R.
N
1 0 1 2 (km)

Fig. 1. Location of rivers in the city of Osaka and the observed abnormal high waters in three typical cases.

● Stations along Aji River. ■ Stations along Shirinashi River.
▲ Stations along Kizu River. ◎ Tidal Stations where the amplitude ratios to that at Tempozan (the station marked with ○) are given in the text.
Observed abnomal high waters. —·—·— Typhoon "Muroto", Sept. 21, 1934. —— Typhoon "Jane", Sept. 3, 1950. - - - - - Typhoon "Ruth", Oct. 15, 1951.

§ 2. Remarkable differences are seen in the distributions of wave heights along the rivers of Osaka for the cases of three typhoons, "Muroto" on 21 Sept. 1934, "Jane" on 3 Sept. 1950 and "Ruth" on 15 Oct. 1951, as shown in fig. 1, where the observed wave heights along several rivers are plotted with respect to the distances from the mouth, and we can see that the decrement of wave heights is conspicuous in the cases of the former two typhoons, whereas it is almost unnoticeable in the latter typhoon, though the wave heights at the mouths of the rivers are far smaller. This difference is considered to be due to the different property of the meteorological tides in the former two cases and due to the fact that the embankments built after the typhoon "Jane" prevented the flood in the downstream region and thus the waters flowing from Osaka Bay went, without losing their water volume, up the rivers.

In this section the first effect is discussed from the theory of long waves going up a river. The high waters at the stations near the mouth of a river or on the sea coast are shown in fig. 2 and 3, where the mareograms and the meteorological tides (deviations of observed tides from the astronomical ones) at Kobe in the case of Typhoon "Jane" and those at Osaka in Typhoon "Ruth" are inserted. The characteristic difference between these two cases consists in the time rate of the change of tidal height, and the wave height was increased by 140 cm within 2 hours in the case of "Jane", whereas it took almost 6 hours for the increase of the same height, and thus the mareogram had a remarkable peak in the former case, but in the latter case the maoeogram indicated no singularities and only an extreme high tide, We apply the next linearized equations to the motion of waves going up the river[1]:

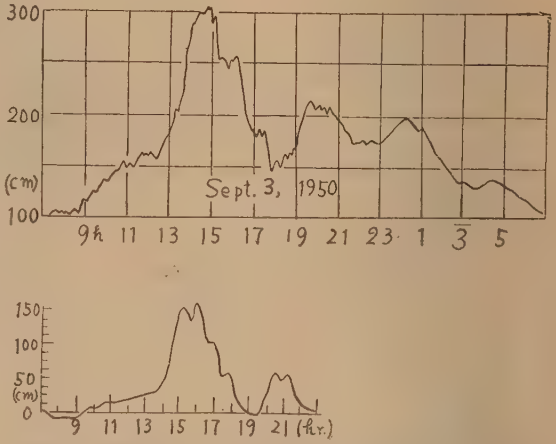

Fig. 2. Mareogram (above) and high tide (deviation from astronomical tide) (below) at Kobe on the occasion of Typhoon "Jane".

$$\frac{\partial u}{\partial t}+fu+g\frac{\partial \zeta}{\partial x}=0\ ,\qquad \frac{\partial \zeta}{\partial t}+R\frac{\partial u}{\partial x}=0\ , \tag{1}$$

where R is the hydraulic radius of the river, and f the friction coefficient represented by gu_0/C^2R, in which u_0 is the proper current velocity of the river, C Chezy's roughness parameter. The general solution of eqs. (1) for the boundary condition that $\zeta|_{x=0}=F(t)(t>0),=0(t<0)$ at $x=0$ is given by

$$\zeta=0 \quad (t<\sqrt{gR})$$

$$=e^{-fx/2\sqrt{gR}}F\left(t-\frac{x}{\sqrt{gR}}\right)$$

$$+e^{-ft/2}\int_0^{t-x/\sqrt{gR}}\frac{f\cdot x}{2\sqrt{gR}}\frac{I_1(\frac{f}{2}\sqrt{(t-p)^2-x^2/gR})}{\sqrt{(t-p)^2-x^2/gR}}e^{fp/2}F(p)dp \quad (t>\sqrt{gR}) \ . \ (2)$$

The mean value of R is about 7 m, and computing C from Bazin's formula $C=87/\{1+\gamma\sqrt{R}\}$ with $\gamma=1.75$, we obtain $c=17$, and further assuming $u_0=1(m/s)$, $f=0.0047\,(\sec^{-1})$. By taking these numerical values and putting $F(t)=\zeta_0te^{-\alpha t}$ ($\alpha=1/2(\mathrm{hr}^{-1})$), the maximum height along the distance from the mouth of the river is calculated from eq. (2) and is shown in the curve I in fig. 4. For comparison, the amplitude of the semi-diurnal tide obtained from eq. (1),

$$\exp\left[-\Re((i\sigma f-f^2)/gR)^{1/2}x\right],$$

is also shown in the curve II in this figure. From these curves we can see that the decrement of the maximum height of the solitary-type wave corresponding to the high waters due to "Jane" is more conspicuous than the amplitude of semi-diurnal tide which seems to be almost similar to the high waters in "Ruth".

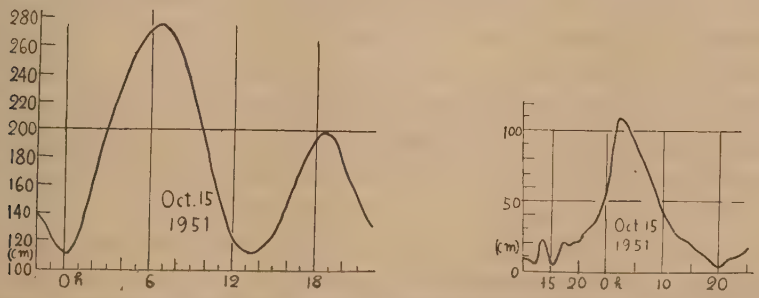

Fig. 3. Mareogram (left) and high tide (deviation from astronomical tide) (right) at Osaka on the occasion of Typhoon "Ruth".

Both theoretical curves show more rapid decrease in height than the observed ones shown in fig. 1, which is due to the overestimation of the friction coefficient f. In fact, I. Tsuboi[2] gave the amplitude ratios at several stations shown in fig. 1 to that of the Tidal Station Tempozan as

St. 1	St. 2	St. 3	St. 4	St. 5	St. 6	St. 7
0.988	1.015	1.009	0.994	1.032	0.985	0.944

for M_2 tide from the tidal observations during one month. However, the general tendency for the change of wave height along the river is consistent with each other between the observed and theoretical curves.

§ 3. The eqs. (1) for the waves progressing up the river becomes linearized ones under the assumption that the wave height is small in comparison with the hydraulic depth of the river. In a general case these equations should be taken as[3]

$$\frac{\partial u}{\partial t}+(u-u_0)\frac{\partial u}{\partial x}=-fu-g\frac{\partial \zeta}{\partial x}\,, \qquad \frac{\partial \zeta}{\partial t}=-\frac{\partial}{\partial x}\{(h+\zeta)(u-u_0)\}\,, \qquad (3)$$

and since they are of non-linear type, the solution under the given boundary conditions should be computed by the method of successive approximation or the integration by use of the concept of characteristic curves. Recently some discussions about the non-linear shallow water waves[4][5] have been given by several authors and from their results it has been clearly shown that the breaking of sea waves or swells near the shore is due to the non-linearity of the fundamental equation system, and accordingly it is necessary to discuss the effect of the long wave going up the river, since the maximum height of the wave caused by the high waters due to typhoons sometimes reach about 4~5 m at the mouth of the river where the depth is 9~10 m at most, as shown in the above examples. When the changes in the height of the wave and in the velocity of the current with time are given at the mouth, the method of successive approximation can be developed in two ways, one of which is to expand the solutions for u and ζ in power series of the maximum amplitude of the wave height at the mouth and the other to expand them in power series of the distance from the mouth if the wave length is large enough and the considered region is not so distant from the mouth as compared with the wave length. For these methods of successive approximation it is more convenient to transform all the variables in eqs. (3) to dimensionless quantities[5] such as

$$\tau=\omega\sqrt{gh}\,t,\quad \alpha=\omega x\,,\quad U=u/\sqrt{gh}\,,\quad Y=\zeta/h\,,\quad U_0=u_0/\sqrt{gh}\,,\quad a=f/\sqrt{gh}\omega$$

where the depth h is assumed to be constant and ω is the characteristic length of the wave which is taken to be equal to the wave length for the periodic wave, and then the initial eqs. (3) are transformed to[6]

$$\frac{\partial U}{\partial \tau}+(U-U_0)\frac{\partial U}{\partial \alpha}=-aU-\frac{\partial Y}{\partial \alpha}\,,\qquad \frac{\partial Y}{\partial \tau}=-\frac{\partial}{\partial \alpha}[(1+Y)(U-U_0)]. \tag{4}$$

In this section the first approach to the successive approximation is discussed; when we take the boundary conditions:

$$Y=AF(\tau)\,,\quad \text{at}\quad \alpha=0\,,$$

where $F(\tau)\leqslant 1$, then we put $Y=Y_1A+Y_2A^2+\cdots+Y_nA^n+\cdots$,

$$U=U_1A+U_2A^2+\cdots\,,$$

and we obtain as the equations for Y_1 and U_1 the following relations by equating the coefficients of the same powers of A in eqs. (4).

$$\frac{\partial U_1}{\partial \tau}-U_0\frac{\partial U_1}{\partial \alpha}=-aU_1-\frac{\partial Y_1}{\partial \alpha}\,,\qquad \frac{\partial Y_1}{\partial \tau}=-\frac{\partial}{\partial \alpha}U_1\,, \tag{5}$$

$$\frac{\partial U_2}{\partial \tau}+U_1\frac{\partial U_1}{\partial \alpha}-U_0\frac{\partial U_2}{\partial \alpha}=-aU_2-\frac{\partial Y_2}{\partial \alpha}\,,\qquad \frac{\partial Y_2}{\partial \tau}=-\frac{\partial}{\partial \alpha}(U_2-U_0Y_2+U_1Y_1)\,, \tag{6}$$

$$\left.\begin{aligned}&\frac{\partial Y_n}{\partial \tau}-U_0\frac{\partial}{\partial \alpha}U_n+aU_n+\frac{\partial Y_n}{\partial \alpha}=-\Big(U_1\frac{\partial}{\partial \alpha}U_{n-1}+U_2\frac{\partial}{\partial \alpha}U_{n-2}+\cdots\\&\qquad+U_{n-1}\frac{\partial}{\partial \alpha}U_1\Big)\,,\\&\frac{\partial Y_n}{\partial \tau}+\frac{\partial}{\partial \alpha}U_n-U_0\frac{\partial}{\partial \alpha}Y_n=-\frac{\partial}{\partial \alpha}(Y_1U_{n-1}+Y_2U_{n-2}+\cdots+U_1Y_{n-1}),\end{aligned}\right\} \tag{7}$$

where the boundary conditions for Y_n are

$$\text{at}\quad \alpha=0\quad Y_1=F(\tau),\quad Y_n=0\ (n\neq 1);\quad \text{at}\quad \alpha=\infty,\quad Y_n=\text{finite}.$$

The solutions of these linearized equations can be computed most simply by the operational method for the arbitrary function $F(\tau)$, and the eq. (5) is given by the operational form as

$$pY_1-U_0\frac{dY_1}{d\alpha}=-\frac{dU_1}{d\alpha}\,,\qquad pU_1-U_0\frac{dU_1}{d\alpha}=-aU_1-\frac{dY_1}{d\alpha}\,, \tag{8}$$

or

$$(1-U_0^2)\frac{d^2Y_1}{d\alpha^2}+(2pU_0+aU_0)\frac{dY_1}{d\alpha}-p(p+a)Y_1=0\,, \tag{9}$$

and thus,

$$Y_1=\varphi(p)e^{\lambda\alpha}\,, \tag{10}$$

where

$$\varphi(p)\subset F(\tau)\,,$$

$$\lambda=\frac{1}{2}\frac{1}{(1-U_0^2)}\left\{-U_0(a+2p)-\sqrt{4p^2+4pa+aU_0^2}\right\}. \tag{11}$$

When we transform these solutions into the usual form, we obtain

$$Y_1=e^{-a\alpha/2(1-U_0)}F\left(\tau-\frac{\alpha}{1-U_0}\right)$$
$$+\frac{a}{2}\gamma\int_\gamma^\tau F\left(\tau-\frac{U_0\alpha}{1-U_0^2}-\mu\right)\cdot\frac{e^{-a\mu/2}I_1\{\frac{a}{2}\sqrt{1-U_0^2}(\mu^2-\gamma^2)\}}{\sqrt{\mu^2-\gamma^2}}d\mu\,, \qquad (12)$$
$$(\gamma=\alpha/(1-U_0^2))\,.$$
$$U_1=\left(U_0-\frac{p}{\lambda}\right)Y_1$$

or
$$U_1=U_0Y_1+\int_\alpha^\infty\frac{dY_1}{d\tau}d\alpha\,.$$

The higher-order approximations can be also computed similarly by solving the unhomogeneous equations given by (7), when the solutions as far as the order $n-1$ are computed. However, these solutions are generally more complicated and here only the solution for Y_2 is given below. First, the operational form of eqs. (6) is given by

$$(1-U_0^2)\frac{d^2Y_2}{d\alpha^2}+(2p+a)U_0\frac{dY_2}{d\alpha}-p(p+a)Y_2$$
$$=\frac{d}{d\alpha}\left\{(p+a)U_1Y_1-\frac{1}{2}\frac{dU_1^2}{d\alpha}-U_0\frac{dU_1Y_1}{d\alpha}\right\}, \qquad (13)$$

and the solution under the boundary conditions that $Y_2=0$ at $\alpha=0$, $Y_2=$finite at $\alpha=\infty$ is in operational form:

$$Y_2=\frac{1}{(\lambda_2-\lambda_1)(1-U_0^2)}\int_0^\alpha\left\{(p+a)U_1Y_1-U_1\frac{dU_1}{d\xi}\right.$$
$$\left.-U_0\frac{dU_1Y_1}{d\xi}\right\}\left\{\lambda_2e^{\lambda_2(\alpha-\xi)}-\lambda_1e^{\lambda_1(\alpha-\xi)}\right\}d\xi\,, \qquad (14)$$

where
$$\lambda_2,\lambda_1=\frac{1}{(1-U_0^2)}\left\{-\left(\frac{a+2p}{2}\right)U_0\pm\sqrt{p^2+pa+a^2U_0^2/4}\right\}.$$

In this case the transformation is not so simple, and when we put

$$F_1(\tau,\alpha)=aU_1Y_1+\frac{\partial}{\partial\tau}(U_1Y_1)-U_1\frac{\partial U_1}{\partial\alpha}-U_0\frac{\partial U_1Y_1}{\partial\alpha}\,,$$

the formal expression of Y_2 is given by

$$Y_2=\frac{1}{2(1-U_0^2)}\int_0^\alpha\{P_1(\alpha-\xi,\tau)+P_2(\alpha-\xi,\tau)+Q_1(\alpha-\xi,\tau)+Q_2(\alpha-\xi,\tau)\}d\xi\,, \qquad (15)$$

where $P_1(\alpha,\tau)$ is given by replacing F with F_1 in eq. (12) and we indicate it by $P_1=P_1[F_1]$, where the brackets [ ] indicate that the function P_1 is deduced from the function F_1. Then the function $P_2(\alpha,\tau)$ can be expressed as

$$P_2=\int_\gamma^\infty P_1\left[\frac{1}{2(1-U_0^2)}\left(aF_1+2\frac{\partial}{\partial\tau}F_1\right)\right],$$

where the first term in the right hand side of the equation corresponding to the functional P_1 for the argument F_1 function which is similar to eq. (12) is written as

$$e^{-U_0\alpha/(1-U_0^2)-\gamma\alpha}F_1\left(\tau-\frac{U_0\alpha}{1-U_0^2}-\gamma\alpha\right),$$

and then we integrate the function P_1 with the variable γ from γ to ∞ and after the integration about γ we replace γ with $\alpha/(1-U_0^2)$. Q_1 and Q_2 are the terms corresponding to P_1 and P_2, which are obtained by replacing γ with $-\gamma$ and the above integration interval about γ with $\int_{-\gamma}^{-\infty}$. So far as the functional form of F in eq. (12) or the initial value of the elevation is not given, the detailed discussion about the nature of the second-order approximation is impossible and only the schematical representation is given here. The first-order solution (12) is somewhat different from the solution (2) in its form, but this is due to the expression of the friction coefficient f or a and not of the fundamental property. The numerical computation of the 2nd-order approximation is so complicated in this method that it is not fulfilled here. From the operational form of the solution for Y_2 (14), the value of Y_2 seems to become infinite at $\alpha\to\infty$, owing to the terms involving $e^{\lambda_2\alpha}$, but since the function consists in terms such as U_1Y_1, U_1^2 and their operational form has a factor as $e^{\lambda_1\alpha}$, the operatinal form for F_2 has a factor $e^{2\lambda_2\alpha}$ from Borel's theorem and thus it is necessary to add the term proportional to $e^{\lambda_1\alpha}$ to eq. (14) for the convergence at $\alpha=\infty$, since the integration with ξ of the term $F_1(\xi)e^{\lambda_1(\alpha-\xi)}$ is

$$\int_0^\alpha e^{2\lambda_2\xi+\lambda_1(\alpha-\xi)}d\xi=\frac{e^{2\lambda_2\alpha}-e^{\lambda_1\alpha}}{2\lambda_2-\lambda_1},$$

and the additive term $e^{\lambda_1\alpha}$ makes the value at $\alpha=\infty$ infinitive. The proportional constant for $e^{\lambda_1\alpha}$ is undetermined, so far as the functional form (or its operational form) of F_1 is not given.

§ 5. In this section the second approach to the successive approximation is discussed, since in the practical examples as shown in § 2 the value of ω^{-1} becomes

5.94×10^4 (m) for $h=7$ (m), $\beta=1/2\,(\mathrm{hr}^{-1})$, where the functional form of ζ $(x=0)$ is taken as $te^{-\beta t}$ as given in § 2 and therefore $\alpha\ll1$ in the considered region, since the distance from the mouth is 5 or 6 km at most. Thus the convergence of the expansions of the solutions in power series of α is good in the considered range. When we put

$$Y=\sum_{i=0}^{\infty}y_i\alpha^i\ ,\quad U=\sum_{i=0}^{\infty}u_i\alpha^i\ ,$$

the coefficients y_i and u_i can be determined from the following system of equations successively, which is obtained by equating the coefficients of α of the same power, substituting the series of Y and U in eqs. (4).

$$u_0'+(u_0-U_0)u_1=-au_0-y_1\ ,\quad y_0'+(1+y_0)u_1+y_1(u_0-U_0)=0\ ,$$
$$u_1'+2(u_0-U_0)u_2+2u_1^2=-au_1-2y_2\ ,\quad y_1'+2(1+y_0)u_2+2u_1y_1+2y_2(u_0-U_0)=0\ ,$$
$$u_{n-1}'+n\left\{(u_0-U_0)\,u_n+u_1u_{n-1}+\cdots+\begin{bmatrix}u_{n/2}^{\,2}\\ u_{(n-1)/2}u_{(n+1)/2}\end{bmatrix}\right\}=-au_{n-1}-ny_n\ ,$$
$$y_{n-1}'+n\{(1+y_0)u_n+y_1u_{n-1}+y_2u_{n-2}+\cdots+y_{n-1}u_1+(u_0-U_0)y_n\}=0\ .$$

The solutions so far as the second-order terms u_2, y_2 are given by

$$Ru_1=(u_0-U_0)(u_0'+au_0)-y_0\ ,$$
$$Ry_1=(u_0-U_0)y_0'-(1+y_0)(au_0+u_0')\ ,$$
$$Ru_2=\tfrac{1}{2}(u_0-U_0)(u_1'+au_1+2u_1^2)-\tfrac{1}{2}(y_1'+2u_1y_1)\ ,$$
$$Ry_2=\tfrac{1}{2}(u_0-U_0)(y_1'+2u_1y_1)-\tfrac{1}{2}(1+y_0)(u_1'+au_1+2u_1^2)\ ,$$
$$R=1+y_0-(u_0-U_0)^2\ . \qquad (16)$$

The general solutions for y_n and u_n are given by

$$Ru_n=(u_0-U_0)\left(\frac{a}{n}u_{n-1}+\frac{1}{n}u_{n-1}'+u_1u_{n-1}+\cdots\right)-\left(\frac{y_{n-1}'}{n}+y_1u_{n-1}+\cdots+y_{n-1}u_1\right),$$

$$Ry_n=(u_0-U_0)\left(\frac{1}{n}y_{n-1}'+y_1u_{n-1}+\cdots+y_{n-1}u_1\right)$$
$$-(1+y_0)\left(\frac{a}{n}u_{n-1}+\frac{1}{n}u_{n-1}'+u_1u_{n-1}+\cdots\right), \qquad (17)$$

from which we can compute u_n, y_n by using the values u_0 to u_{n-1} and y_0 to y_{n-1}. The general discussions of convergence of such series were given in the previous paper[5] and here only the effect of the frictional term is discussed. When the dimensionless friction coefficient is large (in fact $a=33.8$ if we take $f=0.0047\,\mathrm{sec}^{-1}$ and the value of $\omega\sqrt{gh}=1/2\,(\mathrm{hr}^{-1})$ corresponding to the case given above), then for some value of n the condition $a\ll n$ is valid, and in this case we can put

$$u_n \sim \frac{(u_0-U_0)}{nR} a u_{n-1} \quad \text{and} \quad y_n \sim -\frac{(1+y_0)}{nR} a u_{n-1}$$

from the above solutions for u_n, y_n (17). Then

$$u_1 \sim \frac{(u_0-U_0)}{R} a u_0 \quad \text{and} \quad u_n \sim \frac{u_0}{n!}\left(\frac{Pa}{R}\right)^n,$$

$$y_n \sim -\frac{u_0(1+y_0)}{n!\,P}\left(\frac{P}{R}a\right)^n, \quad (P=u_0-U_0)$$

or

$$u \sim u_0 e^{Pa\alpha/R}, \quad y \sim y_0 + \frac{u_0(1+y_0)}{P}\{1-e^{Pa\alpha/R}\}.$$

According to these estimation, the current velocity increases with the distance from the initial point, owing to the friction term, and this seems to be somewhat paradoxical. However, this is explained from the fact that in such estimation the effect of change with time is neglected, since the terms u_n', y_n' are not taken into account, as compared with au_n, and in such condition the equation for the stationary motion is valid and from it

$$(U-U_0)\frac{dU}{d\alpha} = -aU - \frac{dY}{d\alpha}, \quad (1+Y)(U-U_0) = c = \text{const}.$$

and thus

$$\{1+Y-(U-U_0)^2\}\frac{dU}{d\alpha} = a(U-U_0)U.$$

Therefore when $(U-U_0)\{1+Y-(U-U_0)^2\} > 0$, U increases with the distance. (The exact solution of the above equations is simply given by putting $U(0)=u_0$, as

$$\frac{c}{U_0}\left(\frac{1}{U_0}\log\frac{U}{u_0}\frac{u_0-U_0}{U-U_0} + \frac{1}{u_0-U_0} - \frac{1}{U-U_0}\right) - \left(U-u_0-U_0\log\frac{U}{u_0}\right) = a\alpha,$$

and as is seen from computing this solution the increase of U is verified.)

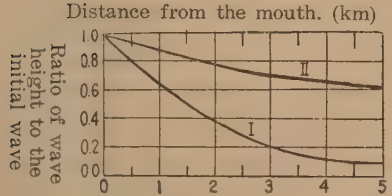

Fig. 4. Theoretical curves for the decrease of wave heights.
curve I, for the wave $\zeta_0 te^{-\alpha t}$.
curve II, for the semi-diurnal tide.

When we put $u_0 = A\sin\tau$, $y_0 = A\sin\tau$, corresponding to the condition that the waves of oscillatory type progress without change of their profile for the region $\alpha < 0$ and then go up the river, where the friction has an effect and the water depth is shallow as compared with the amplitude, we can investigate the change of wave profiles due to the friction and non-linear terms

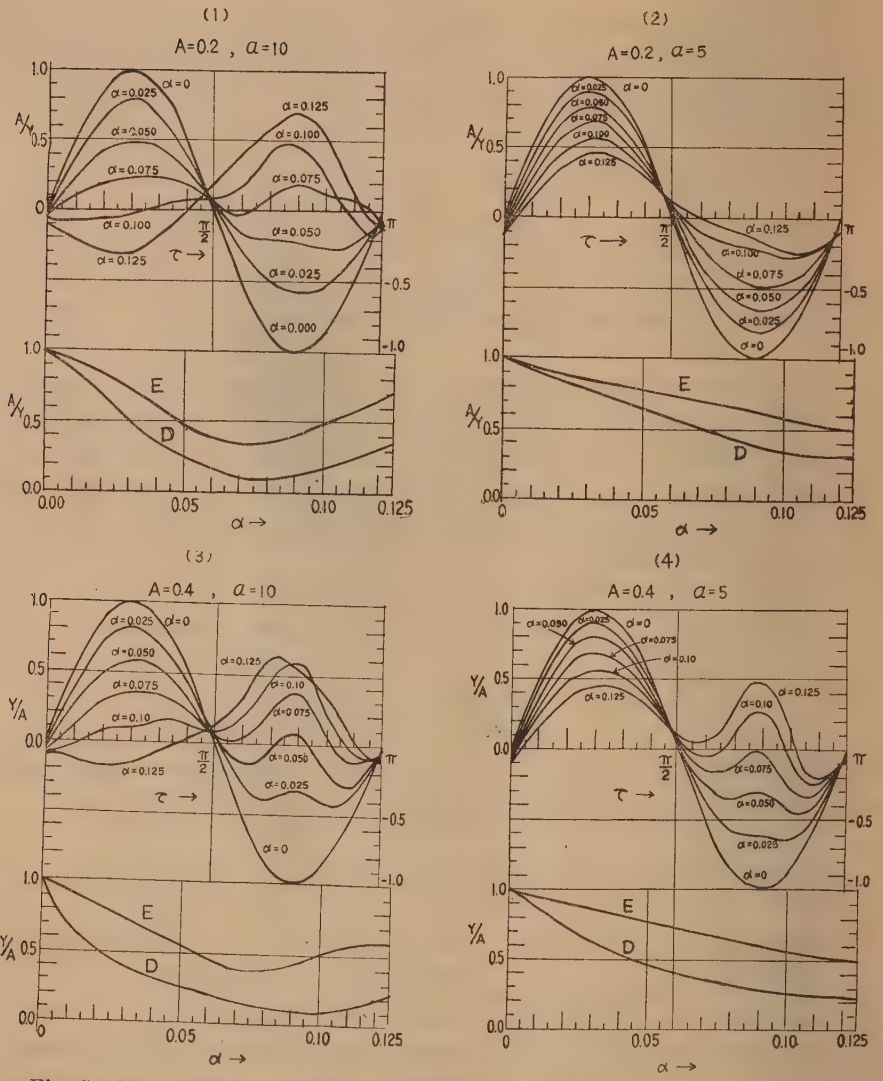

Fig. 5. The changes of profiles of oscillatory waves at stations (above) and the variations of maximum elevation and depression with the distance from the initial point (below). (E=elevation, D=depression)

by computing the coefficients u_n, y_n of any order corresponding to the distance from the initial point. The results of such computations are shown in fig. 5, where the wave profiles at the distances $10\alpha=0.25, 0.50, 0.75, 1.00, 1.25$ are shown

for $U_0=0.1$ and for the intial amdlitudes $A=0.2$, 0.4 and for the frictional coefficients $a=5$, 10, respectively. Further the variations of maximum elevation and depression with the distance are also shown in respect to each case. From these curves we can see the follwing properties about the changes of wave profiles in relation with the friction and the initial wave height.

(i) The change of wave profiles or the occurence of the over-tides are more conspicuous in the depression region than in the elevation region, and such tendency is larger when the amplitude of the initial point is larger.

(ii) The decrease of maximum height of elevation with the distance is more gradual than that of depression and the wave portion of depression seems to be smaller when the waves go further up the river.

(iii) The amplitude decreases with the distance from the initial point at the first region of α, owing to the friction term, but it again increases at some distance and such increase is probably due to the effect of non-linear terms which causes the breaking of the waves.

(iv) When a is small and the initial wave height is large, the change of wave profiles is more conspicuous for the same absolute distance x from the initial point, as seen from comparing the wave profiles at $\alpha=0.05$ for $a=10$ with those at $\alpha=0.10$ for $a=5$, since $x=\alpha/\omega=\alpha a\sqrt{g\bar{h}}/f$ and, if the depth f is constant, $\alpha\sim 1/a$ for the constant value of x, this is due to the fact that the initial wave steepness becomes large for a small value of a and a large value of A, and thus the waves are more influenced by the effect of non-lineality for the large initial wave steepness.

Next, the variations of the maximum amplitude of elevation and depression with the initial amplitude A at the distance $\alpha=1/a$ from the mouth are shown for $a=10$ in fig. 6, which shows that the amplitude at the absolute distance $x=\sqrt{g\bar{h}}/f$ decreases abruptly as the initial wave height increases at the first stage, whereas it increases again after a certain value of A and further it approaches to infinity for the value $A=0.566$ ($U_0=0.1$), since the minimum value of P is given by $1-A+(A+U_0)^2$ for $\tau=3\pi/2$ and since, when $A\geqslant\{(U_0+\frac{1}{2})^2+1\}^{1/2}-(U_0+\frac{1}{2})$, P vanishes at a certain value of τ. Such changes of the maximum amplitude with the values of the initial amplitude A

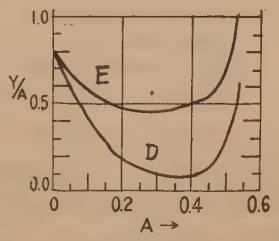

Fig. 6. The variations of maximum elevation (E) and depression (D) with the initial height (A). ($a=10$, $\alpha=0.1$)

seems to be explained, if we consider that the friction acts more effectively upon the decrease of the amplitude till the increase of the initial steepness attains some critical value, and that for larger values of steepness above such critical value the effect of non-lineality becomes predominant, and that at the value $A=0.566$ almost instantaneously the breaking of the waves occurs. Further, Such decrease of the amplitude is more conspicuous for the above-mentioned depression part. In the limit case for $A=0$ the decrease of the amplitude is computed by the solution of the linearized equation for the first order approximation given by eqs. (5), which becomes

$$(\text{periodic term})\times\exp\left(-\frac{1}{a}\Re\sqrt{ia-1-U_0^2/4}\right)$$

for the value $a\alpha=1$. In fig. 7 the variations of the maximum amplitude of elevation at $\alpha=1/a$ with the values of a are shown for $A=0$, 0.2 and 0.4, where the curve for $A=0$ has been obtained by using the above solution for the linearized equation, and in this case the maximum elevation and depression have the same value, as easily seen from the above equation. These curves indicate the effect of the wave length or wave period upon the amplitude at the constant absolute distance $x=\sqrt{gh}/f$, since a is inversely proportional to the wave length, and from these curves we can see that the decrease of the short waves, or in other words steeper waves, is more remarkable for the constant initial wave height till a certain value of wave length, and when the wave length decreases further or the steepness increases above this critical value the amplitude increases rapidly with the steepness, in the same manner as the previous case of the changes of height with the intial amplitude A, due to the effect of non-lineality. Further, the value of a increases infinitely or the wave length becomes infinity, and then the amplitude approaches to the curve for the limit case $A=0$, since in this case the wave steepness almost vanishes and the linearized equation of the shallow water waves become valid. By comparing it with the case $A=0$, we can see that the finite amplitude waves are, in the short wave region or for the small value of a, quite different from the small amplitude waves, which have the

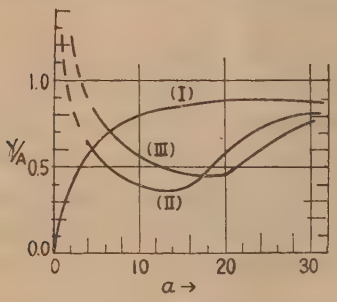

Fig. 7. The variations of maximum elevation with the values of a at $\alpha=1/a$. (Curve I. $A\sim0$, Curve II. $A=0.2$, Curve III. $A=0.4$)

amplitude decreasing monotonously with the decrease of the wave length and their amplitude vanishes at $a=0$ since $a=0$ corresponds to $\alpha\to\infty$.

Summarizing the above analysis, we can see that the decrease of the amplitude is more remarkable for the finite amplitude waves of shorter period than for the small amplitude waves up to a certain distance from the mouth, and the observed fact shown in sec. 2 is explained even by taking account of the effect of the non-lineality, at least qualitatively. In the practical case the breaking of waves caused by high waters seems to have been replaced with the phenomena of overflow of the waters over the banks of rivers, because the increase of wave height was not observed.

§ 6. The approximation stated in § 5 is effective only in the neighbourhood of $\alpha=0$, since more terms of power series should be taken into account at larger values of $\alpha=0$. Therefore the method of characteristic curves is the most useful in a wider range of α. For this purpose the original equations (4) are transformed into the following forms:

$$\left.\begin{aligned}&\left\{\frac{\partial}{\partial\tau}+(U-U_0+C)\frac{\partial}{\partial\alpha}\right\}(U+2C)+aU=0\,,\\&\left\{\frac{\partial}{\partial\tau}+(U-U_0-C)\frac{\partial}{\partial\alpha}\right\}(U-2C)+aU=0\,,\end{aligned}\right\}\qquad(18)$$

where $C=\sqrt{1+Y}$. Further they can be expressed by

$$\left.\begin{aligned}&\left\{\frac{\partial}{\partial\tau}+(U-U_0+C)\frac{\partial}{\partial\alpha}\right\}(U+2C+a\Psi)=0\,,\\&\left\{\frac{\partial}{\partial\tau}+(U-U_0-C)\frac{\partial}{\partial\alpha}\right\}(U-2C+a\Phi)=0\,,\end{aligned}\right\}\qquad(19)$$

by introducing the functions Ψ and Φ which satisfy the relations:

$$\left.\begin{aligned}&\left\{\frac{\partial}{\partial\tau}+(U-U_0+C)\frac{\partial}{\partial\alpha}\right\}\Psi=U\,,\\&\left\{\frac{\partial}{\partial\tau}+(U-U_0-C)\frac{\partial}{\partial\alpha}\right\}\Phi=U\,.\end{aligned}\right\}\qquad(20)$$

Then, from the theory of characteristic curves

$$U+2C+a\Psi=\text{const.}$$

at the characteristic curve G_1 which is defined by

$$\frac{d\tau}{d\alpha}=U-U_0+C$$

in the $\alpha-\tau$ plane and

$$U-2C+a\Phi=\text{const.}$$

at the curve C_2 which is given by

$$\frac{d\tau}{d\alpha}=U-U_0-G\,, \tag{21}$$

and the functions Ψ and Φ can be obtained from

$$\frac{D\Psi}{Ds_1}=U\,, \qquad \frac{D\Phi}{Ds_2}=U\,, \tag{22}$$

where Ds_1 and Ds are the line elements of C_1 and C_2, and D/Ds_1, D/Ds_2 mean the derivatives of the curves C_1 and C_2, respectively. For numerical calculation it is necessary to obtain two families of characteristic curves on the $\alpha-\tau$ plane, and thus the above system of ordinary differential equations should be replaced with the system of difference equations, and then the construction of a network of characteristic curves is possible, as shown by J. J. Stoker[4], although the friction terms are added in this example. However, the method of construction of the network is somewhat different from the frictionless case and it is not useless to describe it from a general point of view. Among three neighbouring points of a network on the $\alpha-\tau$ plane (fig. 8) the points 1 and 2 are considered as the starting points and all the quantities $\alpha,\tau,U,C,\Psi,\Phi$ at them are assumed to be known. Then the coordinates of the third point 3 and the values of U,C,Ψ,Φ at this point can be computed from the following system of difference equations :

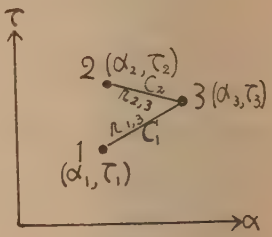

Fig. 8.

$$\frac{\alpha_3-\alpha_1}{\tau_3-\tau_1}=\frac{1}{2}(U_3+C_3+U_1+C_1)-U_0\,,$$

$$U_3+2C_3+a\Psi_3=U_1+2C_1+a\Psi_1\,,$$

$$\Psi_3-\Psi_1=\frac{1}{2}\sqrt{(\alpha_3-\alpha_1)^2+(\tau_3-\tau_1)^2}\,(U_1+U_3)\,;$$

$$\frac{\alpha_3-\alpha_2}{\tau_3-\tau_2}=\frac{1}{2}(U_3-C_3+U_2-C_2)-U_0\,,$$

$$U_3-2C_3+a\Phi_3=U_2-2C_2+a\Phi_2\,,$$

$$\Phi_3-\Phi_2=\frac{1}{2}\sqrt{(\alpha_3-\alpha_2)^2+(\tau_3-\tau_2)^2}\,(U_2+U_3)\,, \tag{23}$$

where all the quantities with the subscript 3 are considered as unknown, since the distances between these points are assumed to be infinitely small and the differential about τ and α can be replaced with the difference. In practical numerical calculations it is much labourious to solve these equations and a simpler method is applied. When the slopes of the characteristic curves C_1, C_2 at the points 1 and 2 are determined from the initial values of U, C, ϕ, ψ, then the position of the point 3 is given as the intersection of these curves, and the distances r_3 between points 1 and 3 and $r_{2,3}$ between points 2 and 3 are determined graphically, and from the equations:

$$\begin{aligned} &U_3+2C_3+\frac{l_1}{2}(U_1+U_3)=U_1+2C_1\,,\\ &U_3-2C_3+\frac{l_2}{2}(U_2+U_3)=U_2-2C_2\,,\\ &l_1=ar_{1,3}\,,\quad l_2=ar_{2,3}\,, \end{aligned} \tag{24}$$

the values of U_3 and C_3 are

$$\begin{aligned} &\left(2+\frac{l_1}{2}+\frac{l_2}{2}\right)U_3=U_1\left(1-\frac{l_1}{2}\right)+U_2\left(1-\frac{l_2}{2}\right)+2(C_1-C_2)\,,\\ &2\left(2+\frac{l_1}{2}+\frac{l_2}{2}\right)C_3=\left\{U_1\left(1-\frac{l_1}{2}\right)+2C_1\right\}\left(1+\frac{l_2}{2}\right)\\ &\qquad\qquad -\left\{U_2\left(1-\frac{l_2}{2}\right)-2C_2\right\}\left(1+\frac{l_1}{2}\right). \end{aligned} \tag{25}$$

When we put U_3^0 and C_3^0 as the values of U and C at the point 3 for the frictionless case and further we assume that the values of U, C at the starting points 1 and 2 are the same for two cases, then

$$\begin{aligned} &4\left(2+\frac{l_1}{2}+\frac{l_2}{2}\right)(C_3^0-C_3)=\frac{U_1}{2}(3l_1-l_2)+\frac{U_2}{2}(l_1-3l_2)+\frac{C_1}{2}(l_1-l_2)+\frac{C_2}{2}(l_2-l_1)\,,\\ &2\left(2+\frac{l_1}{2}+\frac{l_2}{2}\right)(U_3^0-U_3)=\frac{1}{2}(l_1+l_2)(C_1-C_2)+\frac{1}{2}(3l_1+l_2)U_1+\frac{1}{2}(l_1+3l_2)U_2\,, \end{aligned}$$

by neglecting $l_1 l_2$ in comparison with l_1, l_2, since we can take l_1, l_2 as little as possible. From these relations we can observe that $U_3^0 > U_3$ when $C_1 > C_2$, and this means that the velocity becomes smaller with the friction term where the wave height decreases with time and further when $l_1 \sim l_2$, $C_3^0 > C_3$ in the region $U_1 > U_2$, and since these two conditions are satisfied in the tail of the solitary wave with one peak of elevation, we can generally conclude that the wave becomes

lower in the rear part of the solitary wave, or in other words, the tail of the solitary wave is retarded when the friction acts, whereas in the frontal region

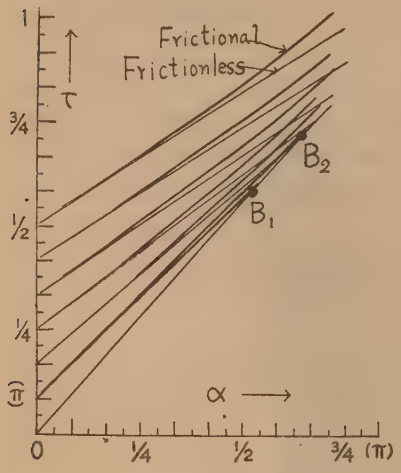

Fig. 9. Characteristic curves G_1 for $a=0$ (frictionless) and $a=10$ (frictional) when $A=0.4$. B_1=Breaking point for $a=0$, B_2=breaking point for $a=10$.

such general conclusion is not easily obtained, and in fig. 9 we show the characteristic curve G_1 for the wave $Y=A\sin\tau$, $\pi>\tau>0$, $=0$ $\tau<0$, $\tau>\pi$ for $A=0.4$ and $a=0$, $a=10$, and from this figure we can see that the frontal part of the wave becomes lower with the friction term than in the frictionless case, and thus the breaking of the wave occurs at $\alpha=2.02$ in the frictional case, whereas it occurs at $\alpha=1.40$ in the frictionless case. Therefore the breaking is somewhat retarded in the frictional case. In this paper, only one numerical example is shown, and further discussions shall be given in the follwing paper.

(To be continued.)

References

1) M. Kusunoki: On the flow of the river tide. Journ. Civ. Engineering, **17**, 1931. (In Japanese.)
2) I. Tsuboi: On the changes of water levels in the rivers of the City of Osaka. Umi to Sora, Vol. 18, No. 1, 1938. (In Japanese.)
3) G. Okamoto: Tides in a river. Chikyu Butsuri, Vol. 4, 1940. (In Japanese.)
4) J. J. Stoker: Formation of breakers and bores. Communications on Applied Mathematics, I (1), 1948.
5) T. Ichiye: On the waves on a sloping beach. (To be published in Ocean. Mag.)
6) In eq. (4) the friction coefficient a is proportional to the wave length or wave period, and at first sight the effect of friction increases with the wave length, but as seen below it is only superficial and the friction coefficient usually appears in the form as $a\alpha$ or $a\tau$.

OCT 7 1955